

12-2014

Enhancement Techniques of Boiling Heat Transfer

Basim Qasim Ali Al-Sukaini

Follow this and additional works at: <https://commons.erau.edu/edt>



Part of the [Mechanical Engineering Commons](#)

Scholarly Commons Citation

Al-Sukaini, Basim Qasim Ali, "Enhancement Techniques of Boiling Heat Transfer" (2014). *Dissertations and Theses*. 261.

<https://commons.erau.edu/edt/261>

This Thesis - Open Access is brought to you for free and open access by Scholarly Commons. It has been accepted for inclusion in Dissertations and Theses by an authorized administrator of Scholarly Commons. For more information, please contact commons@erau.edu.

ENHANCEMENT TECHNIQUES FOR BOILING HEAT TRANSFER

by

Basim Qasim Ali Al-Sukaini

A Thesis Submitted to the College of Engineering, Department of Mechanical
Engineering in Partial Fulfillment of the Requirements for the Degree of
Master of Science in Mechanical Engineering

Embry-Riddle Aeronautical University

Daytona Beach, Florida

November 2014

ENHANCEMENT TECHNIQUES FOR BOILING HEAT TRANSFER

by

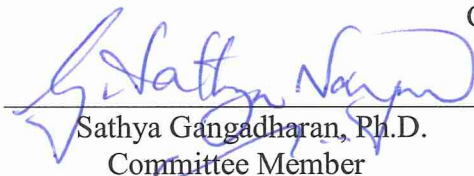
Basim Qasim Ali Al-Sukaini

This thesis was prepared under the direction of the candidate's Thesis Committee Chair, Dr. Birce Dikici, Assistant Professor, Daytona Beach Campus, and Thesis Committee Members Dr. Sathya Gangadharan, Professor, Daytona Beach Campus, And Dr. Marc Compere, Associate Professor, Daytona Beach Campus, and has been approved by the Thesis Committee. It was submitted to the Department of Mechanical Engineering in partial fulfillment of the requirements for the Degree of Master of Science in Mechanical Engineering

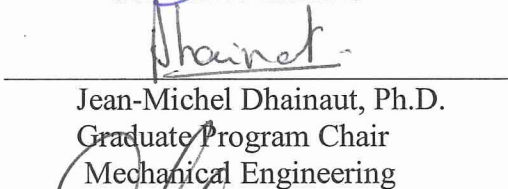
Thesis Review Committee:



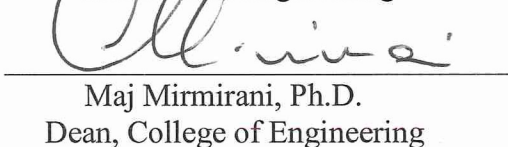
Birce Dikici, Ph.D.
Committee Chair



Sathya Gangadharan, Ph.D.
Committee Member



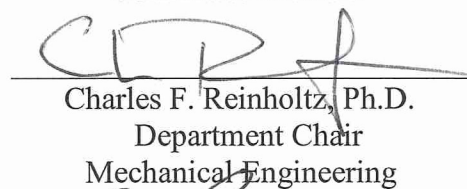
Jean-Michel Dhainaut, Ph.D.
Graduate Program Chair
Mechanical Engineering



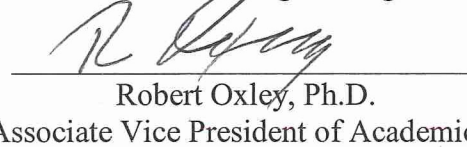
Maj Mirmirani, Ph.D.
Dean, College of Engineering



Marc Compere, Ph.D.
Committee Member



Charles F. Reinholtz, Ph.D.
Department Chair
Mechanical Engineering



Robert Oxley, Ph.D.
Associate Vice President of Academics

11-20-14
Date

Acknowledgments

First and above all, I praise God, the almighty for providing me this opportunity and granting me the capability to proceed successfully.

I would like to express my sincere gratitude to my advisor Dr. Birce Dikici for the continuous support of my master's research, for her patience, motivation, and enthusiasm. Her guidance helped me in all the time of research and writing of this thesis.

I would also like to thank my committee members, Dr. Sathya Gangadharan and Dr. Marc Compere for brilliant comments and suggestions, for their excellent advises and detailed review during the preparation of this thesis.

Also, my sincere thanks go to the lab supervisors, Jordan and Russo, who helped me working on the project.

I would also like to thank all of my friends, especially Abdullah, Hussien, Marwan, Mohanad, Sam, and Sultan, and for all the fun that we have had in the last two years.

A special thanks to my family members. Words cannot express how grateful I am to my parents, sisters, and brothers for all of the sacrifices that you've made on my behalf.

I would like to express my special appreciation and thanks to my sponsor of HCED (The Higher Committee for Education Development in Iraq), who, through their support and generosity, have helped me to make this success possible.

Finally, I would like to thank all the members and employees of Mechanical Engineering Department at Embry-Riddle Aeronautical University for their everlasting support.

Abstract

Researcher: Basim Qasim Ali Al-Sukaini

Title: Enhancement Techniques of Boiling Heat Transfer

Institution: Embry-Riddle Aeronautical University

Degree: Master of Science in Mechanical Engineering

Year: 2014

The aim of this study is to investigate pool boiling performance of water under atmospheric pressure by two techniques. The first method is by adding small amounts of surfactants, and the second way is by using structured surfaces.

The first technique is investigated experimentally with environmentally friendly surfactants. The surfactants chosen for the study are an ionic sodium lauryl sulfate (SLS), nonionic ECOSURF™ EH-14, and nonionic ECOSURF™ SA-9. It is observed that adding a small amount of surfactant alters the water boiling phenomenon significantly. Boiling curves for different concentrations are shifted to the left. The wall temperature drops greatly with an increase in the concentration of aqueous surfactant solutions. Also, it is found that the optimum boiling heat transfer augmentation of SLS is higher than that of EH-14 and SA-9 compared to water. The maximum enhancement obtained is 66.27% for 300ppm aqueous SLS solution. However, the maximum enhancement in heat transfer coefficient is 24.31% for 1600ppm EH-14 and 22.09% for 200ppm SA-9. Boiling visualization shows that boiling with surfactant solutions compared with that in pure water is more vigorous. Bubbles are smaller in size, activate continuously, and collapse

quickly. Also, the bubble departure frequency is higher than that of pure water. Compared with water, it is found that time required to reach boiling point for surfactant concentrations is reduced significantly. The maximum reduction for each surfactant was 14.6% for 100ppm SLS, 9% for 800ppm EH-14, and 12.49% for 300ppm SA-9.

For the second technique, an experimental study is conducted to investigate the performance of various structured surfaces in pool boiling. Surfaces with rectangular channels, holes, and mushroom fins are manufactured first and then studied. The results show that boiling heat transfer can be augmented by structured surfaces. The maximum enhancement is 51.66% achieved by Holed 3 surface compared with plain surface. As the spacing between channels or holes is decreased, the heat transfer coefficient is increased. The bubbles with holed surfaces and mushroomed surface have almost spherical shape, while in plain and grooved surfaces they have an irregular shape. Time to reach boiling point is measured. It is found that some enhanced surfaces show a higher reduction to others. For heat flux of 27.91 kW/m^2 , 8.58% enhancement in time to reach boiling point for Grooved 1 surface is attained, while at a heat flux of 35.08 kW/m^2 the maximum reductions achieved are 8.74% for Mushroomed surface and 8.19% for Holed 1 surface.

Also, the different regimes of pool boiling are observed by droplet dropping tests. Also, the total evaporation time of a water droplet was measured and compared with the results of other studies. The results show that the evaporation times in the natural convection and nucleate boiling regimes are significantly shorter than those in film boiling regime. For natural convection and nucleate boiling regimes, the droplet evaporation time varies between 1s to 31s, while for film boiling regime it varies between 104s to 123s.

Table of Contents

Thesis Review Committee:	ii
Acknowledgments.....	iii
Abstract	iv
Table of Contents	vi
List of Tables	viii
List of Figures	ix
Nomenclature	xi
Structure of the Thesis	xiii
1 Introduction	1
1.1 Statement of the Problem	2
1.2 Boiling Heat Transfer.....	2
1.2.1 Boiling Curve	3
1.2.2 Nucleate Boiling.....	5
1.2.3 Critical Heat Flux for Nucleate Pool Boiling	6
1.3 Surfactants.....	7
1.4 Literature Review.....	9
1.4.1 Surfactants	9
1.4.2 Structured Surfaces.....	12
1.5 Scope of the Present Work.....	15
1.5.1 Surfactants	15
1.5.2 Structured Surfaces.....	16
1.5.3 Droplet Boiling Evaporation Time Observations	16
2 Experimental Test Setup.....	17
2.1 Surfactants	17
2.1.1 Main Components.....	18
2.1.1.1 Beaker.....	19
2.1.1.2 Heater and Stirrer	19
2.1.1.3 Thermocouples	20
2.1.1.4 4-Channel Data Logger Thermometer	20

2.1.1.5	IR Camera	21
2.1.1.6	Digital Camera	21
2.1.1.7	Scales.....	22
2.1.2	Experimental Procedure	22
2.1.2.1	Calculation of the Heat Flux	24
2.1.3	Pool Boiling in Aqueous Surfactant Solutions.....	27
2.1.3.1	Sodium Lauryl Sulfate (SLS).....	28
2.1.3.2	ECOSURF TM EH-14.....	29
2.1.3.3	ECOSURF TM SA-9	29
2.2	Structured Surfaces	30
2.2.1	Production of Structured Surfaces.....	30
2.2.2	Experimental Setup.....	33
2.2.3	Test Procedure	34
2.3	Droplet Boiling Evaporation Time Observations	36
2.3.1	Experimental Procedure	38
3	Experimental Results and Discussion.....	39
3.1	Surfactants.....	39
3.1.1	Boiling Curve of Water	39
3.1.2	Experimental Results and Discussion.....	41
3.1.2.1	Discussion on Heat Transfer Coefficient (h) Enhancement.....	43
3.1.2.2	Discussion on Heat Transfer Coefficient Enhancement Ratio.....	45
3.1.2.3	Discussion on Optimum Heat Transfer.....	49
3.1.2.4	Discussion on Time Required to Reach Boiling Point.....	51
3.1.3	Boiling Visualization.....	53
3.1.3.1	Visualization in Aqueous Anionic Surfactant Solutions.....	54
3.1.3.2	Visualization in Aqueous Nonionic Surfactant Solutions.....	57
3.2	Structured Surfaces	59
3.2.1	Discussion on the Effect of Geometry.....	59
3.2.2	Discussion on the Effect of Spacing.....	62
3.2.3	Discussion on Boiling Visualization	63
3.2.4	Discussion on Bubble Departure Diameter	66
3.2.5	Discussion on Time to Reach Boiling Point.....	68
3.3	Droplet Boiling Evaporation Time Observations	69
3.3.1	Evaporation Time of Water Droplet.....	72
4	Conclusions	75
4.1	Surfactants.....	75

4.2	Structured Surfaces	76
4.3	Droplet Boiling Evaporation Time Observations	77
4.4	Practical Engineering Drawbacks	77
5	Future work.....	79
5.1	Surfactants.....	79
5.2	Structured Surfaces	79
5.3	Droplet Boiling Evaporation Time Observations	80
	References.....	81
	Appendix A: Thermocouple Calibration	87
	Appendix B: Experimental Data of Calculating Heat Flux for Boiling with Surfactants	88
	Appendix C: Experimental Data of Nucleate Boiling of Water and Surfactants	90
	Appendix D: Experimental Data of Water on Structured Surfaces	92
	Appendix E: Experimental Data of Droplet Evaporation Time.....	94

List of Tables

Table 1.1:	Values of the $C_{s,f}$ for various surface- fluid combination [6].....	6
Table 2.1:	Calculation of heat flux	27
Table 2.2:	Physico- chemical properties of surfactants	29
Table 2.3:	Characteristics of enhanced surfaces	32
Table 2.4:	The values of heat flux for boiling with structured surfaces	36
Table 3.1:	Properties of saturated water at 100 °C [6]	40
Table3.2:	Comparison of heat flux rate for theoretical and experimental methods.....	41

List of Figures

Figure 1.1: Boiling classification [9]	3
Figure 1.2: Experimental test setup by Nukiyama [10]	4
Figure 1.3: Boiling curve of water [11]	4
Figure 1.4: The process of CMC [20].....	8
Figure 1.5: Classification of surfactants [21].....	9
Figure 1.6: Structured surfaces by Das. et al. [34].....	13
Figure 1.7: Finned tubes [37].....	14
Figure 2.1: Experimental test setup	18
Figure 2.2: Schematic of experimental setup.....	18
Figure 2.3: Beaker.....	19
Figure 2.4: Heater	20
Figure 2.5: Thermocouple type K.....	20
Figure 2.6: 4-Channel data logger thermometer	21
Figure 2.7: IR camera [44].....	21
Figure 2.8: CASIO camera	22
Figure 2.9: Scales.....	22
Figure 2.10: Stirring process.....	23
Figure 2.11: Temperature profiles of different heater settings	26
Figure 2.12: Surfactants used in the present investigation	28
Figure 2.13: Chemical structure of sodium lauryl sulfate [50].....	28
Figure 2.14:(a):Dimensions of surface in inches (b): Pictorial view of structured surfaces	31
Figure 2.15: Cross section of structured surfaces (dimensions in inches).....	32
Figure 2.16: Experimental setup.....	33
Figure 2.17: Boiling vessel with dimensions in inches.....	34
Figure 2.18: Wall temperature measurements using IR camera (a) plain ($T_s =$ $107.04\text{ }^\circ\text{C}$) (b) Holed 1 ($T_s = 105.44\text{ }^\circ\text{C}$) at heat flux 35.08 kW/m^2	35
Figure 2.19: Experimental setup.....	37
Figure 2.20: Droplet dropping plate.....	38
Figure 3.1: Comparison boiling curve of water with Ref. [26]	40
Figure 3.2: Pool boiling data of aqueous solutions of SLS	42
Figure 3.3: Pool boiling data of aqueous solutions of EH-14.....	43
Figure 3.4: Pool boiling data of aqueous solutions of SA-9.....	43
Figure 3.5: Nucleate boiling heat transfer coefficient as a function of heat flux for aqueous solutions of SLS.	44
Figure 3.6: Nucleate boiling heat transfer coefficient as a function of heat flux for aqueous solutions of EH-14.....	45

Figure 3.7: Nucleate boiling heat transfer coefficient as a function of heat flux for aqueous solutions of SA-9.....	45
Figure 3.8: Heat transfer coefficient enhancement ratio vs. heat flux of SLS.....	46
Figure 3.9: Heat transfer coefficient enhancement ratio vs. heat flux of EH-14.....	47
Figure 3.10: Heat transfer coefficient enhancement ratio vs. heat flux of SA-9.....	47
Figure 3.11: Effect of temperature on CMC of SDS [56].....	49
Figure 3.12: Optimum heat transfer among water and all surfactants.....	51
Figure 3.13: Time to reach boiling point vs. heat flux for SLS.....	52
Figure 3.14: Time to reach boiling point vs. heat flux for EH-14.....	52
Figure 3.15: Time to reach boiling point vs. heat flux for SA-9.....	53
Figure 3.16: Boiling behavior at heat flux 30.38kW/m ²	54
Figure 3.17: Boiling behavior of water and 300ppm SLS at various heat fluxes.....	55
Figure 3.18: Comparison of boiling behavior for pure water and various aqueous SLS solutions at heat flux =30.38 (kW/m ²).....	56
Figure 3.19: Comparison of boiling behavior for pure water and various aqueous EH-14 solutions at heat flux =30.38 (kW/m ²).....	58
Figure 3.20: Comparison of boiling behavior for pure water and various aqueous SA-9 solutions at heat flux =30.38 (kW/m ²).....	59
Figure 3.21: Boiling curves data for enhanced surfaces.....	60
Figure 3.22: Boiling heat transfer coefficient as a function of heat flux for enhanced surfaces.....	60
Figure 3.23: Pictorial view of boiling phenomena before reaching boiling point.....	63
Figure 3.24: Pictorial view of boiling phenomena at different values of heat flux.....	65
Figure 3.25: Boiling behavior of water on different structured surface at 35.08 kW/m ²	66
Figure 3.26: Bubble departure diameter measurements at heat flux of 35.08 kW/m ²	67
Figure 3.27: Bubble departure diameter as a function of heat flux.....	68
Figure 3.28: Time to boiling point vs. heat flux.....	69
Figure 3.29: Natural convection boiling regime.....	70
Figure 3.30: Nucleate boiling regime.....	71
Figure 3.31: Transition boiling regime.....	71
Figure 3.32: Film boiling regime.....	72
Figure 3.33: Leidenfrost drop in cross section [69].....	72
Figure 3.34: Evaporation time vs. excess temperature in the natural convection and nucleate boiling regimes.....	74
Figure 3.35: Evaporation time vs. excess temperature in the film boiling regime.....	74

Nomenclature

A	area, (m ²)
A_r	area augmentation ratio
D	diameter, (m), depth, (m)
S	spacing, (m)
H	height, (m)
C_p	specific heat capacity at constant pressure, (J/kg. K)
C	concentration(ppm)
I	electric current, (Amp)
g	gravitational acceleration, (m/s ²)
h	convection heat transfer coefficient, (W/m ² . k)
h_{fg}	latent heat of vaporization, (J/kg)
k	thermal conductivity, (W/m. K)
m	mass, (kg)
L	length, m
\dot{m}_b	evaporation rate, (kg/s)
M	molecular weight, (kg/kmol)
\dot{q}	heat transfer rate, W
q''	heat flux, (W/m ²)
T	temperature, (°C)
t	time, s
ΔT_e	excess temperature [$T_s - T_{sat}$](°C)
V	voltage, (Volt)
Pr	Prandtl number
Re	Reynolds number
Nu	Nusselt number

V	velocity, m/s
q_{losses}	heat losses, (W)
q_{liquid}	heat transferred to the liquid, (W)

Greek Symbols

β	dimensionless parameter
μ	viscosity, (kg/s. m)
ρ	mass density, (kg/m ³)
σ	surface tension, (N/m)
\emptyset	contact angle, (deg)
α	heat transfer coefficient enhancement ratio

Subscripts

b	bulk, bubble, boiling
l	saturated liquid conditions
v	saturated vapor conditions
sat	saturated conditions
w	water, wall
s	surface conditions, solid properties, solution
f	fluid properties
e	excess
L	based on characteristic length
fc	forced convection

Abbreviation

CMC	critical micelle concentration (ppm)
SLS	sodium lauryl sulfate

Structure of the Thesis

This thesis consists of five chapters. Chapter one is devoted to explain boiling fundamentals. In addition, this chapter contains a comprehensive literature view for boiling with surfactants and boiling on structured surfaces. Chapter two illustrates the experimental setup, and all equipment used in the test are described in detail. Chapter three presents the experimental results of surfactant solutions, structured surfaces, and droplet boiling evaporation time observations. Chapter four gives a general conclusion of the study. Chapter five contains some recommendations for future work.

Boiling Heat Transfer Enhancement with Surfactants

Boiling enhancement studies began in 2012 with Dr. Dikici and her graduate student Eddiong Eno. In their study, same surfactants (SLS, EH-14, and SA-9) are studied. However, the boiling curves are drawn only for selected concentrations, and the results are compared. The results are represented in [1] and [2].

In this thesis, boiling curves of a wider composition range of surfactant solutions are drawn separately as well, and they are compared to boiling of other surfactants and boiling of water.

1 Introduction

Extreme use of fossil fuels has led to many serious issues like reducing energy sources and causing global warming, which is considered the main reason of climate change [3]. Therefore, the energy efficiency improvement and environmental protection are become urgent requests for the world. One of the essential techniques of reducing the effect of global warming is to improve the efficiency of the many engineering applications such as evaporators in refrigeration systems, boilers in power plants, and numerous heat exchangers for various uses. Particularly, many of these heat exchangers have boiling heat transfer process. Therefore, great research and attention have been paid to enhance boiling phenomena [4]. Enhancement techniques of boiling heat transfer can be categorized into two methods: passive and active enhancement techniques. Passive techniques do not need an external source of power. They comprise extended surfaces, rough surfaces, enhanced surfaces, additives for gases, additives for liquid, swirl flow devices, coiled tubes, surface tension devices, and displaced enhancement devices.

However, an external power is required for active techniques. They contain fluid vibration, jet impingement electric or magnetic fields, surface vibration, mechanical aids, injection or suction, and compound techniques [5]. In this thesis, the focus will be narrowed to the addition of surfactants and structured surfaces to enhance boiling heat transfer. In addition, a water droplet is used to investigate the different boiling regimes.

1.1 Statement of the Problem

The literature survey showed that boiling heat transfer can be enhanced significantly by surfactants and with careful selection of structured surfaces. In this thesis, a study is carried out to obtain optimum concentrations of surfactant solutions and various structured surfaces for increasing boiling heat transfer coefficient.

1.2 Boiling Heat Transfer

Boiling is the liquid-to-vapor phase change process. Boiling happens at the solid–liquid interface when the temperature of the surface (T_s) is higher than the saturation temperature (T_{sat}) corresponding to the pressure of the liquid, and the proper form of Newton’s law of cooling is in the following expression [6]:

$$q_s'' = h(T_s - T_{sat}) = h\Delta T_e \quad (1.1)$$

ΔT_e is the excess temperature. The rapid formation of vapor bubbles at the solid–liquid interface is the main characteristic of the boiling process. The vapor bubbles begin to depart from the surface and move to the free surface of the liquid when they reach a certain size [7].

Boiling also is classified as sub-cooled boiling and saturated boiling, depending on the liquid temperature. When the temperature of the liquid is below the saturated

temperature (T_{sat}), boiling is called sub-cooled, and when the temperature of the liquid is equal to the saturated temperature (T_{sat}), boiling is called saturated [7].

In addition, it is important to recognize the difference between pool boiling and flow boiling, shown in Figure 1.1. Pool boiling occurs when the liquid is stagnant, and the heating surface is immersed in the liquid. However, in flow boiling, the fluid is forced to move in a heated pipe or over a surface by external means such as a pump. Therefore, it is also known as forced convection boiling [8].

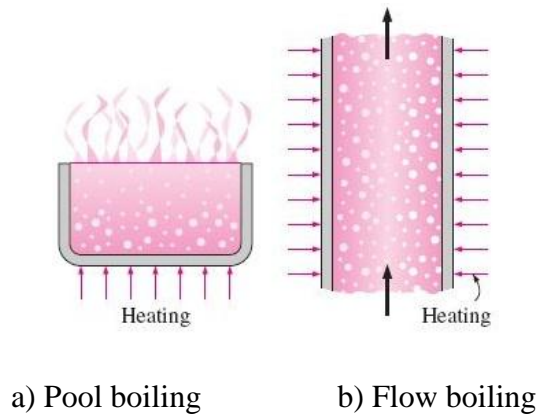


Figure 1.1: Boiling classification [9]

1.2.1 Boiling Curve

In order to understand pool boiling heat transfer, the best method refers to the pool boiling curve. The first published pool boiling curve based on experimental results was done by Nukiyama [10]. The experiments were conducted by using a metal wire submerged in water at atmospheric pressure, shown in Figure 1.2.

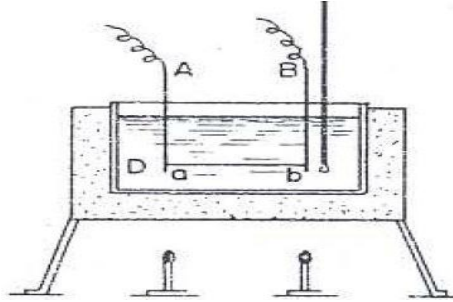


Figure 1.2: Experimental test setup by Nukiyama [10]

The pool boiling curve represents the correlation between the heat flux of heating surface and the wall superheat, which is the temperature difference between the hot surface temperature and the saturation temperature of the liquid [10].

The boiling curve for pool boiling of water at atmospheric pressure is represented in Figure 1.3. It is characterized into four different regions: the natural convection Region I, the nucleate pool boiling Region II, the transition Region III, and the film boiling Region IV [11].

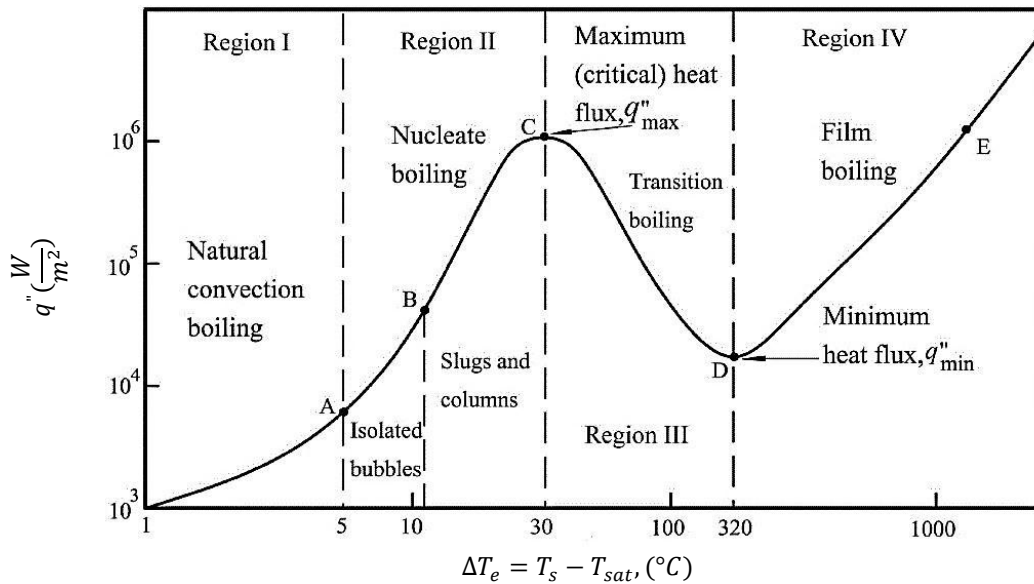


Figure 1.3: Boiling curve of water [11]

1.2.2 Nucleate Boiling

The nucleate boiling is a very effective thermal process. It is widely used in the industrial equipment because of its ability to transfer a large amount of heat with the small difference of temperatures. Therefore, a lot of research on many features of boiling heat transfer has been conducted to improve the boiling heat transfer [12]. One focus is on predicting the number of nucleation sites and heat transfer rate, which was studied first by Yamagata et al [13]. They were able to correlate the surface heat flux with the excess temperature by the following correlation [6]:

$$q_s'' \propto \Delta T_e^3 \quad (1.2)$$

In nucleate boiling regime, most of the heat exchange transfers directly to the liquid. Therefore, the nucleate boiling is considered as phase change forced convection type. The forced convection correlations are usually taken the form [6]:

$$\overline{Nu}_L = C_{fc} Re_L^{m_{fc}} Pr^{n_{fc}} \quad (1.3)$$

Where m_{fc} has an experimental value of 2/3. The Nusselt and Reynolds number identify a characteristic velocity and a length scale. Bubble diameter is the proper length scale for large heater surface. The bubble departure diameter can be calculated by the following expression [6]:

$$D_b \propto \sqrt{\frac{\sigma}{g(\rho_l - \rho_v)}} \quad (1.4)$$

The characteristic velocity can be determined by using the following correlation [6]:

$$V \propto \frac{D_b}{t_b} \propto \frac{D_b}{\left(\frac{\rho_l h_{fg} D_b^3}{q_s'' D_b^2}\right)} \propto \frac{q_s''}{\rho_l h_{fg}} \quad (1.5)$$

Substituting equations (1.4) and (1.5) in equation (1.3) gives the resulting expression for h , which can be substituted in equation (1.1) to get the following expression [6]:

$$q_s'' = \mu_l h_{fg} \left[\frac{g(\rho_l - \rho_v)}{\sigma} \right]^{1/2} \left[\frac{C_{p,l} \Delta T_e}{C_{s,f} h_{fg} Pr_l^n} \right]^3 \quad (1.6)$$

$C_{s,f}$ and n are constants. This correlation, proposed by Rohsenow, is the most well-known correlation for nucleate boiling [14]. Values of $C_{s,f}$ and n are determined experimentally for various liquid-surface combinations, given in Table 1.1. Small values of $C_{s,f}$ are desirable because that leads to increase the value of heat flux, according to equation (1.6).

Table 1.1: Values of the $C_{s,f}$ for various surface- fluid combination [6]

Fluid-Surface Combination	$C_{s,f}$	n
Water-copper		
Scored	0.0068	1.0
Polished	0.0128	1.0
Water–stainless steel		
Chemically etched	0.0133	1.0
Mechanically polished	0.0132	1.0
Ground and polished	0.0080	1.0
Water -brass	0.0060	1.0
Water-nickel	0.0060	1.0
Water-platinum	0.013	1.0

1.2.3 Critical Heat Flux for Nucleate Pool Boiling

The boiling curve of water shows an important point, which is the critical heat flux. It is desirable to operate close to critical heat flux. Therefore, many correlations have been proposed. An expression was obtained by Kutateladze [15], through dimensional

analysis, and Zuber [16], through a hydrodynamic analysis. This correlation is taken the form [6]:

$$q_{max}'' = Ch_{fg}\rho_v \left[\frac{\sigma g(\rho_l - \rho_v)}{\rho_v^2} \right] \quad (1.7)$$

Where C is the leading constant. The value of C varies from an application to another. For large horizontal cylinders, for spheres, and for many large heated surfaces, the value of C equals to 0.131. However, a value of C =0.149 is taken for large horizontal plates [6].

1.3 Surfactants

Surfactants are chemicals that have the ability to dissolve in water or other solvents. As a result, the properties of the solvent will be changed after dissolution [17]. It was found that adding a small amount of surfactants affect the surface tension of the solution. The surface tension decreases significantly with the concentration of the surfactant until reaching the critical micelle concentration (CMC). CMC is defined as the concentration of surfactants above which micelles form and all additional surfactants added to the system go to micelles, shown in Figure 1.4 [18]. After reaching the CMC, the variation in the surface tension becomes quite constant. The value of the CMC for a given medium is affected by many factors such as pressure, temperature, and on the existence and concentration of other surfactants [19].

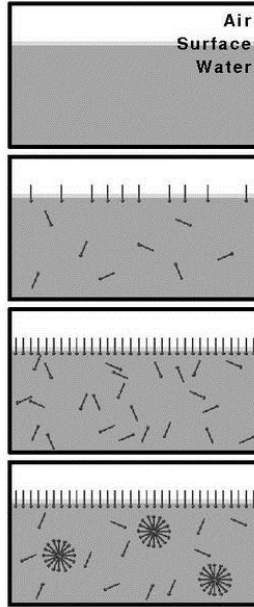


Figure 1.4: The process of CMC [20]

Surfactants also have a common molecular, which consists of two parts: nonpolar (commonly hydrocarbon, hydrophobic) chain, which is water insoluble component, and a polar (hydrophilic) portion, which is water soluble component. A chain of 8 to 18 carbon atoms can form the hydrophobic part [17].

According to polar head part, surfactants can be categorized into four common groups: nonionic surfactants, anionic surfactants, cationic surfactants, and amphoteric surfactants, shown in Figure 1.5. The molecular structure of nonionic surfactants has no charge parts of its head. However, anionic surfactant has a negative charge, while cationic surfactant has the positive charge. Amphoteric surfactant has a molecular that is able to have both a positive and a negative charge [21].

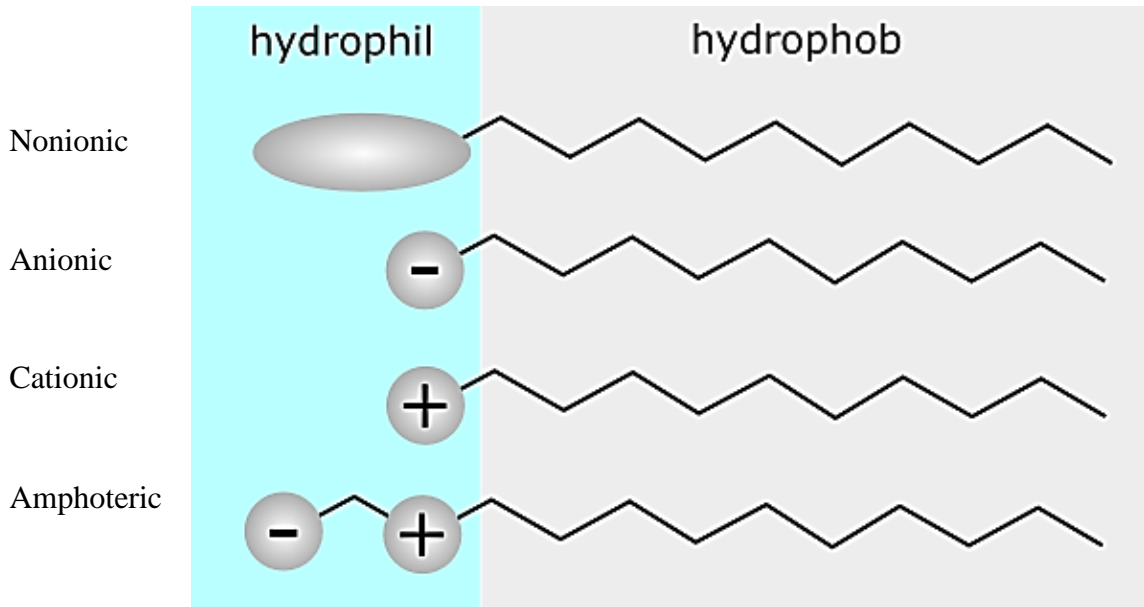


Figure 1.5: Classification of surfactants [21]

1.4 Literature Review

The literature review is divided in two parts. The first one is assigned for surfactants, while the second part is for structured surfaces.

1.4.1 Surfactants

It was found that adding small amounts of certain surfactant additives can improve the boiling heat transfer significantly. Therefore, the interest in boiling phenomena has been increased, and many studies have been conducted with different surfactants. Researchers have been addressing many factors that have an influence on the boiling phenomena. These factors include surface tension, viscosity, contact angle, bubble dynamics, bubble diameter, and bubble growth.

Surface tension has been recognized as an essential characteristic that has a big effect on the boiling heat transfer coefficient. Yang et al. [22] studied the effect of surface tension of the surfactant solution. They found that the surface tension had a significant

influence on the heat transfer. Wasekar et al. [23] proposed that the dynamic surface tension of the aqueous surfactant solution is the main parameter of the nucleate boiling process. Zhang [12] confirmed the hypothesis by measuring many interfacial properties like dynamic and equilibrium surface tensions, and wettability for different surfactant solutions. It was shown that a dynamic surface tension, which decreases to an equilibrium value after a long time duration, is the most critical factor of the phase-change phenomenon because it has a big impact on the surfactant adsorption-desorption process, which is time-dependent. Wu et al. [24] studied the effects of surfactant additives on saturated nucleate pool boiling. Their results showed that the boiling mechanisms cannot be described effectively by neither equilibrium nor dynamic surface tension. However, the authors were able to correlate the heat transfer coefficient increase and the enhancement of the vapor bubble occupied area. Hetsroni et al. [25] conducted an experimental study to investigate subcooled boiling of surfactant solutions in a pool from horizontal stainless steel tubes. Habon G was used as a surfactant. It was observed that the boiling curves of surfactant solutions were not the same of boiling curve of water. As the concentration of Gabon G increased, the heat transfer augmented significantly. Also, it was noticed that the enhancing of heat transfer could not be described by the influence of either equilibrium surface tension or the viscosity. Elghanam et al. [26] carried out an experimental study to enhance saturated nucleate pool boiling by means of surfactant additives. Sodium dodecyl sulfate (SDS) and sodium laurel ether sulfate (SLES) as anionic and Triton X-100 as nonionic were used as surfactants, and the working fluid was distilled water. The percentages of heat transfer enhancement reached to 133% for Triton X-100, 185% for SLES and 241% for SDS. They concluded the depression of surface

tension is the main reason. Nafey et al. [27] studied the effect of surfactant additives on solar water distillation process. Different concentrations of sodium lauryl sulfate (SLS) including 50, 100, 200 and 300ppm were used in this work. The results showed that the system daily productivity (DP) did not be affected when the concentration of surfactant reached more than 300ppm. On the contrary, it was observed that DP was reduced by 6% at surfactant concentration more than 400ppm. The authors attributed the increase of the DP to the depression of surface tension.

Besides surface tension effect, the viscosity could be an effective correlating factor. Hetsroni et al. [28] investigated the nucleate pool boiling of pure water and water with cationic surfactant. They found that the surface tension and the kinematic viscosity have a big impact on heat transfer coefficient. At low concentration less than 530ppm, the heat transfer coefficient increases due to the decreasing of surface tension. However, for high concentration (1060ppm), the heat transfer coefficient decreased because of the increase in kinematic viscosity.

The effect of contact angle on boiling heat transfer was studied by many researchers. Zicheng et al. [29] investigated the performance of surfactant additives (99% sodium dodecyl sulfate (SDS) and Triton X-114) in the nucleate pool boiling heat transfer. The experimental results showed that an optimum heat transfer augmentation was attained near the critical micelle concentrations (CMC) of the surfactants. The authors attributed the heat transfer increase to many characteristics like the influence of surfactant species, the decrease of surface tension, and the effect of the contact angle.

Also, efforts have been made to understand the effect of bubble diameter, and bubble dynamics on boiling performance. Levitskiy et al. [30] suggested that decreasing in bubble sizes was due to the change in the wetting angle along with a reduction in surface tension, and they attributed the variations in the interfacial characteristics to a direct result of the molecular adsorption dynamics of the additive. Kotchaphakdee et al. [31] investigated nucleate pool boiling heat transfer with dilute aqueous polymer solutions. They showed that there are significant differences in bubble size and dynamics between polymeric and non-polymeric liquids.

The literature survey shows that the pool boiling heat transfer can be enhanced by adding small amounts of surfactant additives. Researchers have found many factors that affect boiling phenomena such as viscosity, contact angle, and bubble dynamics, but the reduction of surface tension is the main reason of boiling heat transfer enhancement.

1.4.2 Structured Surfaces

Many studies have been carried out regarding pool boiling heat transfer using structured surfaces. Research has shown that structured surfaces can enhance boiling performance. Therefore, extensive research has been done to investigate the effect of nucleation site, geometry, and spacing, and other parameters on boiling heat transfer.

The creation of artificial nucleation sites was one of the initial ideas to enhance boiling heat transfer. Griffith et al. [32] were the first to study the influence of artificial nucleation sites on boiling performance. They found that the boiling enhancement can be achieved by reentrant cavity. Fujikaka [33] created the commercial boiling surface ECR-

40. This surface has orthogonally intersecting tunnels with reentrant base over tubular surface. The results showed the boiling heat transfer was enhanced significantly.

Efforts have been made to study the effect of geometry on boiling heat transfer. Das et al. [34] conducted an experimental study to investigate the performance of many enhanced surfaces in nucleate pool boiling, shown in Figure 1.6. The experimental results showed that the surfaces with inclination had better performance compared to ones normal to the surface. Also, the surfaces with orthogonal intersecting tunnels and circular base cavities gave the highest enhancement in the heat transfer rate.

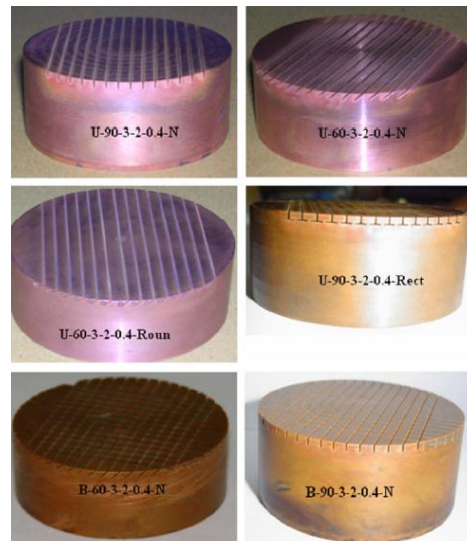


Figure 1.6: Structured surfaces by Das. et al. [34]

Cooke et al. [35] investigated the influence of open micro-channel geometry on pool boiling. They studied the performance of 10 different micro-channeled surfaces. The study showed that the surfaces with wider and deeper channels and thinner fins increased the heat transfer rate significantly. Yu et al. [36] conducted an experimental study to investigate the performance of copper rectangular fin array surfaces in pool boiling. The results showed that the surfaces with closer and higher fins increased the heat transfer

rate because these surfaces provided a bigger flow resistance for the bubble/vapor lift-off. It was observed that the surface with 0.5 mm fin spacing and a 4.0 mm fin length had the maximum value of CHF. It was $9.8 \times 10^5 \text{ Wm}^{-2}$, which was five times the value of CHF on the plain surface. Hubner et al. [37] investigated the influences of the fin geometry and surface roughness on pool boiling. Many finned tubes with different geometries of fins (trapezoid-shaped, T-shaped, or Y-shaped), shown in Figure 1.7, were examined. The experimental results showed that the finned tubes with trapezoid-shaped fins performed better than plain tube because of the surface roughness at the top fins.

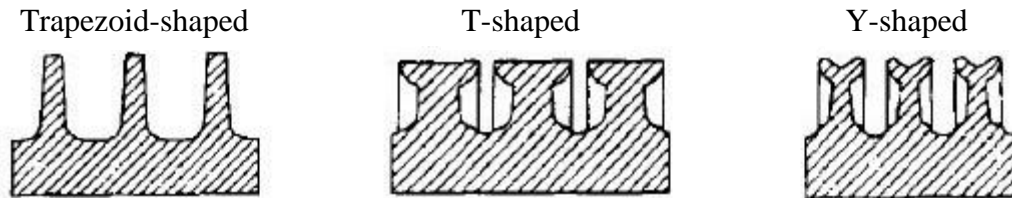


Figure 1.7: Finned tubes [37]

Also, the effect of nucleation spacing was studied. Nimkar et al. [38] boiled FC 72 on structured surfaces with micro-pyramidal shaped re-entrant cavities to investigate the effect of nucleation site spacing on the pool boiling performance. The results indicated that the cavity spacing did not have any influence on the bubble departure diameter and frequency. Also, it was observed that the cavity spacing had a big impact on the active site density. Ramaswamy et al. [39] conducted an experimental study to visualize the boiling mechanism from structured surfaces. These enhanced surfaces had different pore diameters and pitches. The experimental results showed that the pore diameter has a big effect on the bubble detachment diameter. Also, it was observed that when the wall superheat increased, the nucleation site density, the bubble frequency, and the bubble

growth rate were increased as well. In addition, the increasing in the pore pitch, and pore diameter caused reducing in bubble frequency.

The literature survey indicates that the pool boiling heat transfer can be enhanced by structured surfaces, which can be achieved by the creation of artificial nucleation sites and different geometries. Researchers have found that the structured surfaces increase the heat transfer coefficient, active nucleation sites, and bubble frequency.

1.5 Scope of the Present Work

The main goal of this research is to enhance boiling heat transfer. Therefore, surfactant additives and structured surfaces are used as two boiling enhancement techniques. Each research is done separately. Besides, there is an investigation of droplet evaporation regimes in order to compare with boiling.

1.5.1 Surfactants

The main objective of the surfactant study is to investigate the saturated nucleate pool boiling heat transfer of environmentally friendly surfactant solutions at various concentrations and different heat fluxes. The surfactants chosen for the study are sodium lauryl sulfate (SLS), ECOSURF™ EH-14, and ECOSURF™ SA-9. The aims of this investigation are summarized in the following points:

- 1- Conducting experiments to obtain boiling curves of aqueous surfactant solutions.
- 2- Comparing heat transfer coefficients of surfactant solutions with heat transfer coefficient of water.
- 3- Studying the effects of concentration, heat flux, and molecular weight on the nucleate boiling performance of water

- 4- Comparing the results of this study for water and SLS surfactant with findings of other studies and correlations.
- 5- Using a digital camera to visualize the nucleate pool boiling of aqueous surfactant solutions in order to understand boiling heat transfer phenomenon.

1.5.2 Structured Surfaces

The purpose of studying the structured surfaces is to investigate the pool boiling of different enhanced surfaces using distilled water under atmospheric pressure. These surfaces have rectangular channels, holes, and mushroom fins with different sizes. The aims of this investigation are summarized in the following points:

- 1- Conducting experiments to obtain boiling curves of enhanced surfaces.
- 2- Comparing heat transfer coefficients of water on structured surfaces with that of pure water on a plain surface.
- 3- Using a digital camera to visualize the pool boiling of water on enhanced surfaces in order to understand boiling heat transfer phenomenon.

1.5.3 Droplet Boiling Evaporation Time Observations

For this study, a droplet of distilled water at atmospheric pressure on a plate was used, and the plate was heated to a temperature more than the boiling point of water. The objectives are listed below:

- 1- Investigating the different regimes of pool boiling with droplet dropping tests.
- 2- The total evaporation time of a droplet of sub-cooled water was measured.

2 Experimental Test Setup

In this chapter, the experimental test setup for each project is explained in detail. This chapter contains three parts. For the first part, nucleate pool boiling experiments of three surfactant solutions were carried out at atmospheric pressure to study the influence of surfactant additives on boiling heat transfer performance. Many parameters were studied like the effects of surfactant concentration, ionic nature, and molecular weight. Boiling curves for many surfactant concentrations were presented. The surfactants used in this study were SLS, ECOSURFTM EH-14, and ECOSURFTM SA-9. Wide range of surfactant concentrations was investigated at different heat fluxes. The second part of this chapter deals with an experimental investigation of pool boiling using enhanced surfaces under atmospheric pressure. The goal of the experiments is to investigate the influence of structured surfaces on pool boiling heat transfer. The last part explains the experimental setup to investigate the different regimes of pool boiling (natural convection boiling, nucleate boiling, transition boiling, and film boiling) with droplet dropping tests. The total evaporation time of a droplet of sub-cooled water was measured. Therefore, a droplet of distilled water at atmospheric pressure on a plate was used, and the plate was heated to a temperature more than the boiling point of water.

2.1 Surfactants

The experimental setup is simple and designed to provide controlled, repeatable boiling conditions for surfactant solutions. A photograph of the experimental setup is shown in Figure 2.1, while Figure 2.2 displays the schematic diagram of the experimental apparatus.



Figure 2.1: Experimental test setup

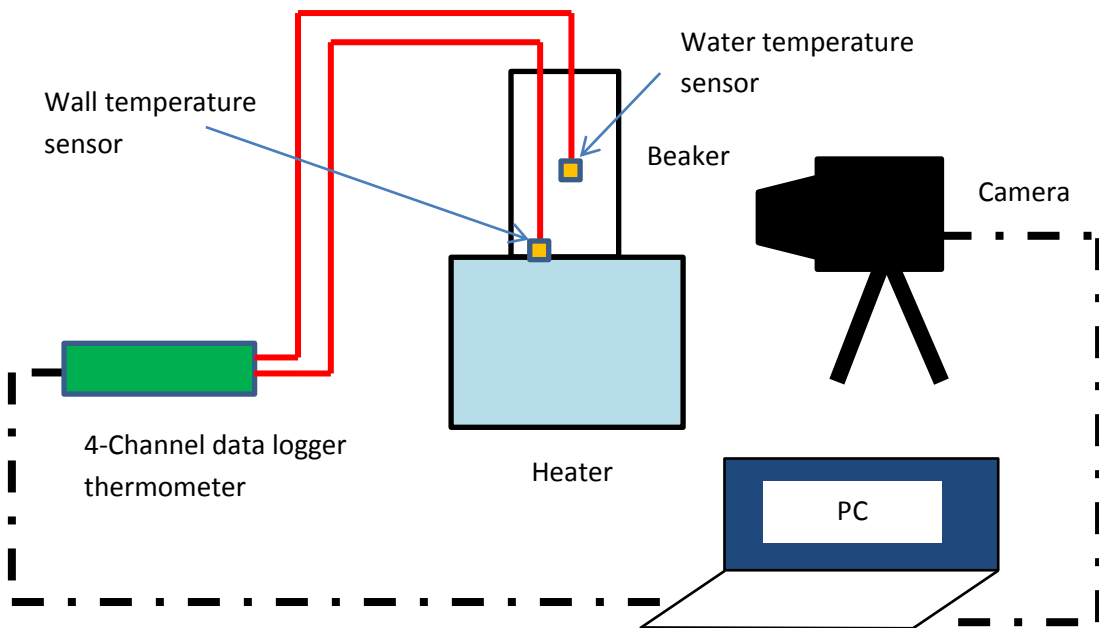


Figure 2.2: Schematic of experimental setup

2.1.1 Main Components

The experimental apparatus primarily consists of the following main components: beaker, heater, thermometer, thermocouples, image acquisition, and scales.

2.1.1.1 Beaker

United beaker shown in Figure 2.3 is used as a pool for conducting the experiments. The beaker has white printed graduations that enable calculating the amount of evaporated water easily. In addition, it allows boiling in a clear view for the camera and allows quick water changes to evaluate surfactant solutions. The beaker has 0.102 m diameter and is made from low expansion borosilicate glass, which is able to resist to high temperature up to 500 °C [40].



Figure 2.3: Beaker

2.1.1.2 Heater and Stirrer

This device, which is shown in Figure 2.4, can function as a heater and a stirrer at the same time. The work surface is white and made from ceramic, which makes it durable and chemical resistant. The power supply for the heater is varied by manual control. Therefore, the temperature and speed can be adjusted and maintained easily and precisely to the desired value [41].



Figure 2.4: Heater

2.1.1.3 Thermocouples

Type K thermocouple shown in Figure 2.5 is used to measure the base and water temperatures. This thermocouple is manufactured with ultra-slim silicone rubber, which provides high flexibility, and it is capable to resist a variety of chemicals and oils. Also, it has a self-adhesive foil backing for faster response time. The range of temperature measured by this thermocouple is between -50 to 200 °C (-58 to 392 °F) [42].



Figure 2.5: Thermocouple type K

2.1.1.4 4-Channel Data Logger Thermometer

The portable RDXL4SD model of thermometer shown in Figure 2.6 is used. This data logger can function without being connected to a computer. It has an internal battery, backlight display and built-in analysis functions. Also, the device has four channels for temperature measuring data, real-time SD memory card, and real time data recorder. Therefore, the data logger is able to collect temperature data of four channels with the time information (year, month, date, minute, second) and saves them in an Excel file, which can be moved to a computer for analysis [43].

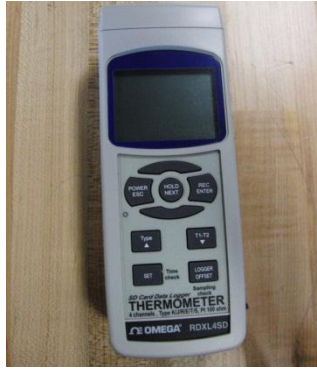


Figure 2.6: 4-Channel data logger thermometer

2.1.1.5 IR Camera

The type of IR camera used is FLIR E40, shown in Figure 2.7. This model is compact and weighs only 880 g (battery included). It has 160 x 120 pixel resolution of infrared images. It is also able to measure temperature range from -20 °C to +650 °C. Its accuracy is high with $\pm 2\%$ reading [44].



Figure 2.7: IR camera [44]

2.1.1.6 Digital Camera

Image acquisition is employed to observe and report the mechanisms of pool boiling heat transfer of surfactant solutions. A camera type CASIO, shown in Figure 2.8, was used to record pool boiling phenomena and bubble dynamics. The camera can record up

to 1000 frames per second of video and shoot continuous high-resolution images at speed 40 images per second [45].



Figure 2.8: CASIO camera

2.1.1.7 Scales

Two types of scales are used. The first one, shown in Figure 2.9a, is Cuisinart DigiPad Digital Scale, which is used to measure the mass of water (400 gram). Its capacity is 11 lbs. The second one shown in Figure 2.9b is a precision scale type of GF-300 used to measure the amount of surfactants that adds to water. This type is capable to measure 0.001 g as minimum and 310 g as maximum.



a) Cuisinart Scale



b) GF-300 precision Scale

Figure 2.9: Scales

2.1.2 Experimental Procedure

Before the experiment, the beaker was rinsed by liquid soap, water, and sponge to ensure a clean pool and was placed above the heater, which was thoroughly cleaned.

After that, the pool chamber was filled with a measured quantity of water (400 grams) to bring the surface to a level 51–52 mm above the heater. Water was selected as a working fluid because it is used in many applications and has negligible environmental effects compared to other refrigerants. After that, the amount of surfactant was measured by using the precision scale depending on concentration, which has parts per million (ppm) unit. Parts per million unit is the mass ratio between the surfactant and the solution, and ppm is defined as [46]:

$$ppm = 1,000,000 m_c / m_s \quad (2.1)$$

Where

$m_c = \text{mass of surfactant (kg)}$

$m_s = \text{mass of solution (kg)}$

Then, the measured sample of surfactant was added and mixed with water for one minute by the stirrer unit in the heater. The stirrer can be adjusted manually for desired speed, which was dial 8. The stirring process creates a vortex as shown in Figure 2.10:

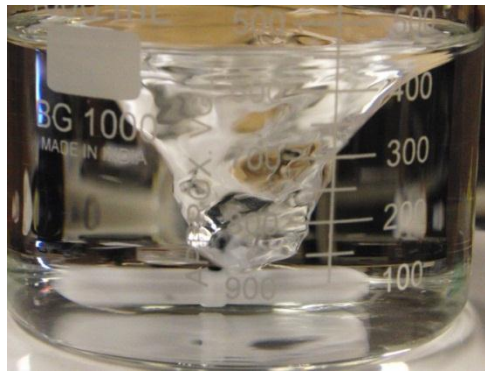


Figure 2.10: Stirring process

To measure wall temperature and bulk water temperature, 4-channel data logger thermometer as a reader and two calibrated K type thermocouples, shown in Appendix A, were used. One temperature sensor was placed on the base of the beaker to measure the

wall temperature. The other temperature sensor was positioned at a level almost 30 mm above the surface of the beaker to measure the bulk water temperature. Then, the heater was turned on and adjusted to desired heat flux. Therefore, the water boiled enough with the purpose of decreasing the influence of any dissolved gasses within the fluid. The boiling process lasts for approximately half an hour. For each value of heat flux, the collected data included the wall temperature, bulk water temperature, and time to reach boiling point for all tests. Also, the digital camera was used to record and capture images of the boiling process (bubble nucleation, growth, and departure). Then, the heat flux was changed, and the same procedure was repeated after test setup was cooled to room temperature. Tap water is used in the tests because boiling temperature, base temperature, and time until reaching the boiling point did not change significantly compared to distilled water. Distilled water comes from recondensed steam because the water has been boiled to purify it. Tap water does not go through that purification process and can contain trace amounts of fluoride, microorganisms, or nitrates [47].

2.1.2.1 Calculation of the Heat Flux

The heat generated from the heater can be measured by using wattmeter [48].

$$Power (W) = I (Amperes) \cdot V (Volts) \quad (2.2)$$

However, at steady state, the heat from the heater is not transferred totally to the test fluid. There are losses due to natural convection from the pool chamber (beaker). Then, the total power can be expressed in the following equation [48]:

$$Power (W) = \dot{q}_{losses}(W) + \dot{q}_{liquid}(W) \quad (2.3)$$

The net heat transfer rate becomes:

$$\dot{q}_{liquid} = power - heat\ transfer\ rate\ of\ losses = \quad (2.4)$$

To determine \dot{q}_{liquid} term, following assumptions are made [6]:

- 1- Steady state condition.
- 2- The surface of the water is exposed to atmospheric pressure.
- 3- Water is at a uniform temperature. T_{sat} equals to 100 °C.

The \dot{q}_{liquid} term, the heat transfer delivered to the water, can be calculated in two methods. First method is by using Fourier's law, given by equation (2.5). Some assumptions have been taken also such as assuming one-dimensional, steady heat conduction from the heater to the water [6].

$$q'' = K \frac{\Delta T}{L} \quad (2.5)$$

Where

$$q'' = heat\ flux \left(\frac{W}{m^2} \right)$$

$$\Delta T = temperature\ difference \ (^\circ C)$$

$$L = thickness\ of\ base\ beaker = 0.003\ m$$

$$K = thermal\ conductivity\ for\ borocilicate\ glass = 1.14 \left(\frac{W}{m \cdot ^\circ C} \right) [49]$$

With the temperature difference between the surface temperature of the heater and the base temperature of the beaker, the heat flux delivered to the water was calculated. The wall temperature was measured by K type thermocouple, while IR camera was used to measure the surface temperature of heater as shown in Figure 2.11. By taking the average of last four readings, the surface temperature of heater was evaluated. The results of heat flux are shown in Table 2.1.

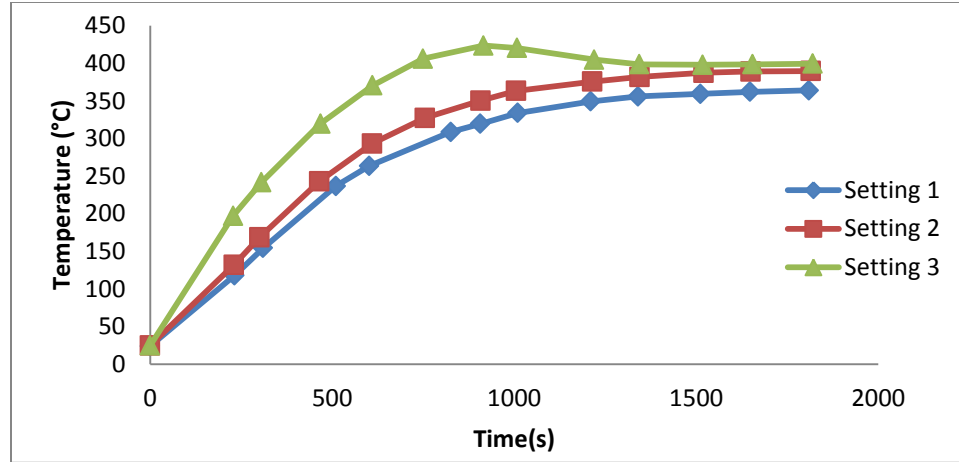


Figure 2.11: Temperature profiles of different heater settings

Second method suggests that when the steady state condition occurs, all the heat added to the water is used to form vapor, and \dot{q}_{liquid} term is calculated by the following equation [6]:

$$\dot{q}_{liquid} = \dot{m}_b h_{fg} \quad (2.6)$$

The evaporation rate for different heater settings was measured by following the below procedure:

- 1- The mass of dry beaker was measured.
- 2- A mass of 400 grams of water was added. So, the total mass is 712 grams.
- 3- The beaker was placed on the heater, and one sensor was used to measure the water temperature. (Note after 30 minutes all tests reaches steady state)
- 4- After each 10 minutes, the mass of beaker was measured. Then, the evaporation rate of boiling was calculated by the equation (2.7).

$$\dot{m}_b = \frac{\Delta m}{\Delta t} = \frac{\Delta m (gram) \times 10^{-3} \left(\frac{kg}{gram}\right)}{10 (minute) * 60 \left(\frac{s}{minute}\right)} \quad (2.7)$$

Table 2.1 shows the results of heat flux values by different methods. It should be noted that the values of heat flux of the second method were used for this investigation because the values of heat flux calculated by Fourier's law are not reasonable as it can be seen from the table, compared with the heater capacity at each setting. Another reason of such high values of heat flux by Fourier's law was the surface temperature of heater was measured without any boiling vessel on it, which led to high surface temperatures of the heater.

Table 2.1: Calculation of heat flux

Heater settings	Capacity of heater (W)	q'' (W/m ²) by Fourier's law	\dot{q} (W) by Fourier's law	q'' (W/m ²) by using the evaporation rate method	\dot{q} (W) by using the evaporation rate method
Setting 1	423	94787.2	774.41	16572.67	135.42
Setting 2	495	102626.6	838.49	25135.22	205.38
Setting 3	785	106179.6	867.48	30383.23	248.27

So that the heat transfer coefficient is given by using Newton's law of cooling [6]:

$$h = \frac{q''}{T_s - T_{sat}} \quad (2.8)$$

2.1.3 Pool Boiling in Aqueous Surfactant Solutions

Two types of surfactants (anionic surfactant (SLS) and nonionic surfactants (ECOSURFTM EH-14 and ECOSURFTM SA-9)) shown in Figure 2.12 are tested for various concentrations. The aqueous solutions of surfactants are prepared by dissolving the measured samples of surfactants in water. The concentrations of each surfactant that used in this study were;

1). Anionic surfactant:

SLS: (50, 100, 200, 300, 400, 500ppm).

2). Nonionic surfactants:

ECOSURF™ EH-14: (200, 400, 800, 1600, 3200ppm).

ECOSURF™ SA-9: (200, 300, 400, 500, 600ppm).



SLS

EH-14

SA-9

Figure 2.12: Surfactants used in the present investigation

2.1.3.1 Sodium Lauryl Sulfate (SLS)

Sodium lauryl sulfate (SLS) is an anionic surfactant. Its structure is displayed in Figure 2.13. It has a lipophilic end, which is saturated 12-carbon chain, and hydrophilic end, which is negatively charged sulfate group. This charged end of the molecule of SLS has an attraction for water. Therefore, it has been used as a foaming and cleaning agent in detergent, wetting agent in textiles, cosmetic emulsifier, and sometimes in toothpastes [50].

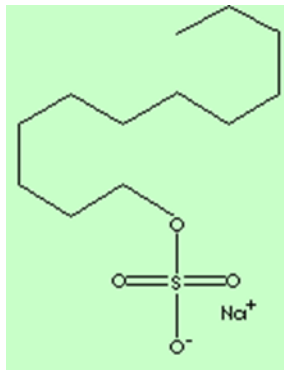


Figure 2.13: Chemical structure of sodium lauryl sulfate [50]

2.1.3.2 ECOSURF™ EH-14

ECOSURF™ EH-14 is a nonionic surfactant. It has many applications such as hard surface cleaners, metal cleaners, high performance cleaners, industrial processing/manufacturing, and agricultural formulations. It is composed of 90 percent of 2-Ethyl Hexanol EO-PO nonionic surfactant and 10 percent water. It has many favorable properties. For example, it is biodegradable component. In addition, it is soluble in water, chemically stable in the existence of acids, bases and salts, and compatible with anionic, cationic, and other nonionic surfactants [51].

2.1.3.3 ECOSURF™ SA-9

ECOSURF™ SA-9, known as a seed oil surfactant, is also a biodegradable nonionic surfactant that composed of alcohols, C6-C12, ethoxylated, and propoxylated. This type of surfactant provides considerable benefits in handling, processing and formation. It is used in hard surface cleaners, prewash spotters, and paints and coatings [52].

Table 2.2: Physico- chemical properties of surfactants

Properties	SLS	ECOSURF™ EH-14	ECOSURF™ SA-9
Surfactant type	anionic	nonionic	nonionic
Molecular weight	288.38	1036	668
Formula	CH ₃ (CH ₂) ₁₁ OSO ₃ Na	-	-
Surface Tension (mN/m)	38.0	31.8	29
Appearance	White powder	Liquid	Pale yellow liquid
Viscosity at 40°C (104°F), cSt	-	85.39	30.225

Density g/cm ³ at 20 °C	1.05	1.0538	0.9831
------------------------------------	------	--------	--------

2.2 Structured Surfaces

An experimental investigation of pool boiling using enhanced surfaces was conducted. The experiments were carried out under atmospheric pressure, and the working fluid was distilled water. The aim of the experiments is to study the effect of enhanced surfaces on pool boiling heat transfer.

2.2.1 Production of Structured Surfaces

The manufactured enhanced surfaces are shown in Figure 2.14. The surfaces can be as the base of the boiling vessel and the studied enhanced surfaces at the same time. Plain and seven structures have been machined of aluminum to dimensions of 4.75 inch length, 3.5 inch width, and 0.25 inch thickness, shown in Figure 2.14a. The goal is to study the effect of the geometry characteristics on boiling phenomenon. Therefore, surfaces with rectangular channels, holes, and mushroom fins are fabricated. Also, these surfaces are varied by changing the fin length and fin spacing. Table 2.3 shows the details of the surfaces used in this investigation. The exposed area of the enhanced surface is not the same as that of the plain surface. Therefore, the increase in the surface area is taken to consideration. The area augmentation ratio is calculated for all surfaces by the following equation [34]:

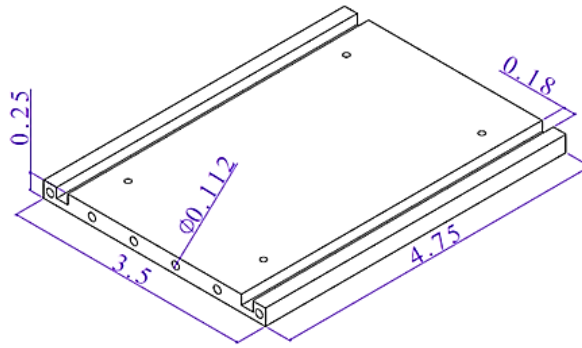
$$A_r = \frac{A_{augmented}}{A_{plain}} \quad (2.9)$$

Where:

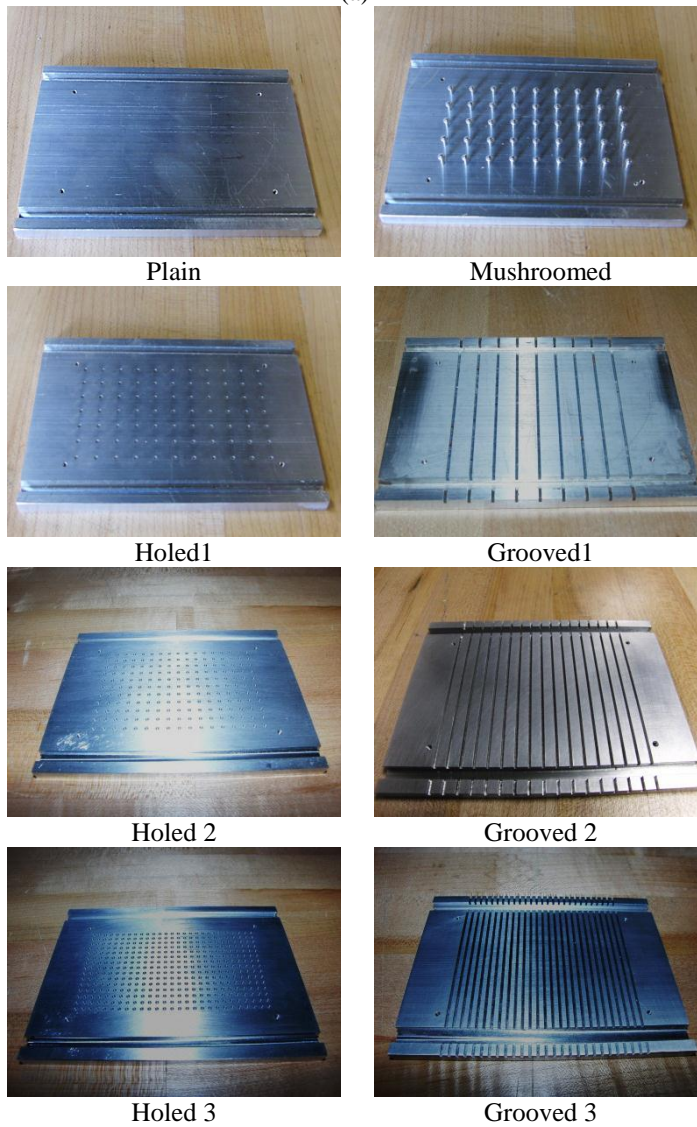
A_r is the area augmentation ratio

$A_{augmented}$ is the area of augmented surface

A_{plain} is the area of plain surface



(a)



(b)

Figure 2.14:(a):Dimensions of surface in inches (b): Pictorial view of structured surfaces

Table 2.3: Characteristics of enhanced surfaces

Surfaces	# of channels/ holes/ mushroom fins	Diameter of the hole (in)/width of channel	Spacing (in)	Depth (in)/Height (in)	Area augmentation ratio(A_r)
Plain	---	---	---	---	--
Mushroomed	45 mushroom fins	0.0625	0.3175	0.125	1.23
Holed 1	77 holes	0.0625	0.25	0.125	1.14
Holed 2	187 holes	0.0625	0.125	0.125	1.35
Holed 3	405 holes	0.0625	0.0625	0.125	1.76
Grooved 1	9 channels	0.04	0.3	0.08	1.30
Grooved 2	17 channels	0.04	0.16	0.08	1.57
Grooved 3	27 channels	0.04	0.08	0.08	1.90

Also, for better comparison and understanding the heat transfer enhancement, an effort has been made to use dimensionless parameter, β [38]. This parameter correlates the spacing to the depth for holed and grooved surfaces or the spacing to the height for mushroomed surface as shown in Figure 2.15.

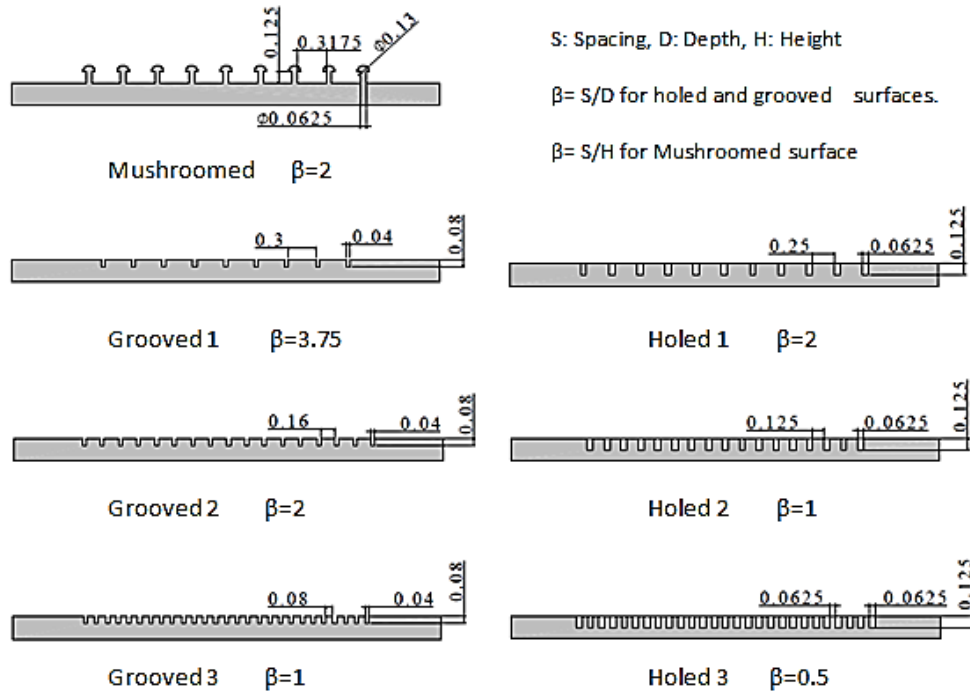


Figure 2.15: Cross section of structured surfaces (dimensions in inches)

2.2.2 Experimental Setup

The experimental set-up, shown in Figure 2.16, consists of an electric heater, a boiling vessel, IR camera, sensor and thermometer, and high speed camera. Most of the equipment is explained in details in part I of this chapter except the boiling vessel.

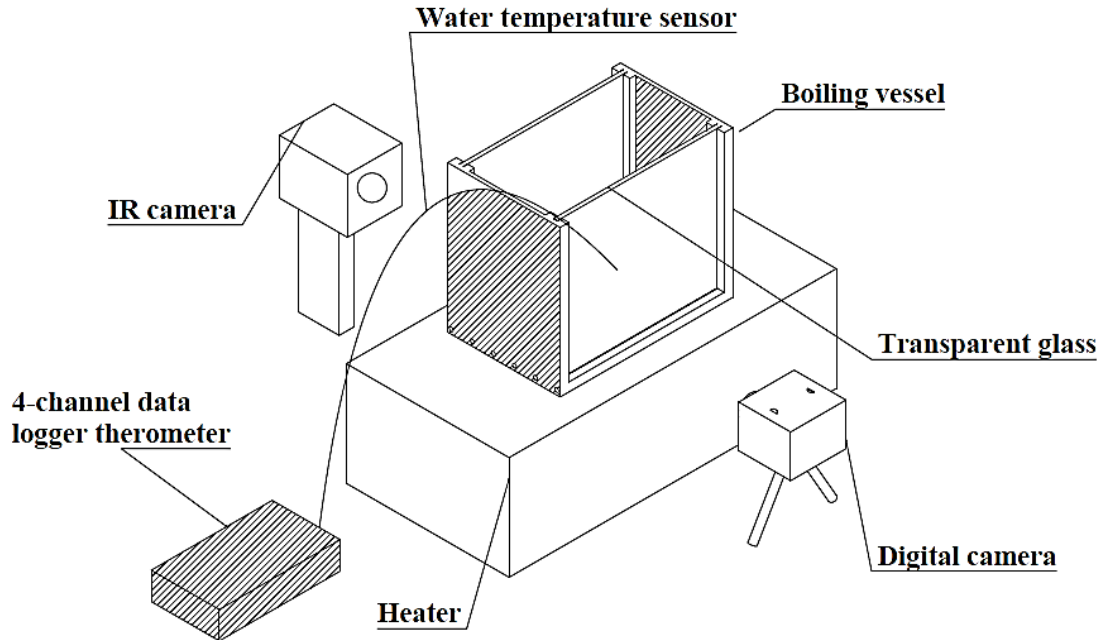


Figure 2.16: Experimental setup

The boiling vessel is made of three pieces of aluminum and two pieces of borosilicate transparent glass. The reasons for choosing borosilicate glass are its low thermal expansion and its ability to resist to high temperature (450 °C) for long time [53]. Three pieces of aluminum are two for the sides, and the other is for the base that functions as the tested surface. These pieces are connected by 12 screws and sealed by silicone to prevent leakage. The dimensions of the box were 5.25 inch length, 3.5 inch width, and 4.5 inch height as shown in Figure 2.17 .

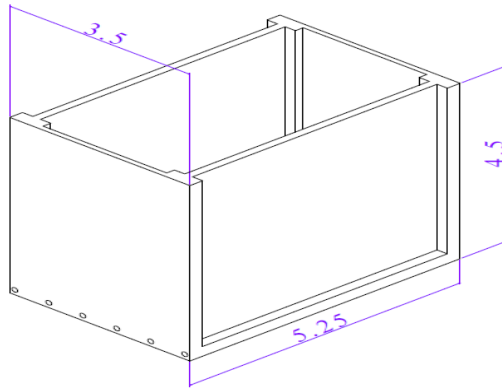


Figure 2.17: Boiling vessel with dimensions in inches

2.2.3 Test Procedure

The first step of preparation was to assemble the box with the desired surface as explained above. The boiling vessel was rinsed by liquid soap, water, and sponge to ensure a clean pool and was mounted above the heater. After that, the pool chamber was filled with a measured quantity of distilled water (400 grams). The reason of using distilled water was to reduce the negative effects of corrosion on boiling vessel. At the same time, Type-K thermocouple was attached to measure the water temperature. Then, the heater was turned on and adjusted to the desired heat flux, and the water was left to boiling. When the water reached boiling temperature, IR camera was used to measure the base temperature, which was evaluated by taking many pictures. The IR camera was put in front of the boiling vessel for each test. Three different pictures were taken at different times. It was found the water reaches boiling point before 20 min. Therefore, the pictures were taken at 20 min, 25 min, and 30 min. After that, the pictures were edited by using FLIR TOOLS software. Each picture has five values of base temperature. Then, the base temperature is evaluated by taking the average of 15 values for each test. Figure 2.18

shows a comparison is made for base temperature measurements between the plain and holed surface at heat flux 35.08 kW/m^2 .

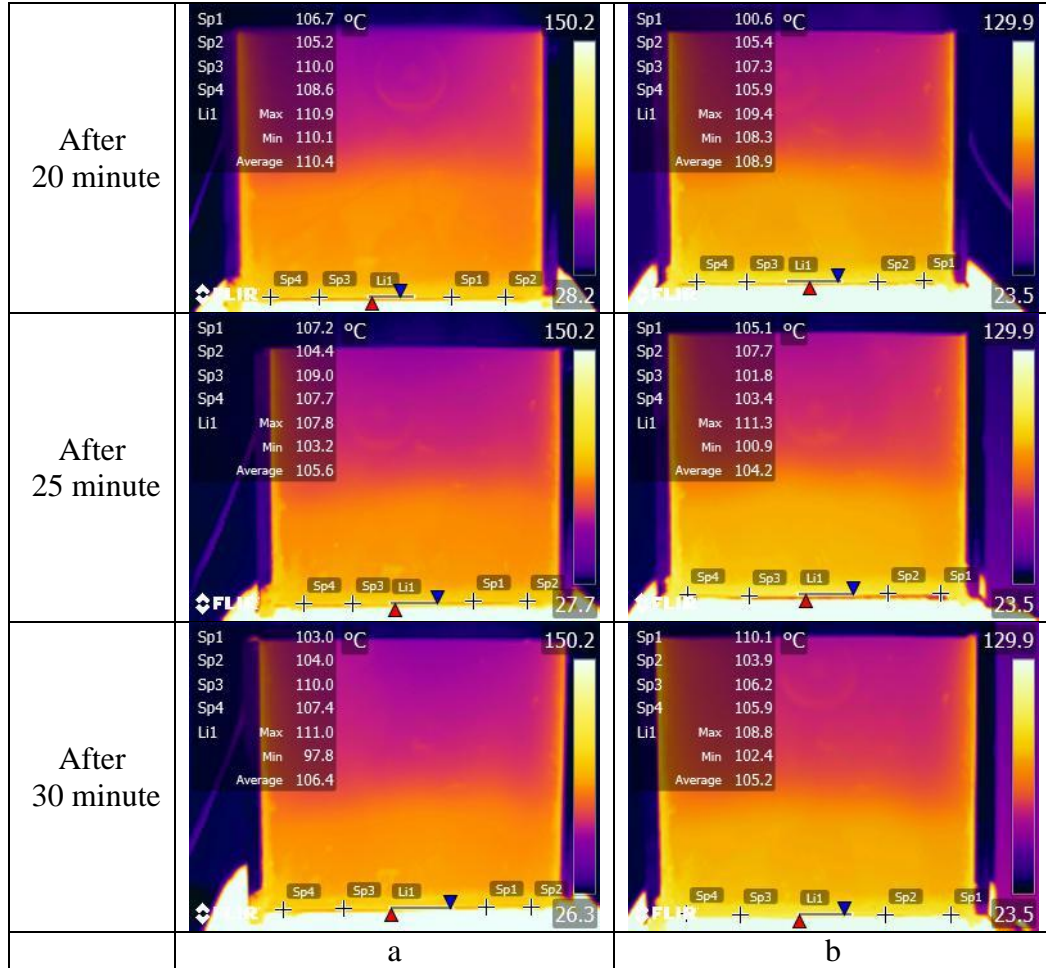


Figure 2.18: Wall temperature measurements using IR camera (a) plain ($T_s = 107.04 \text{ }^\circ\text{C}$) (b) Holed 1 ($T_s = 105.44 \text{ }^\circ\text{C}$) at heat flux 35.08 kW/m^2

Also, the high speed camera was implemented to record and capture images of the boiling process (bubble nucleation, growth, and departure) for improved observation of bubble interaction between nucleation sites. Then, the heat flux was changed, and the same procedure was repeated after test setup was cooled for each surface. To ensure consistency and accuracy of results, the experiments were run two times for each test.

Repeatability studies have confirmed that heat transfer performance from test to test does not change considerably.

To determine the values of heat fluxes that the heater supplied, same procedure in part I in this thesis was followed for the plain surface. The heat flux was calculated by the second method, Appendix D. The results of heat flux are shown in Table 2.4 .

Table 2.4: The values of heat flux for boiling with structured surfaces

Heater settings	\dot{m}_b (kg/s)	q (W)	q'' (kW/m ²)
Setting 1	0.0001039	234.47	27.91
Setting 2	0.0001306	294.66	35.08

2.3 Droplet Boiling Evaporation Time Observations

The experimental setup, shown in Figure 2.19 , is quite simple. It consists of an electric heater, a droplet dropping plate, a liquid dropper, a digital camera, and a gun thermometer. The droplet dropping plate is made of two pieces of aluminum that are assembled together by four screws, shown in Figure 2.20. The lower part has the dimensions of 3 inch in diameter and 0.44 inch thick. The other piece is like a clamp (3 inch in outer diameter, 2.52 inch in inner diameter, and 0.11 inch thick) that acts as a seat for placed droplets of liquid. Gun thermometer type DT8280 is used to measure the temperature of the heated plate, while a digital camera is employed to record boiling phenomena. To measure the total time that the water droplet takes to evaporate, video recording is applied. The mass of the single water droplet is measured using the Escali L-600 digital scale.



Gun thermometer



Heater



Liquid dropper

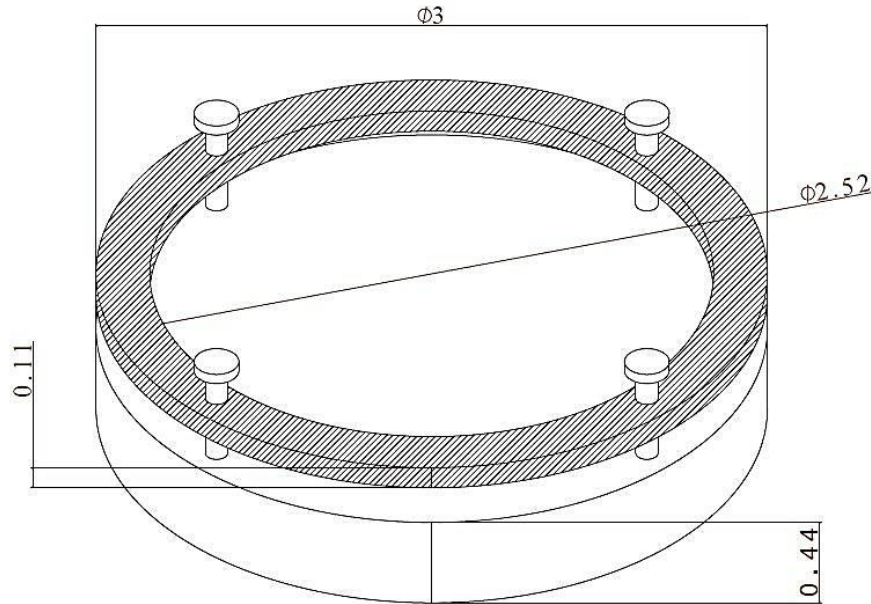


Escali L-600 digital scale

Figure 2.19: Experimental setup



(a) Pictorial view



(b) Schematic view (dimensions in inches)

Figure 2.20: Droplet dropping plate

2.3.1 Experimental Procedure

To prepare the experiments, the plate was cleaned thoroughly and placed above the heater. Then, the heater was turned on and adjusted to desired temperature. When the temperature, measured by the gun thermometer, reached a certain value, the droplet of distilled water was deposited on the heated plate using the liquid dropper. At the same time, the camera was implemented to record the process. This procedure was repeated several times to cover all the regimes of pool boiling.

The results were carefully evaluated, and the characteristics of four zones of pool boiling (natural convection boiling, nucleate boiling, transition boiling, and film boiling) were revealed. The findings showed that the boiling process of water droplet was entirely different from one regime to another. Also, the time of evaporation was evaluated and found to be varied with the excess temperature from one regime to another.

3 Experimental Results and Discussion

This chapter contains the experimental results and discussion of the three projects. Therefore, it is divided into three parts. The first part discusses the experimental results of surfactant, while the experimental results of structured surfaces are discussed in the second part. Final part contains the experimental results of droplet experiments.

3.1 Surfactants

Experiments are carried out to investigate the nucleate pool boiling heat transfer of aqueous solutions of three different surfactants, SLS, EH-14, and SA-9. Many boiling characteristics like bubble behavior and heat transfer enhancement mechanisms are studied for a wide range of surfactant concentrations. Also, time to reach boiling point is evaluated to find out which surfactant concentrations boil faster than the water. The results of solutions of various concentrations are presented, and the optimum enhancement in heat transfer is identified.

3.1.1 Boiling Curve of Water

The experimental data of the nucleate boiling of water are obtained and compared with other experimental data and correlations available in the literature review.

Figure 3.1 shows a comparison between the experimental data of water of this study with results reported by Elghnam et al. [26], who performed the experiments on horizontal stainless steel tubes. Although there is a big difference in the experimental setup between the present study and Elghnam et al's study, it is found there is a fair agreement. Therefore, the experimental data can be an accurate baseline reference for the nucleate boiling performance of the surfactant solutions.

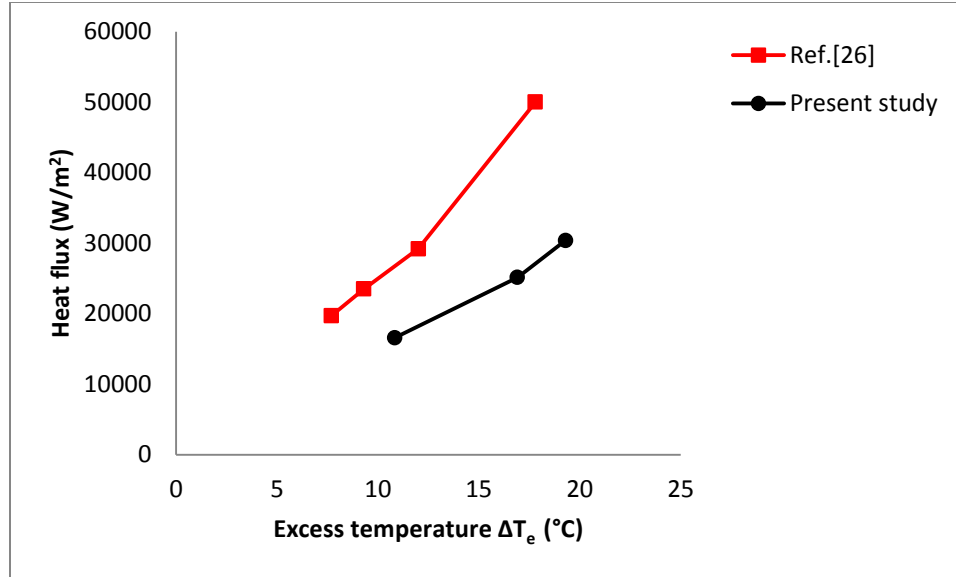


Figure 3.1: Comparison boiling curve of water with Ref. [26]

Also, a comparison is made with the Rohensow correlation. Rohensow correlation is chosen because it is a well-known expression, which is given by equation (1.6). This correlation is used to calculate the heat flux.

The properties of saturated water at 100 °C are provided in Table 3.1:

Table 3.1: Properties of saturated water at 100 °C [6]

$\rho_l = 957.9 \text{ kg/m}^3$	$C_{p,l} = 4.217 \text{ KJ/kg.K}$
$\mu_l = 279 \times 10^{-6} \text{ kg/m.s}$	$Pr_l = 1.76$
$h_{fg} = 2257 \times 10^3 \text{ J/kg}$	$\sigma = 58.9 \times 10^{-3} \text{ N/m}$
$\rho_v = 0.5956 \text{ kg/m}^3$	

Also, the value of n is approximately 1.0 for water, but the value of $C_{s,f}$ for combination of water- borosilicate glass is unknown. This value varies from 0.006 to 0.013 for different fluid- surface combinations (Table 1.1). Therefore, it will be taken as approximation ($C_{s,f}$ as 0.013). By substituting the numerical values, the heat flux is

calculated theoretically, while the experimental values of heat flux were calculated in section 2.1.2.1 in this thesis.

Table3.2 shows that the experimental data of this study do not agree well with Rohsenow correlation because of different test setups. It is found that there is a big difference in values of heat fluxes. The discrepancy between the present study and Rohensow correlation is related to many factors such as different experimental setup and experimental errors.

Table3.2: Comparison of heat flux rate for theoretical and experimental methods

T_s (°C)	Rohsenow correlation	Experimental
	$q_{s,theo}'' \left(\frac{kW}{m^2} \right)$	$q_{s,exp}'' \left(\frac{kW}{m^2} \right)$
110.84	174.41	16.57
116.91	662.08	25.13
119.3	984.36	30.38

3.1.2 Experimental Results and Discussion

The experimental data for nucleate pool boiling of various concentrations of aqueous anionic (SLS) and nonionic (EH-14 and SA-9) surfactant solutions are shown in Figure 3.2, Figure 3.3, and Figure 3.4, respectively. The heat flux, q'' , is graphed against the wall superheat $T_s - T_{sat}$.

Generally, the addition of small amounts of surfactant to water causes the nucleate boiling curve to shift to the left. The wall temperature of the beaker drops greatly with an increase in the concentration of aqueous surfactant solutions. It is found that the maximum reduction in wall temperature for each surfactant was 5.76% for 300ppm SLS, 2.97% for 1600ppm EH-14, and 2.61% for 200ppm SA-9, compared with water.

For SLS surfactant, it can be seen from Figure 3.2 that adding a small amount of SLS has a big effect on the boiling curve, which is evident with 50ppm concentration. With further increase of concentration, the boiling curve continues shifting to the left until reaching certain concentration (300ppm). Then, more adding of SLS makes the boiling curve shifts towards the right. Therefore, it is obvious that the effect of the surfactant on the boiling curve performance has an optimum value of 300ppm, depending on the concentration. However, the effect of EH-14 surfactant on pool boiling is less than that of SLS as it is shown in Figure 3.3 . At low concentrations, the boiling curve shifts slightly to the left, especially at low heat flux, reaches a maximum, and after that it shifts toward right with further increase in concentration. Compared with SLS and EH-14 surfactants, it seems that the SA-9 surfactant has the lowest influence on the excess temperature. The optimum boiling curve behavior is achieved at a concentration of 200ppm for SA-9.

The reducing in wall temperature indicates the enhancement in heat transfer. According to many researchers [25, 54, 55], this behavior is attributed to the role of surface tension and mechanisms of bubble dynamics.

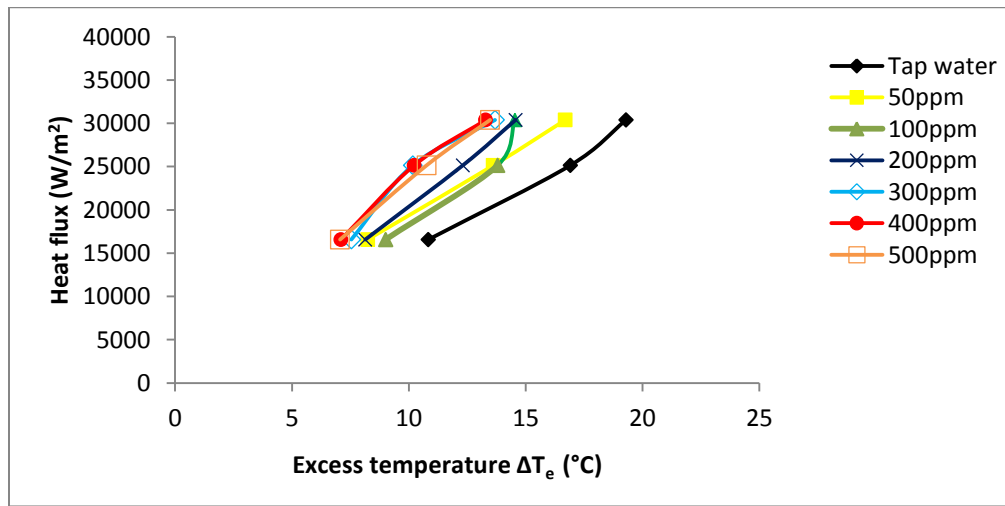


Figure 3.2: Pool boiling data of aqueous solutions of SLS

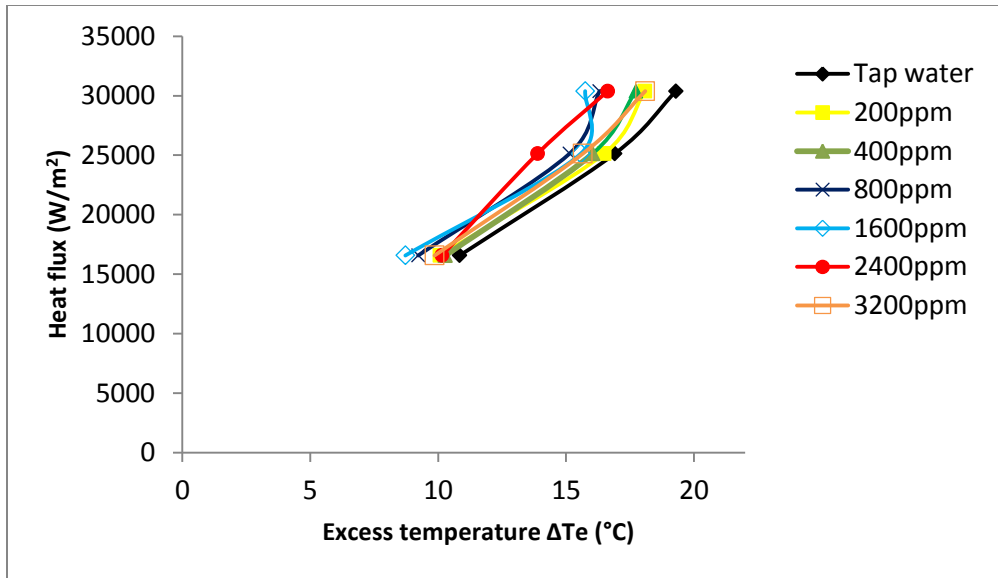


Figure 3.3: Pool boiling data of aqueous solutions of EH-14

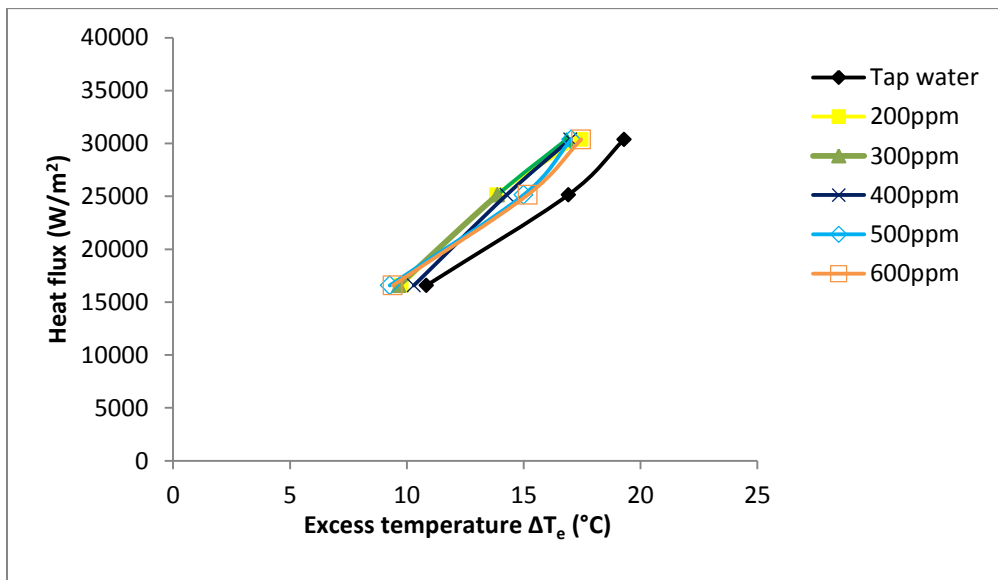


Figure 3.4: Pool boiling data of aqueous solutions of SA-9

3.1.2.1 Discussion on Heat Transfer Coefficient (h) Enhancement

The influence of heat flux, and surfactant concentration on the nucleate boiling heat transfer coefficient of surfactant solutions are shown in Figure 3.5, Figure 3.6, and Figure 3.7. For a given heat flux, the increase in concentration of aqueous solutions leads to considerable enhancement in heat transfer coefficient. Also, for a given concentration,

it is observed that the boiling heat transfer coefficients for almost surfactant solutions are increased slightly as the heat flux is increased. The observed enhancement in (h) is attributed to the role of dynamic surface tension, and bubble dynamics like the nucleation and growth of a vapor bubble. It was found that adding a small amount of surfactants reduces the dynamic surface tension of the solution. Therefore, departure of smaller-sized bubbles will be allowed because of lower values of dynamic surface tension that counters the buoyancy force trying to pull the bubble away from the base of the beaker. This helps to increase the number of active nucleation sites and reduce subsequently the bubble growth time, which leads to an increase in bubble departure frequency [26]. However, at higher surfactant concentration, the solution viscosity is increased, and this may lead to the reduction in heat transfer. There is not surfactant viscosity data available in the other studies, but negligible influence of viscosity can be assumed on boiling heat transfer at low concentrations of surfactant [28].

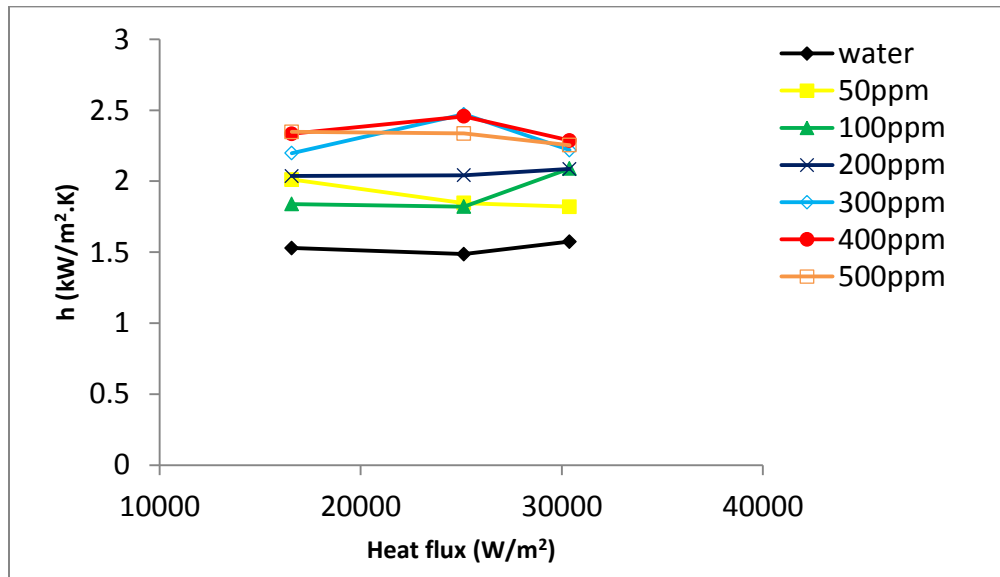


Figure 3.5: Nucleate boiling heat transfer coefficient as a function of heat flux for aqueous solutions of SLS.

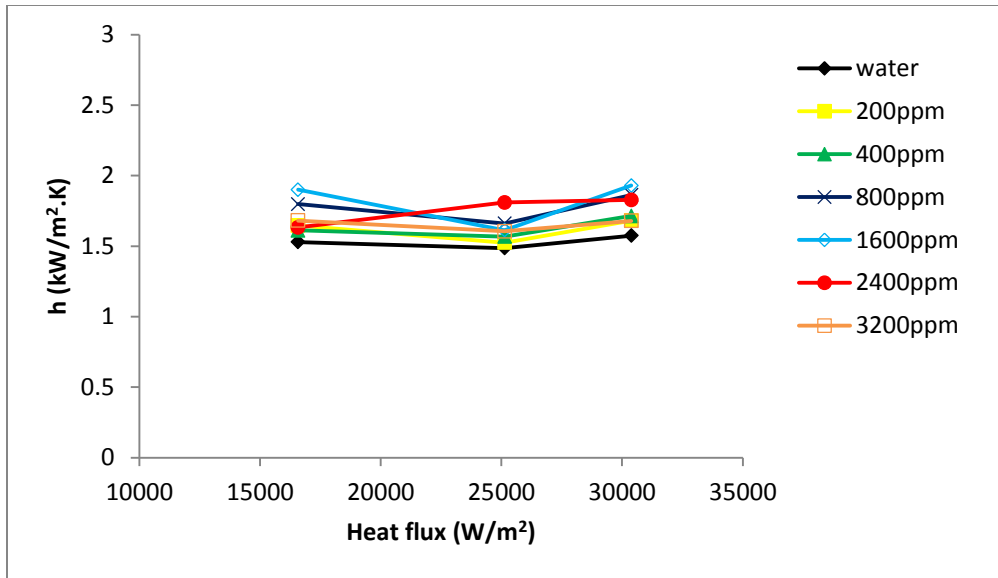


Figure 3.6: Nucleate boiling heat transfer coefficient as a function of heat flux for aqueous solutions of EH-14.

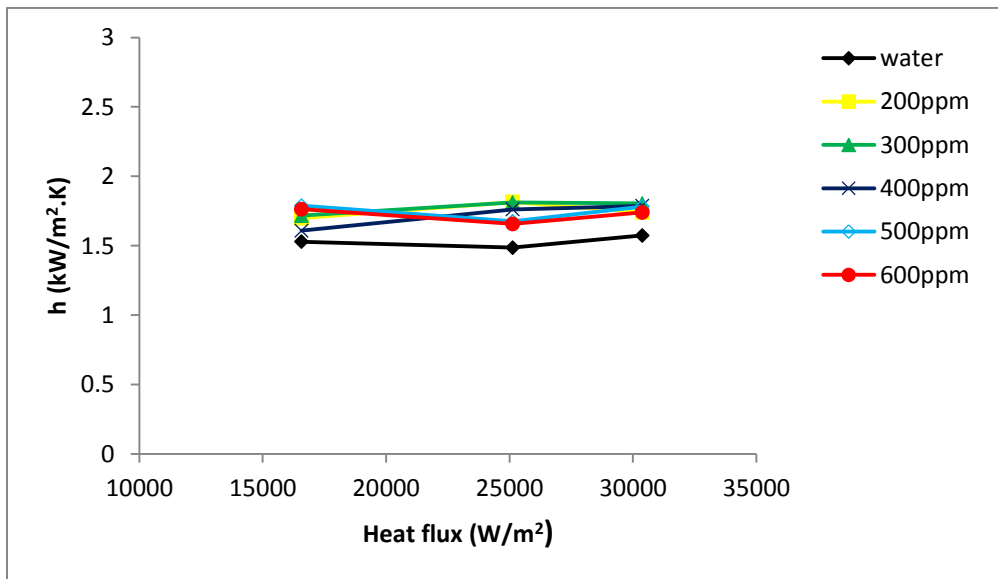


Figure 3.7: Nucleate boiling heat transfer coefficient as a function of heat flux for aqueous solutions of SA-9.

3.1.2.2 Discussion on Heat Transfer Coefficient Enhancement Ratio

Figure 3.8, Figure 3.9, and Figure 3.10 show the enhancement in pool boiling heat transfer performance of three surfactant solutions compared with water. In these figures,

the heat transfer coefficient enhancement ratio is plotted as a function of heat flux. The ratio is defined by the following expression [26]:

$$\alpha = \frac{h - h_w}{h_w} \quad (3.1)$$

Where,

h: heat transfer coefficient of surfactant solution ($kW/m^2 \cdot ^\circ C$)

h_w: heat transfer coefficient of water ($kW/m^2 \cdot ^\circ C$)

α: heat transfer coefficient enhancement ratio

It is found that the performance is seen to be dependent upon the wall heat flux and concentration. In general, as the heat flux and concentration increase, the heat transfer coefficient increases as well.

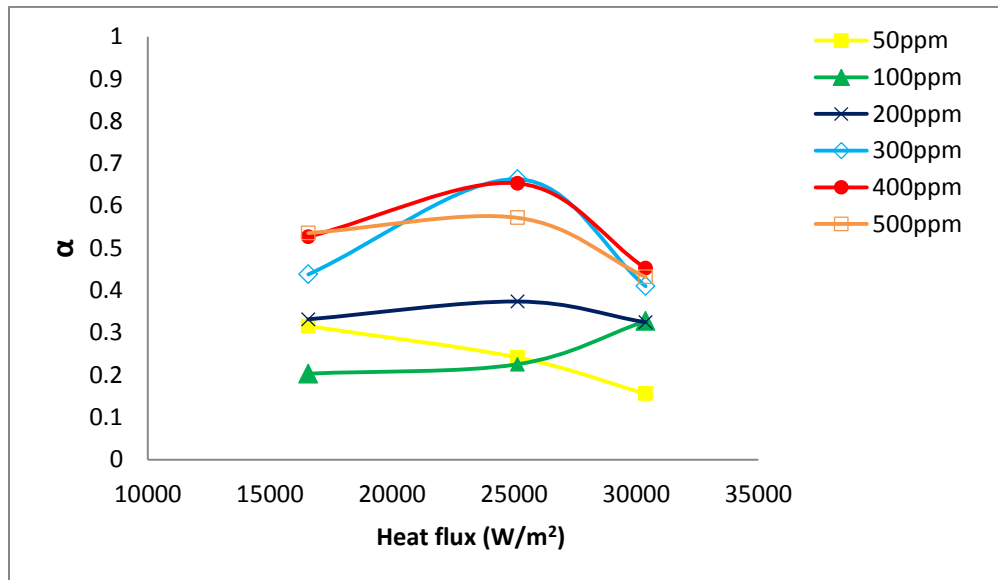


Figure 3.8: Heat transfer coefficient enhancement ratio vs. heat flux of SLS

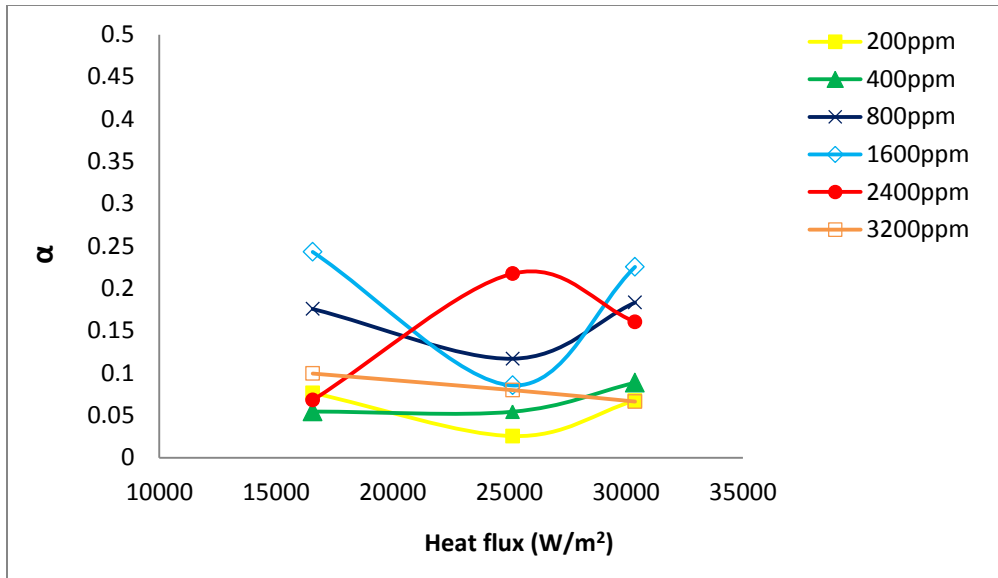


Figure 3.9: Heat transfer coefficient enhancement ratio vs. heat flux of EH-14

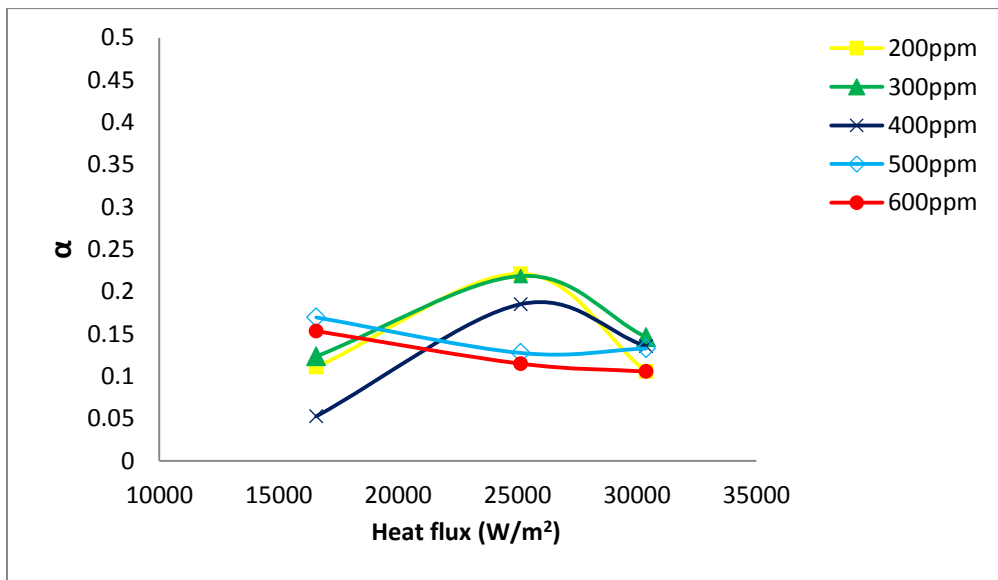


Figure 3.10: Heat transfer coefficient enhancement ratio vs. heat flux of SA-9

For SLS, an optimum heat transfer enhancement is achieved over a concentration range around CMC. The maximum enhancement obtained is 66.27% for 300ppm aqueous SLS solution. In addition, it should be observed that with concentrations more than 400ppm, there is no significant change in h for a given heat flux. This might be attributed to the fact that the reduction of surface tension with concentration for SLS is

constant above a solution concentration of 400ppm. This result agrees well with previous researchers. For example, Nafey et al. [27] observed that daily productivity (DP) was reduced by 6% at surfactant concentration more than 400ppm of SLS. Also, Baloch et al. [56] found that the CMC of SLS depends on the temperature. The CMC value decreases from 2800ppm (8.0×10^{-3} (mole/L)) at 10°C ($C(\text{ppm}) = 10^6 \times C(\text{mole/L}) \times M(\text{g/mole}) / \rho(\text{kg/m}^3)$ [46]) to 537ppm (2.0×10^{-3} (mole/L)) at 40 °C as shown in Figure 3.11. In addition, Tzan and Yang [57] found that there is no enhancement in heat transfer when the concentration of SDS is above 700ppm. However, the findings are in contrast to other researchers, who found that the optimum enhancement with SLS was achieved at different concentration. For instance, Elghanam et al. [26] found that 1500ppm concentration of SDS improves the heat transfer coefficient by 241%, while Zicheng et al. [29] observed that the maximum enhancement was achieved at concentration of 2500ppm. In this study, tests are carried out between [0-500ppm] for SLS.

For nonionic surfactants, the maximum enhancement in heat transfer coefficient is 24.31% for 1600ppm EH-14, which is achieved at low heat flux and 22.09% for 200ppm SA-9. With further increasing above these concentrations, the heat transfer coefficient decreases. It is evident these concentrations are the CMC of the surfactants, although the only data of CMC of these surfactants available at 23 °C show different values. It is shown that the CMC of EH-14 is 4018ppm, while 20ppm is the CMC of SA-9. To our knowledge, this is the first study of using EH-14 and SA-9 as surfactant tests.

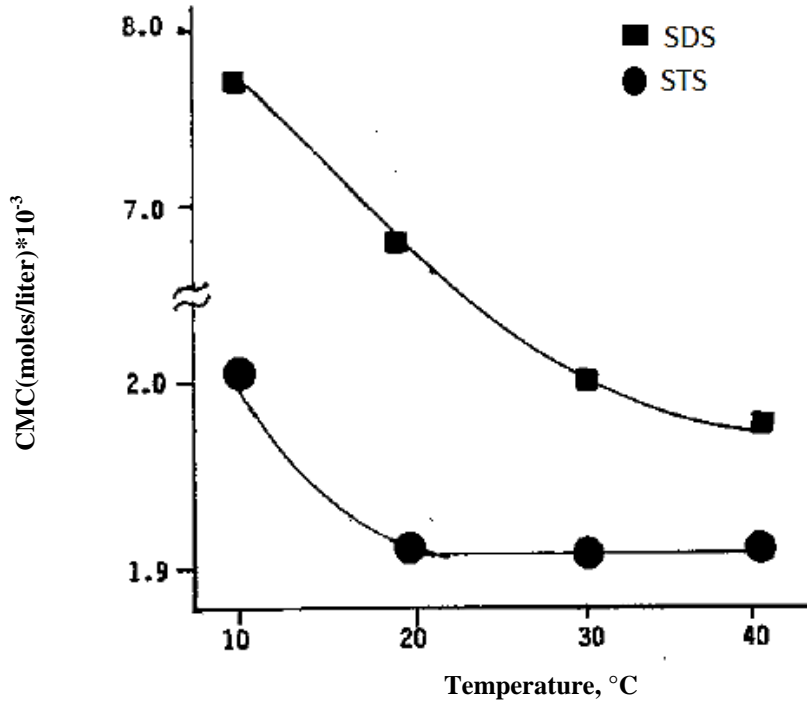


Figure 3.11: Effect of temperature on CMC of SDS [56]

3.1.2.3 Discussion on Optimum Heat Transfer

A comparison has been made between the three surfactants to evaluate the maximum heat transfer. Therefore, measured heat transfer coefficients h are graphed as a function of heat flux q for surfactants at CMC and pure water in Figure 3.12.

It can be seen that the optimum boiling heat transfer enhancement of SLS is higher than that of EH-14 and SA-9 when compared with water. It is found that the main reason is the lowest equilibrium surface tension at CMC. Although the data of surface tension for EH-14 and SA-9 surfactant at high temperatures are not available, but a comparison can be made at 23 °C. The values of surface tension at CMC are 38.0 mN/m for SLS, 31.8 mN/m for EH-14, and 29 mN/m for SA-9. It can be seen that the equilibrium surface tension of SA-9 at CMC is lower than that of the others. Depending on that, a conclusion

can be drawn that the optimum boiling heat transfer enhancement of SA-9 should be higher than that of others. However, it is the disparity as shown in Figure 3.12. As a result, it should be mentioned that the influence of surfactant may not be explained only by the reduction of surface tension. There are many variables that have a big effect on boiling phenomenon such as thermal patterns on the heated surface, Marangoni effects, ionic nature, viscosity, and molecular weight [28]. According to Henneberg et al. [58], the number of active nucleation sites may be dominated by diffusion of surfactant molecules. It was found that surfactants with lower molecular weight diffuse faster than those with higher molecular weight [26]. The molecular weights of tested surfactants are 288.38 for SLS, 1036 for EH-14, and 668 for SA-9. It can be seen that the SLS has the lowest molecular weight, and this agrees well with diffusion controlled mechanism. However, for nonionic surfactants, it was observed the contrast. The heavier molecular weight surfactant improves the heat transfer better than lighter molecular weight counterpart in the present investigation. About the effect of viscosity, Hestroni et al. [28] found that for high concentrations the heat transfer coefficient is decreased because of increasing the kinematic viscosity. The only data available of viscosity at 40 °C are 85.39 cSt for EH-14 and 30.225 cSt for SA-9. It can be seen that the viscosity of EH-14 is higher than that of SA-9. In spite of that, EH-14 performs better than SA-9.

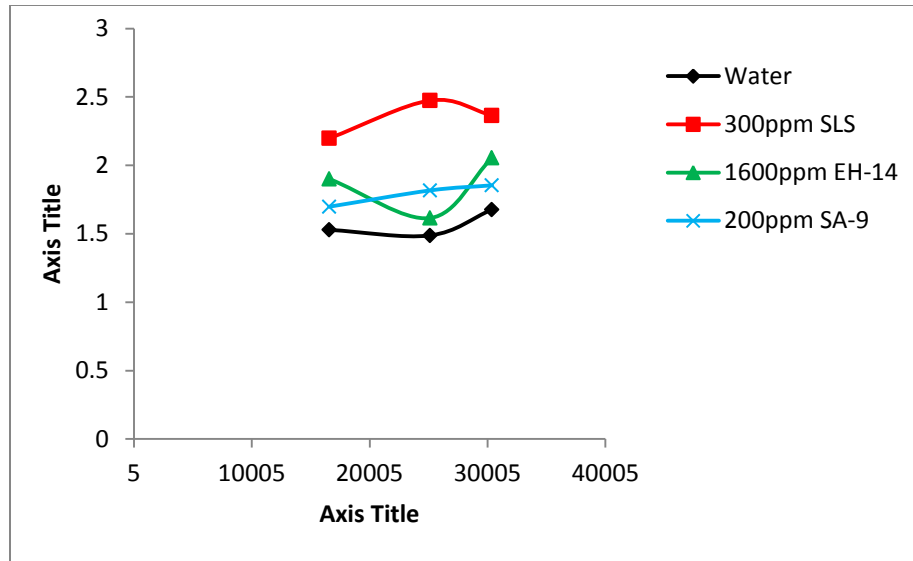


Figure 3.12: Optimum heat transfer among water and all surfactants

3.1.2.4 Discussion on Time Required to Reach Boiling Point

The time required to reach boiling point for surfactant concentrations is measured and compared with water. It was found there was a variation in the initial and boiling temperatures of surfactant solutions. The variation ranges between 19-23 °C for initial temperature and 98C-101 °C for saturated temperature. Therefore, for a fair comparison, time is evaluated from 25 °C until reaching 95 °C. The results show there is a reduction in time to reach 95 °C for most surfactant concentrations as shown in Figure 3.13, Figure 3.14 , and Figure 3.15 . The maximum reduction in time for each surfactant was 14.6% for 100ppm SLS, 9% for 800ppm EH-14, and 12.49% for 300ppm SA-9 compared to water. However, for some concentrations, it was noticed that there is no significant reduction in time to reach 95 °C. The concentrations were 50ppm SLS with -2%, 200ppm EH-14 with -0.9%, and 200ppm SA-9 with -0.4%.

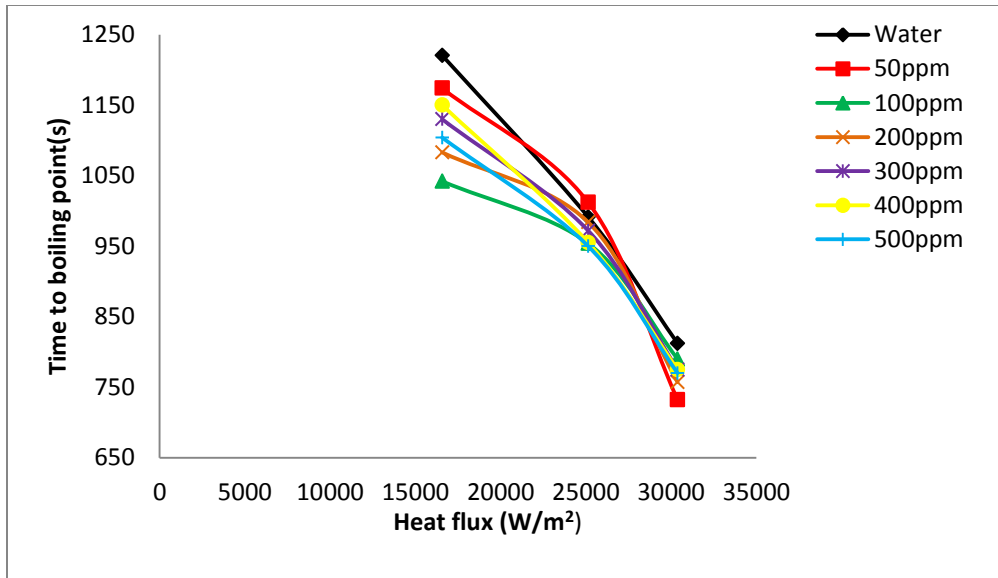


Figure 3.13: Time to reach boiling point vs. heat flux for SLS

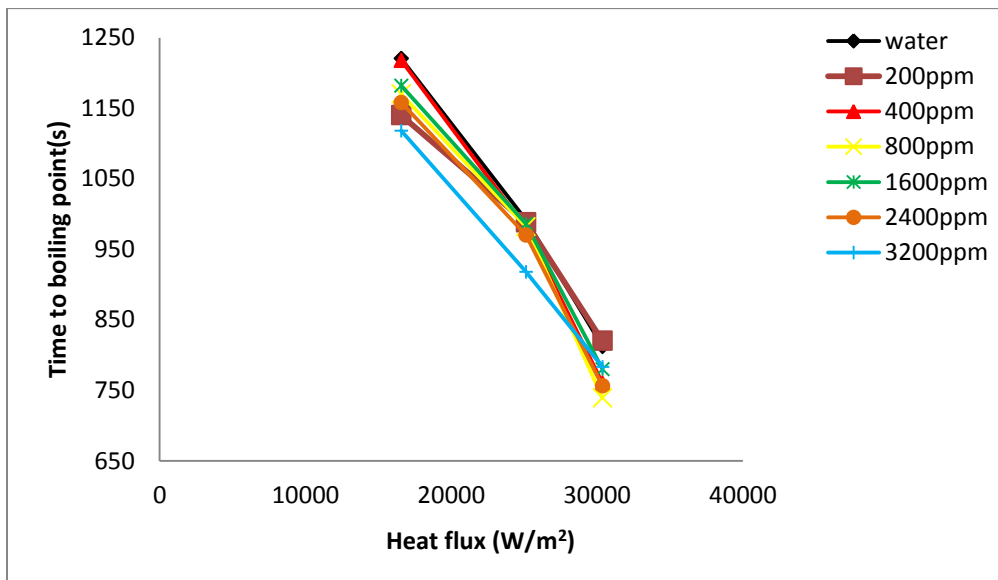


Figure 3.14: Time to reach boiling point vs. heat flux for EH-14

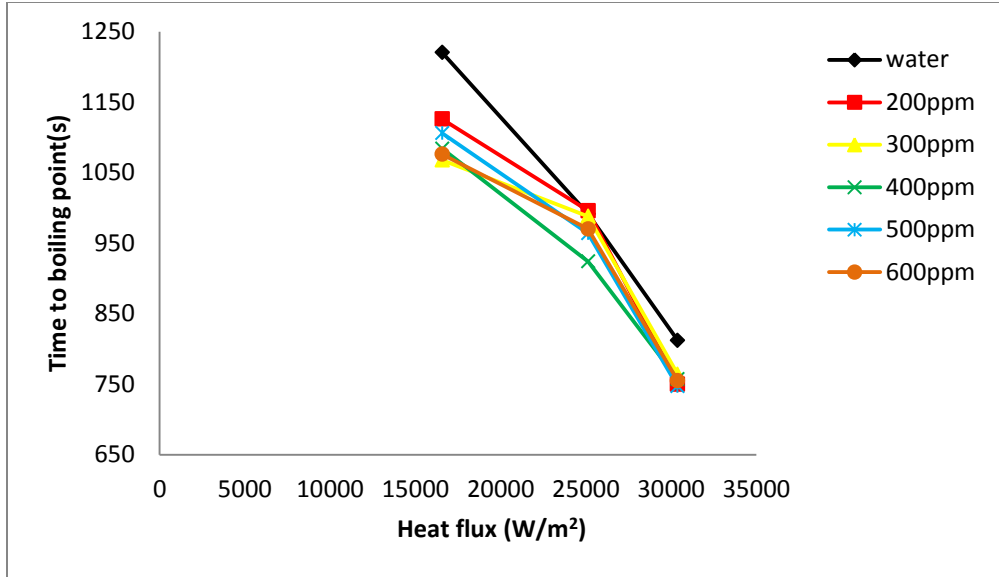


Figure 3.15: Time to reach boiling point vs. heat flux for SA-9

3.1.3 Boiling Visualization

General observations demonstrate that boiling with surfactant solutions, shown in Figure 3.16, is quite different from that of pure water. It was observed that the bubbles in the boiling with additive solutions are more vigorous and smaller in size, activate continuously, and collapse quickly. Also, it was noticed the bubble departure frequency was higher compared to that of water. Bubble departure increases with increasing the heat flux. All these results by adding small amounts of surfactant may be attributed to lower values of surface tension compared to the pure water [48]. According to Fritz [59], the decreasing in surface tension leads to departure of smaller-sized bubbles. Fritz established a well-known equation, which correlates the surface tension proportionally to bubble departure diameter. This correlation is given by equation (3.2).

$$d_b = 0.0208\phi \sqrt{\frac{\sigma}{g(\rho_l - \rho_v)}} \quad (3.2)$$

Here ϕ is the contact angle (deg.). Also, this conclusion is consistent with Wen and Wang [60], and Hetsroni et al. [61], who observed the same conclusion.

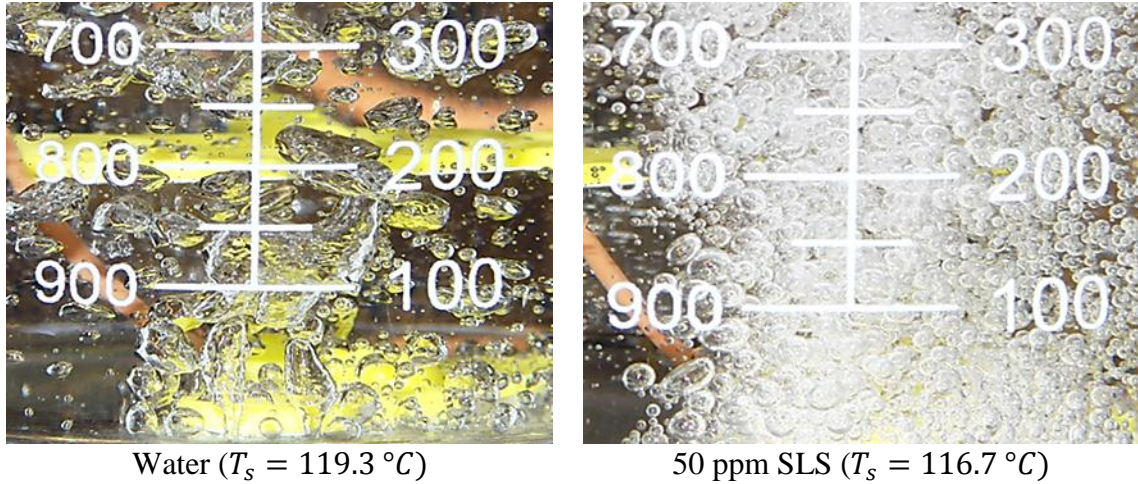


Figure 3.16: Boiling behavior at heat flux 30.38kW/m^2

3.1.3.1 Visualization in Aqueous Anionic Surfactant Solutions

Figure 3.17 shows boiling of water and 300ppm SLS solution on the beaker at different heat fluxes $16.57, 25.13, 30.38 \text{ kW/m}^2$, respectively. It is seen that the heat flux has a big influence on the bubble dynamics. When the heat flux increased, merging of bubbles takes place more. For pure water, bubble behavior is observed to be extremely disordered, with comprehensive coalescence during the ascent. At all values of heat flux, an irregular shape of bubbles is observed [28]. For 300ppm SLS solution, a cluster of small bubbles can be seen. These bubbles are adjacent to each other. They have spherical shape, which is different from water irregular shapes. They also cover the surface faster than the water and form a foam layer, whose thickness depends on the heat flux. As the heat flux increased, the foam layer increased as well. Figure 3.18 shows the boiling behavior of different concentration of SLS surfactant compared with water at the highest heat flux. It was seen that as the concentration of SLS surfactant increases, the number of

bubbles increases as well. It was found that the increased foaming leads to enhancement in boiling heat transfer [62]. The reason is that the decrease in wall temperature is because the collapse of the vapor cluster [25].

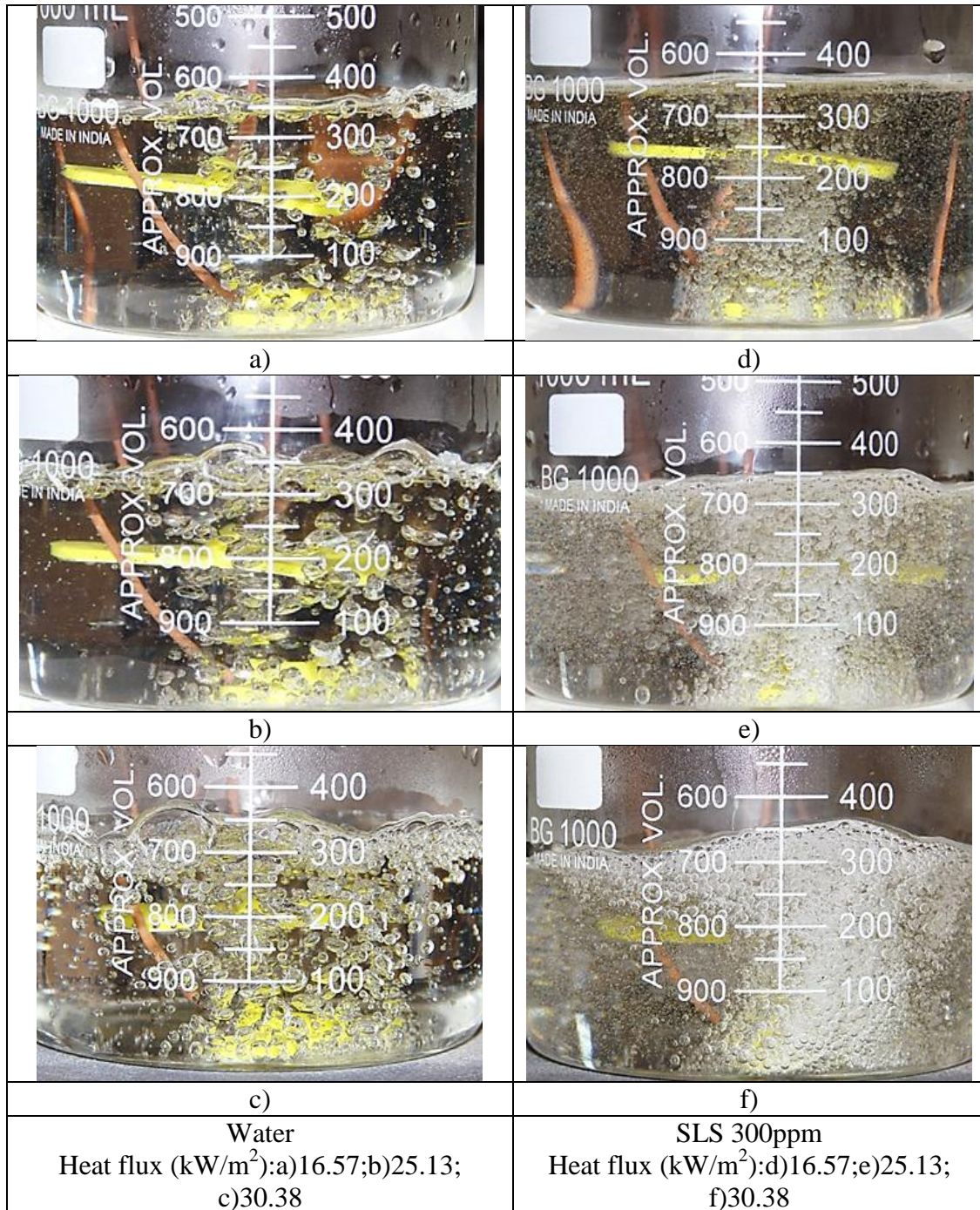


Figure 3.17: Boiling behavior of water and 300ppm SLS at various heat fluxes

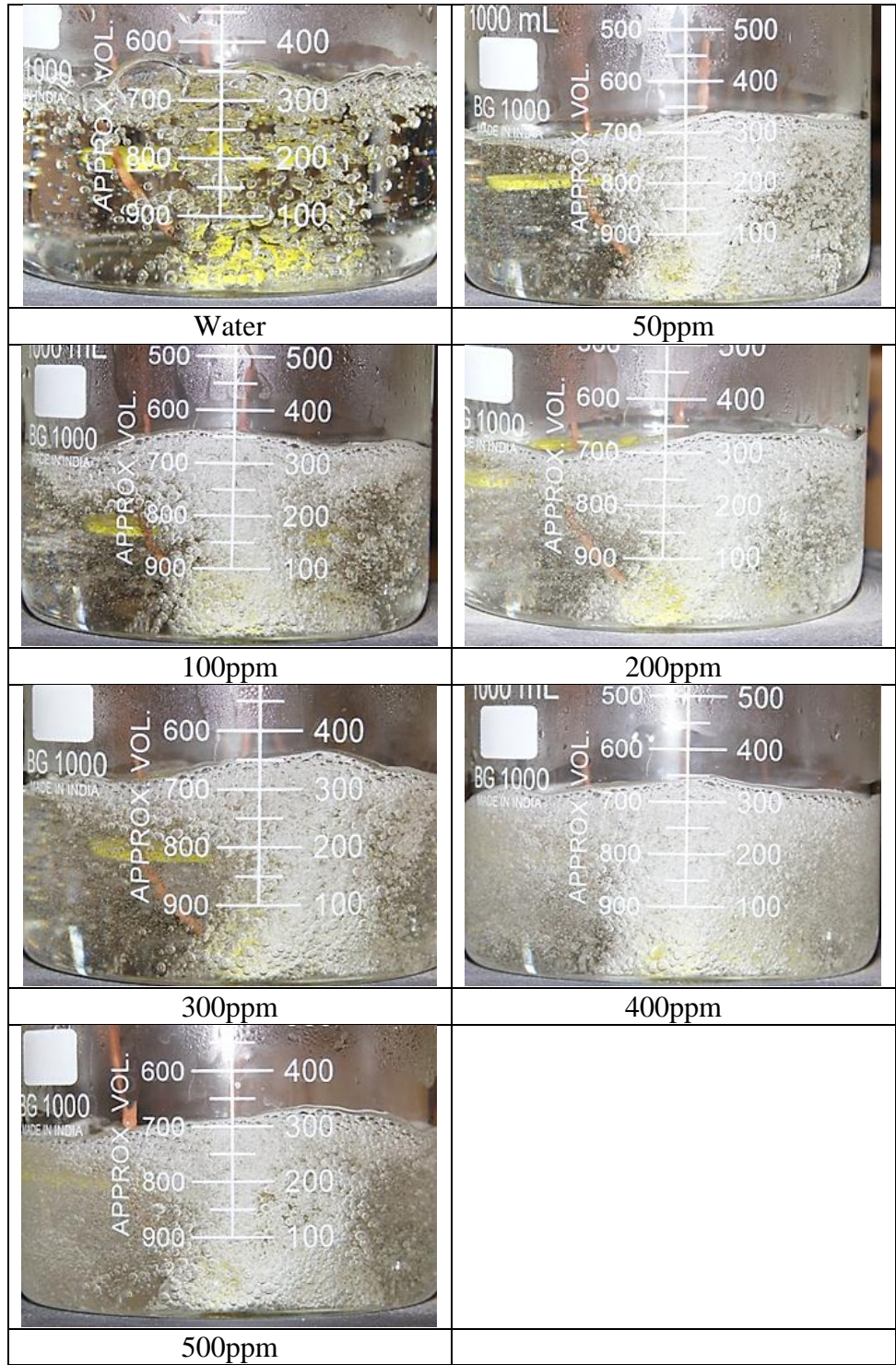
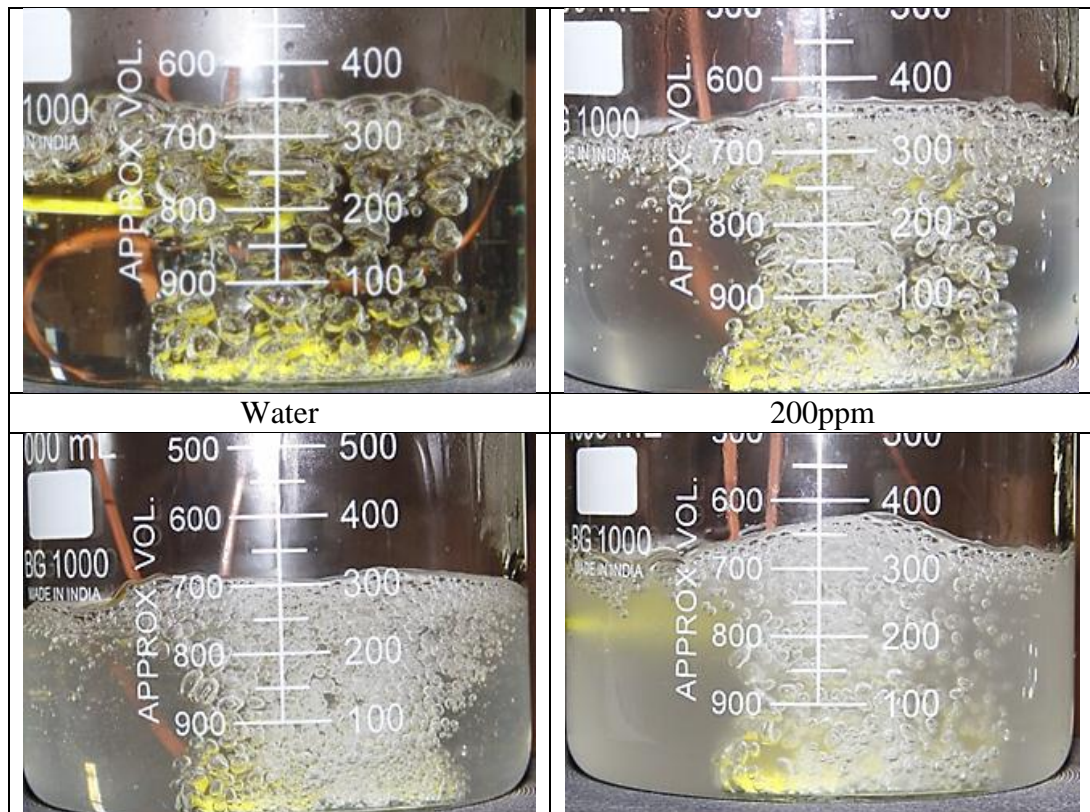


Figure 3.18: Comparison of boiling behavior for pure water and various aqueous SLS solutions at heat flux =30.38 (kW/m²)

3.1.3.2 Visualization in Aqueous Nonionic Surfactant Solutions

Figure 3.19, and Figure 3.20 show the boiling behavior in water, and nonionic EH-14 and SA-9 solutions of different concentrations at the highest heat flux level ($q'' = 30.38 \text{ kW/m}^2$). Boiling in EH-14 solutions is more vigorous than that of water. Clusters of smaller-sized, more regularly shaped bubbles are observed. These bubbles form at the base of the beaker. For concentrations above 400ppm, it was observed that clouding of the solutions was happened when the surfactant solution reached saturation temperature. Also, the top surface was covered by a foam layer, which was much thinner than of SLS surfactant at the same heat flux. In contrast, boiling in SA-9 solutions was observed to be similar to that of water. The bubbles have irregular shapes as it was seen of water, but their size is less than those of water. The top surface was barely covered by the foam layer.



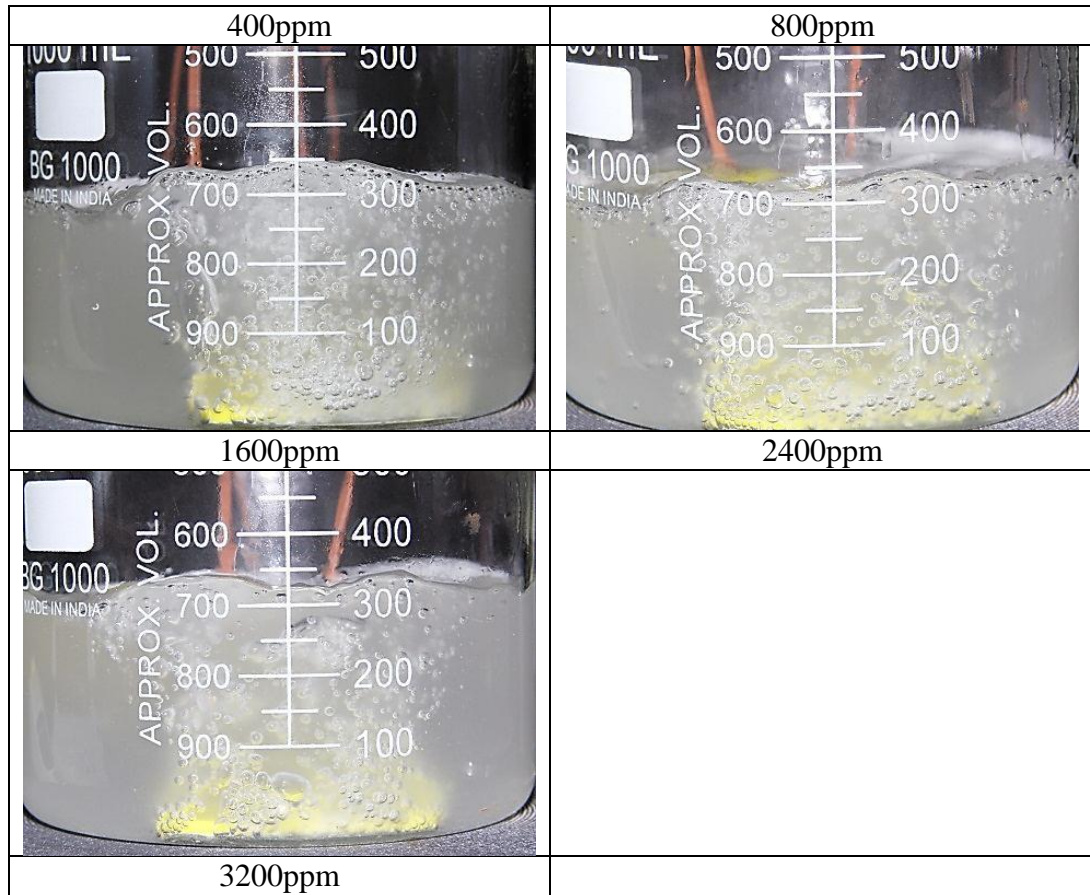
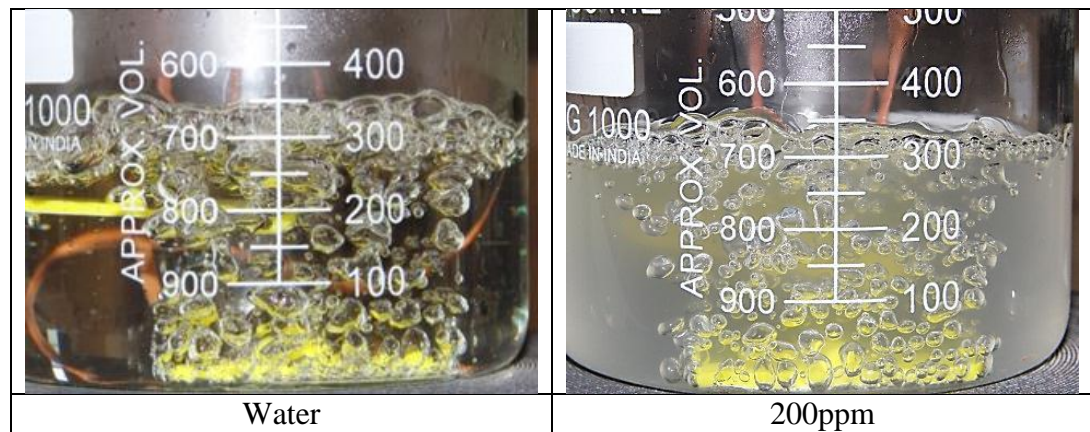


Figure 3.19: Comparison of boiling behavior for pure water and various aqueous EH-14 solutions at heat flux =30.38 (kW/m²)



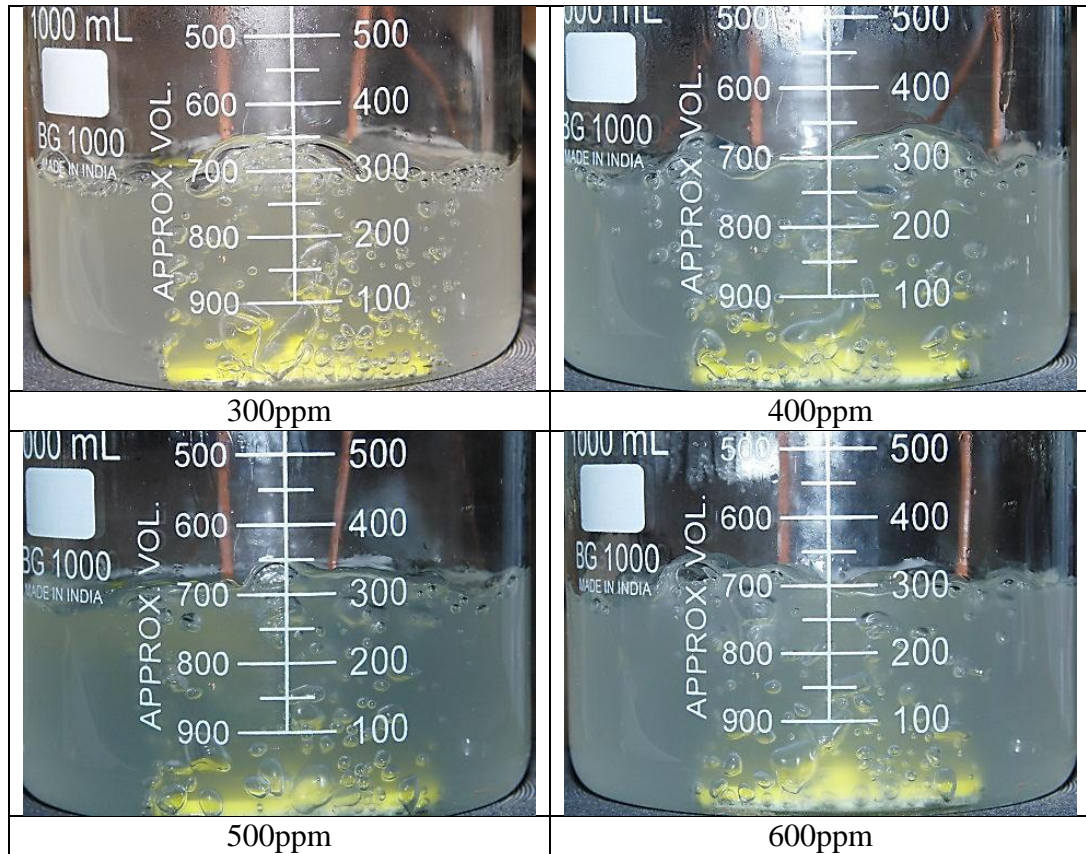


Figure 3.20: Comparison of boiling behavior for pure water and various aqueous SA-9 solutions at heat flux =30.38 (kW/m²)

3.2 Structured Surfaces

Experiments with augmented surfaces are conducted using distilled water. The influence of structured geometries (surfaces with holes, grooves, and mushroom fins) on boiling phenomena is investigated. The results obtained are compared to the plain surface.

3.2.1 Discussion on the Effect of Geometry

The boiling curves and heat transfer coefficients of distilled water on plain and structured surfaces are shown in Figure 3.21, and Figure 3.22, respectively.

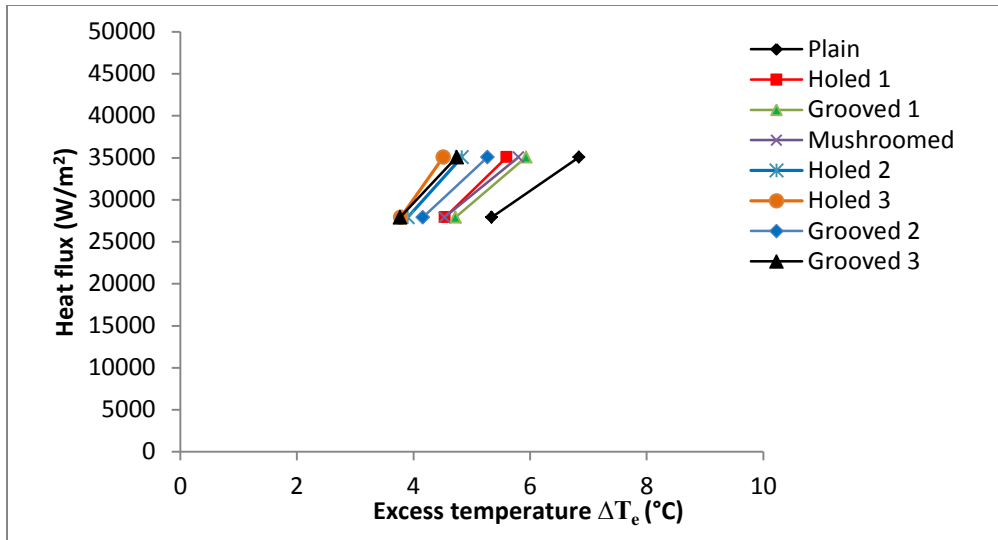


Figure 3.21: Boiling curves data for enhanced surfaces

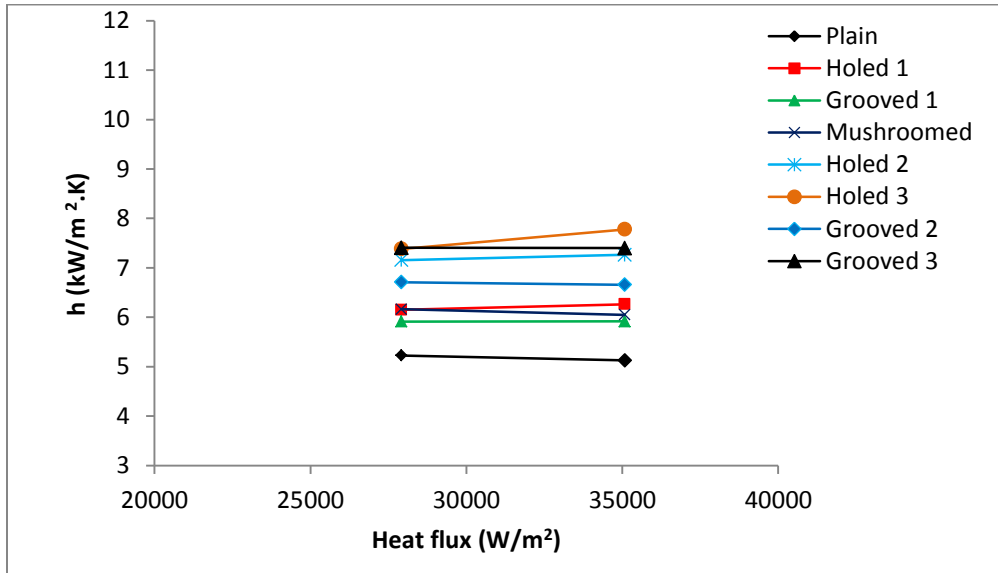


Figure 3.22: Boiling heat transfer coefficient as a function of heat flux for enhanced surfaces.

It can be seen that the boiling curves of the structured surfaces are noticed to shift to the left. Structures can drop the wall temperature, thus the heat transfer coefficient is enhanced considerably. At the same heat flux, heat transfer coefficients of the structured surfaces are higher than the plain surface because of increasing of the effective heat transfer area. In addition to that, structured surfaces increase the bubble frequency, which

will help to dissipate the heat from the surface. As a result, the wall superheat will be decreased [63]. This result is also in agreement with findings of Jun et al. [64].

Figure 6 shows that as the heat flux increases, the heat transfer coefficient increases as well for all surfaces. The plain surface has the poorest performance compared to all the other surfaces, while Holed 3 surface gives the best heat transfer performance. At heat flux 27.91 kW/m^2 , Grooved 3 and Holed 3 surfaces give the best performances compared to the plain surface. Heat transfer coefficient is increased by 41.64% and 41.26%, respectively. However, Grooved 1 surface has the poorest performance among the structured surfaces. The enhancement in heat transfer coefficient is only 13.1%. For Mushroomed surface, it shows enhancement in heat transfer coefficient by 17.8%.

For heat flux of 35.08 kW/m^2 , Holed 3 surface shows the maximum enhancement of heat transfer. It is about a 51.66% increase in the heat transfer coefficient compared to the plain surface, while it was 44.3% for Grooved 3 surface. Again, Grooved 1 surface performs poorly among the other structured surfaces. The enhancement is 15.34%. Also, Mushroomed surface enhances the heat transfer coefficient only by 17.9%. The reasons of maximum enhancement achieved by Holed 3 and Grooved 3 surfaces might be due to increase the effective heat transfer area and bubble dynamics. It can be seen from Table 2.3 there is a significant increase in the effective heat transfer area. For Holed 3, the A_r is 1.76, while area augmentation ratio for Grooved 3 is 1.9. This also shows that the augmentation in surface area is not the only reason of enhancing boiling heat transfer. It can be seen that the A_r of Holed 3 is less than that of Grooved 3. In spite of that, Holed 3 performs better than Grooved 3. Researchers found that the bubble size can be identified by channel width. Bigger bubbles can be produced from larger channels. These

bubbles are able to scatter more heat from the surface [35]. Depending on that, the diameter of hole is 0.0625 inch (1.58 mm), while the width of the channel is 0.04 inch (1.01 mm). It can be concluded that the bubbles from holed surfaces are bigger than those from grooved surfaces. Therefore, the bubble departure diameter was evaluated in this chapter. It was observed among structured surfaces holed surface has the biggest bubble diameter at a heat flux of 35.08 kW/m², while at the heat flux of 27.91 kW/m², it is shown the contrast. Grooved 1 has the biggest bubble diameter. Also, the bubble nucleation can be achieved by high temperature. This can be attained by deep channels, which provide a surface closer to the heater [35]. By taking this point in consideration, Holed surfaces have a depth of 0.125 inch (3.17 mm), while grooved surfaces have 0.08 inch (2.03 mm) depth. It can be concluded that holed surfaces have higher bubble nucleation than the other surfaces.

3.2.2 Discussion on the Effect of Spacing

The spacing between the channels and holes is observed to have a significant impact on the heat transfer performance of the enhanced surfaces. As it can be seen from the Table 2.3, the surfaces with grooved structures have the same channel width and depth, but they vary in spacing between the channels. The same thing is true for holed surfaces. To understand the effect of spacing, dimensionless parameter (β) has been investigated to evaluate the performance of the surfaces. The parameter (β) is shown in Figure 2.15. As the spacing decreases, β is decreased as well. Decreasing the spacing leads to increase the number of grooves or holes, which leads to increase the effective heat transfer area. This is considered the main reason of enhancing heat transfer coefficient besides bubble dynamics. Among holed surfaces, Holed 3 surface performs better than the others. For

example, β was decreased from 2 (Holed 1) to 0.5 (Holed 3), the heat transfer coefficient was increased from $6.26 \text{ kW/m}^2\cdot\text{K}$ (Holed 1) to $7.77 \text{ kW/m}^2\cdot\text{K}$ (Holed 3) at heat flux 35.08 kW/m^2 . The same thing is true for grooved surfaces, Grooved 3 surface performs better than the others. The heat transfer coefficient was increased from $5.91 \text{ kW/m}^2\cdot\text{K}$ to $7.4 \text{ kW/m}^2\cdot\text{K}$ for Grooved 1 ($\beta = 3.75$) and Grooved 3 ($\beta = 1$), respectively at the same heat flux (35.08 kW/m^2).

3.2.3 Discussion on Boiling Visualization

Figure 3.23 shows the boiling phenomena before the water temperature reaching boiling point. It can be seen that the artificial nucleation sites of structured surfaces become activated by the formation of bubbles. This result is consistent with [65].

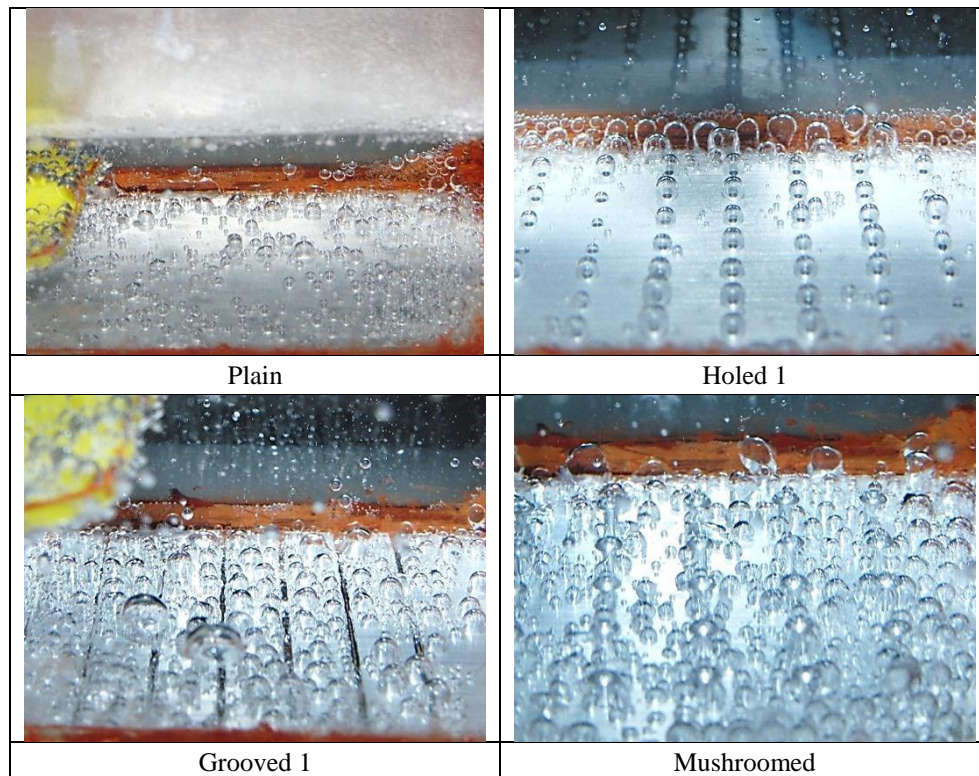


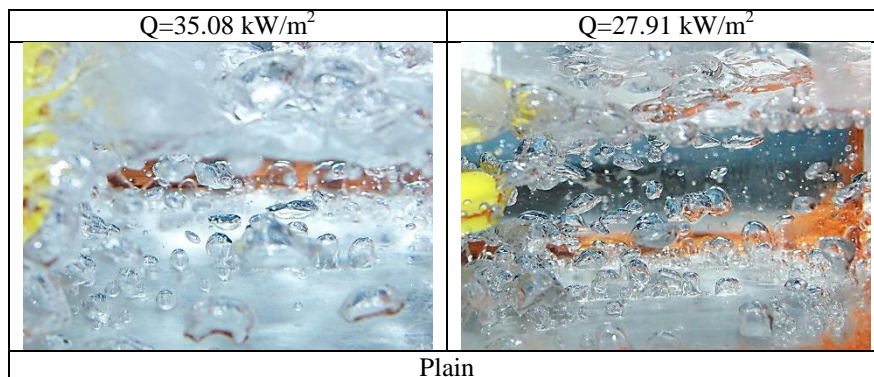
Figure 3.23: Pictorial view of boiling phenomena before reaching boiling point

Figure 3.24 shows the boiling phenomenon on plain and structured surfaces at two values of heat flux. It can be seen that the number of departure bubbles from structured surface seems to be more than that on a plain surface, because of the higher frequency of bubble departure. At low heat flux (27.91 kW/m^2), isolated bubbles form on the surface, and they hardly interact each other during their rise. When the heat flux increases more, the number of active nucleation sites increases as well. The bubbles begin to influence each other as it can be seen at a heat flux of 35.08 kW/m^2 , especially for grooved and mushroomed surfaces.

At heat flux of 35.08 kW/m^2 , the enhanced surfaces are almost covered with a vapor film, which is hardly formed on the plain surface. Also, surfaces with enhanced features have much higher density of active nucleation sites than that on the plain surface because these surfaces can accelerate bubble departure by decreasing the bubble departure diameter and increasing departure frequency. There is Ivey's correlation that relates the bubble departure diameter to departure frequency. This correlation is given by equation (3.2) [66]:

$$f_d \propto D_d^{-n} \quad (3.2)$$

Where $n=1/2, 1, \text{ or } 2$. This correlation suggests that when the bubble departure diameter decreases, the departure frequency increases [66].



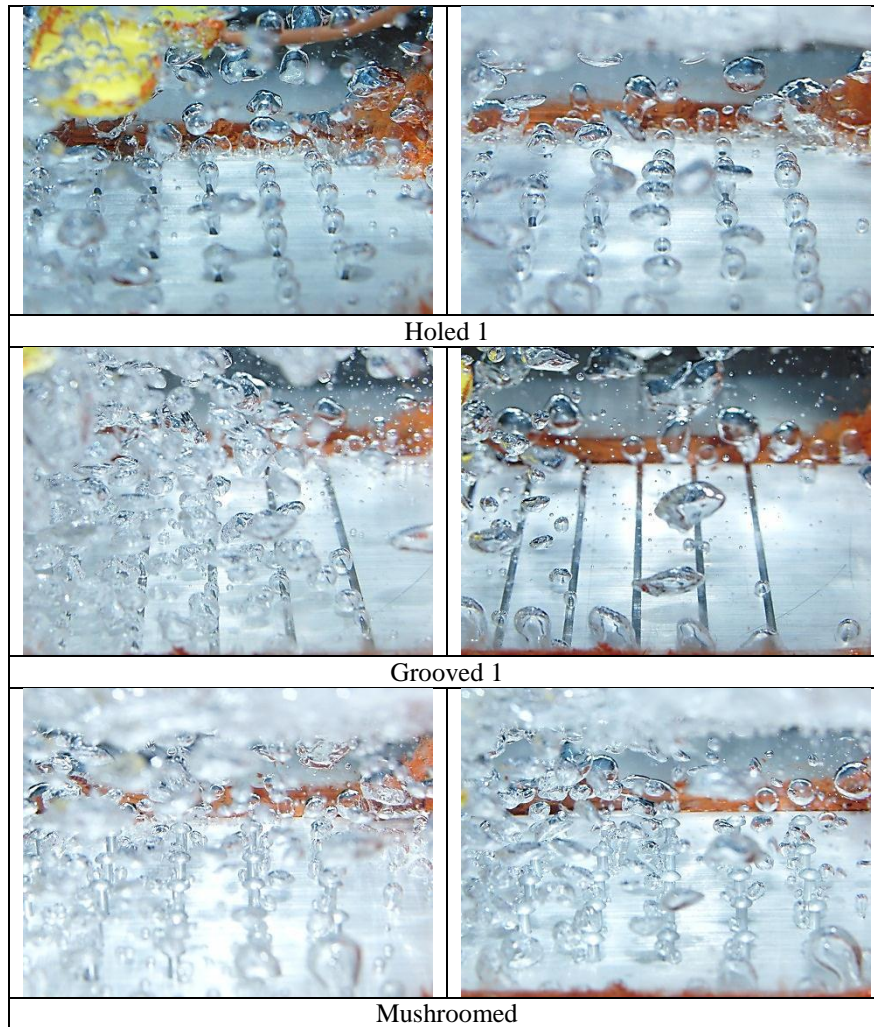


Figure 3.24: Pictorial view of boiling phenomena at different values of heat flux

The bubbles with holed surfaces and mushroomed surface have almost spherical shape, while in plain and grooved surfaces the bubbles have an irregular shape. For holed and grooved surfaces, it is seen that the artificial nucleation sites act as small pumps, and the displaced volume by the bubble leaving the surface is substituted by the liquid [65].

Figure 3.25 shows the boiling behavior of water on different enhanced surface at heat flux of 35.08 kW/m^2 . It can be seen as the number of holes or grooves is increased, the number of bubbles is increased as well because of increasing the number of active nucleation sites.

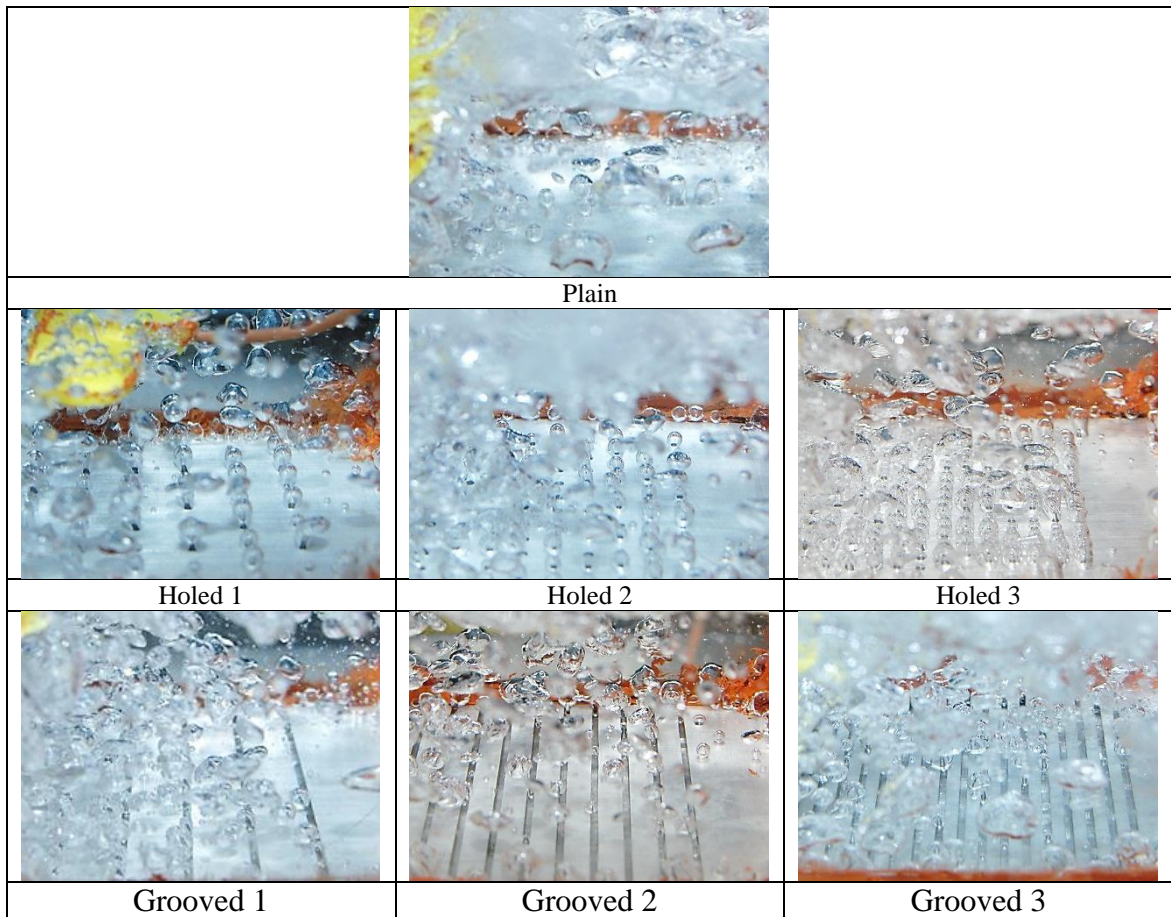


Figure 3.25: Boiling behavior of water on different structured surface at 35.08 kW/m^2

3.2.4 Discussion on Bubble Departure Diameter

With the help of a scale ruler, the bubble diameter is evaluated approximately by taking measurements for obvious bubble as shown in Figure 3.26.

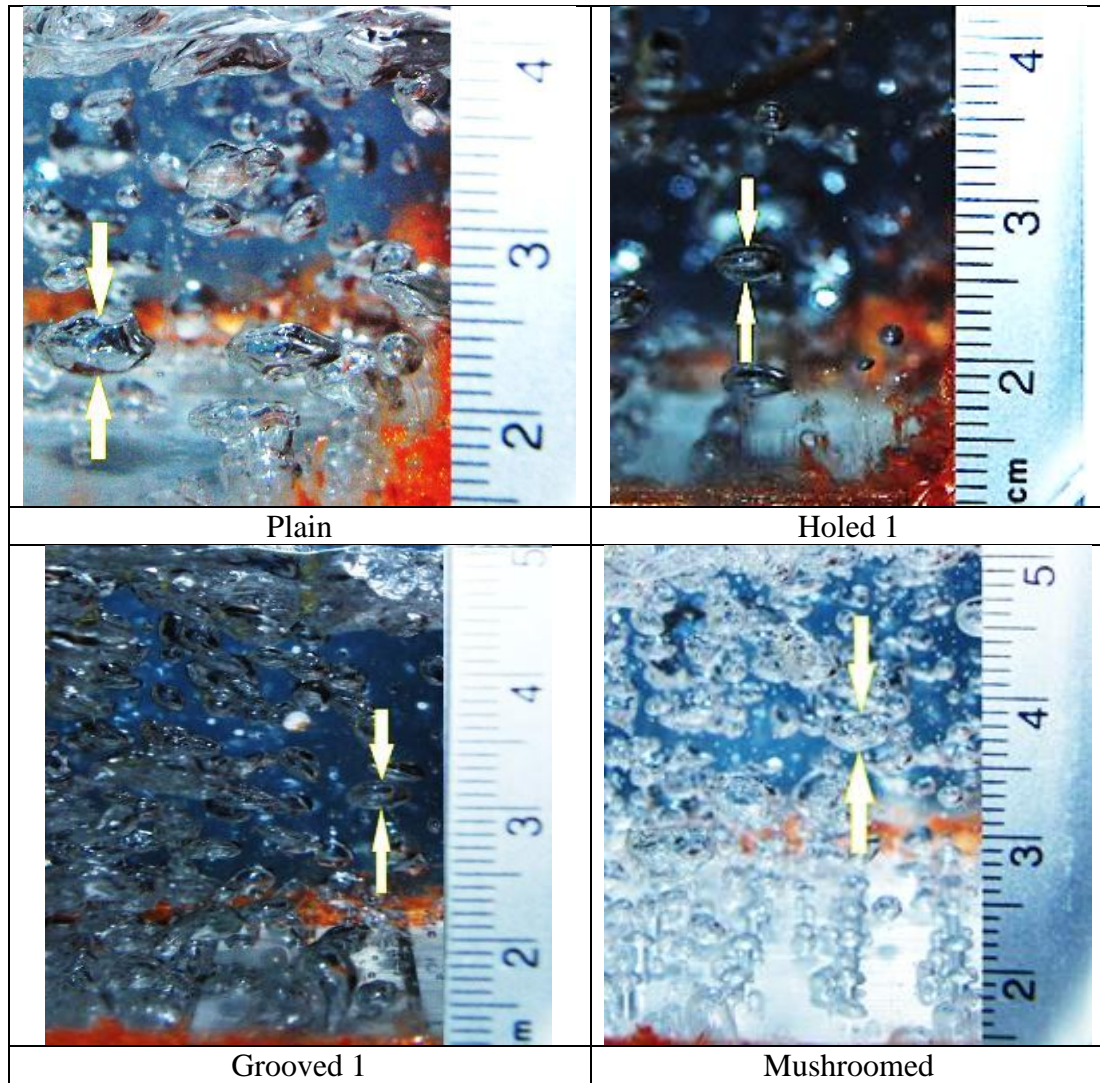


Figure 3.26: Bubble departure diameter measurements at heat flux of 35.08 kW/m^2

Then, the values are graphed as a function of heat flux, shown in Figure 3.27. It is important to mention that the bubble diameter was compared for four surfaces because the surfaces with the same features (same channels or holes) shows almost the same bubble diameter as it can be seen from Figure 3.25. In general, the results show that the bubble diameters decrease with an increase in heat flux values. This finding agrees well with previous studies by Nakayama et al. [67] and Chien et al. [68]. Also, it is shown that the plain surface has the largest bubble diameter among others, while the grooved surface has the smallest bubble diameter.

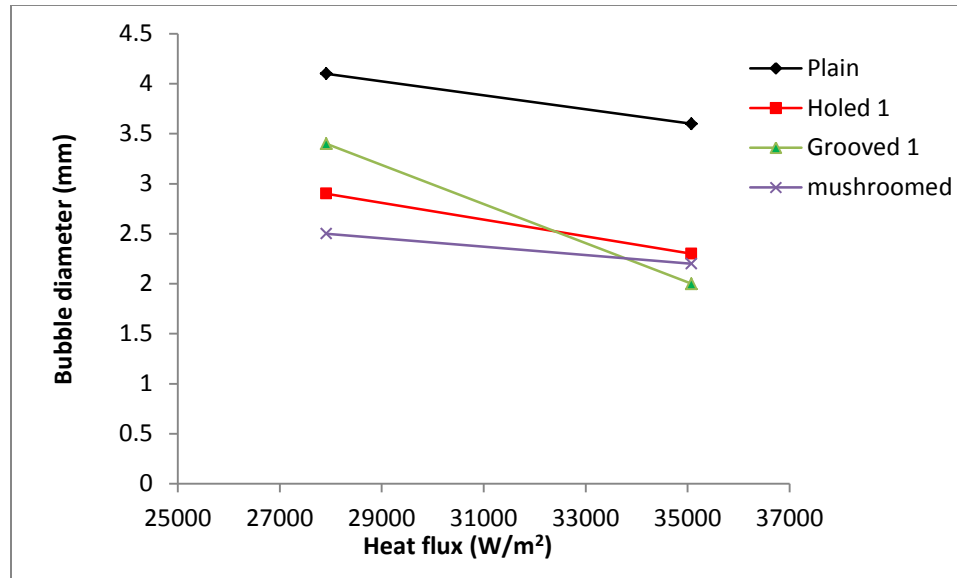


Figure 3.27: Bubble departure diameter as a function of heat flux

3.2.5 Discussion on Time to Reach Boiling Point

The time required to reach boiling point of distilled water on structured surfaces is measured and compared with that on the plain surface. Because of temperature variations in initial and saturated temperatures, comparison is made for time from 25 °C until 95 °C. The experiments for each surface are run twice. Therefore, time to reach boiling point is the average of two values for each heat flux. The results of time to reach boiling point is plotted against the heat flux as shown in Figure 3.28. Figure 3.28 shows there is a big reduction in time to reach boiling point for some enhanced surfaces, while others show no reduction like Holed 3, Grooved 2, and Grooved 3 surfaces. For heat flux of 27.91 kW/m², 8.58% enhancement in time to reach boiling point for Grooved 1 surface was attained, while at a heat flux of 35.08 kW/m² the maximum reduction achieved was 8.74% for Mushroomed surface and 8.19% for Holed 1 surface.

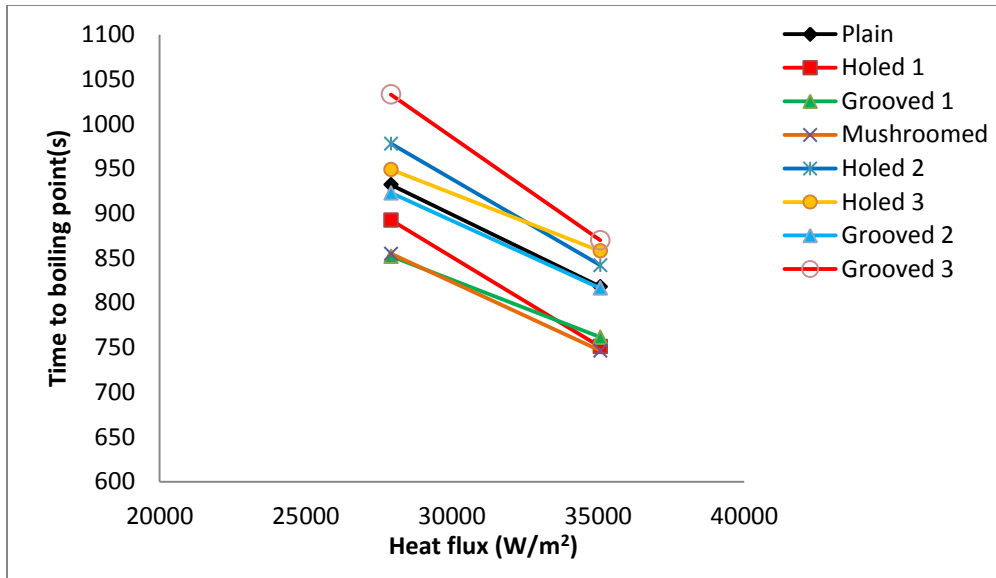


Figure 3.28: Time to boiling point vs. heat flux

3.3 Droplet Boiling Evaporation Time Observations

Different boiling behaviors of a water droplet during pool boiling are shown in Figure 3.29 - Figure 3.32. The natural convection boiling regime at $\Delta T_e = 1^\circ\text{C}$ is shown in Figure 3.29. It can be seen that in this zone many small bubbles form instantaneously at the base. After that, the drop boils until it vanishes [7]. Figure 3.30 illustrates the pool boiling phenomenon in the nucleate boiling regime at $\Delta T_e = 18^\circ\text{C}$. This boiling regime is characterized by transferring a large amount of heat with the small difference of temperatures. That is why it is widely used in the industrial equipment. The figure shows clearly that the water droplet diffuses and swells up so quickly until it disappears [7]. Figure 3.31 shows the transition boiling at $\Delta T_e = 66^\circ\text{C}$. This boiling regime is also called unstable film boiling or partial film boiling. As it can be seen from the figure, one of the balls is normally bigger than the others. The balls jump from one place to another frequently [7]. The film boiling at $\Delta T_e = 170^\circ\text{C}$ of droplet water is illustrated by Figure 3.32. The figure obviously demonstrates that one individual ball is formed, and no shattering is witnessed. The ball becomes smaller and smaller until it totally evaporates

[7]. This boiling regime is known as the Leidenfrost phenomenon, shown in Figure 3.33. If the temperature is at or above the Leidenfrost point, evaporation of the bottom surface of a water droplet is instantly happened. A vapor layer is formed between the plate and the droplet due to heat radiation and conduction from the plate. Hence, the rest of the droplet is protected from touching the plate by this vapor layer [69]. That is why the droplet is protected from touching the plate by this vapor layer [69]. That is why the droplet's life is increased by up to 500 times [70]. In addition, the nucleation of bubbles is inhibited in this regime because of the lack contact between the liquid and the solid. As a result, the droplet does not boil; it just vaporizes [71].

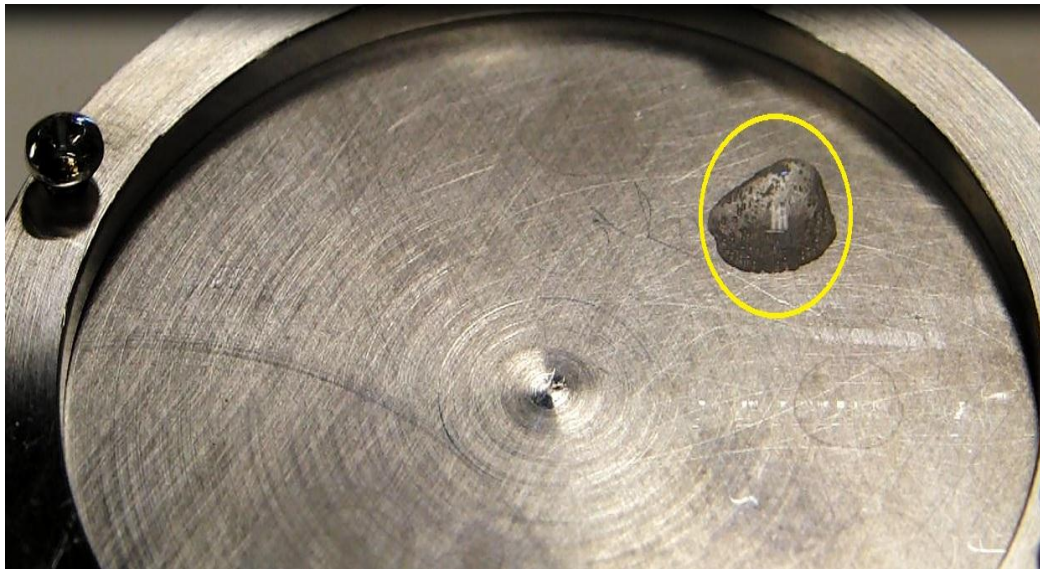


Figure 3.29: Natural convection boiling regime



Figure 3.30: Nucleate boiling regime

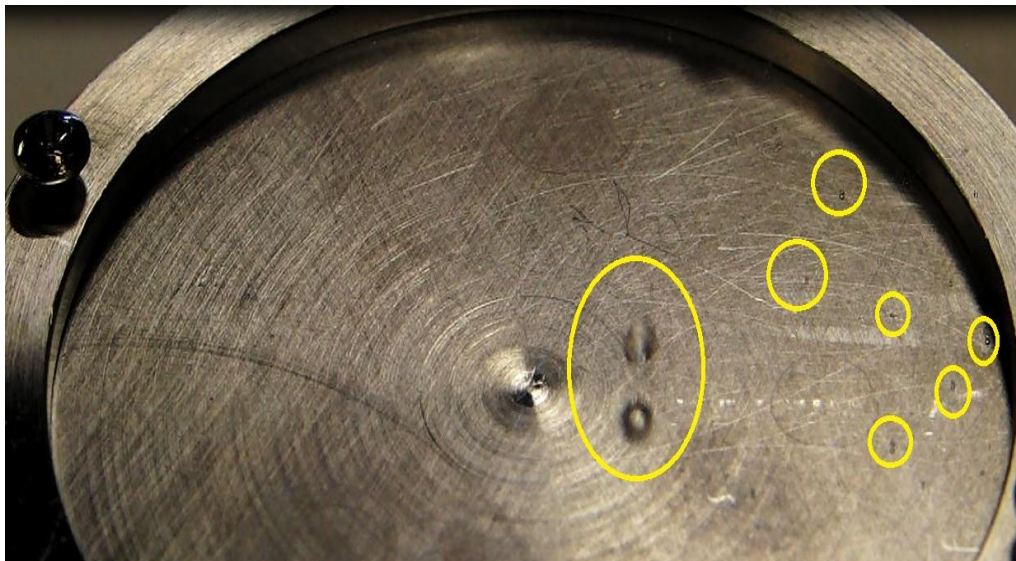


Figure 3.31: Transition boiling regime

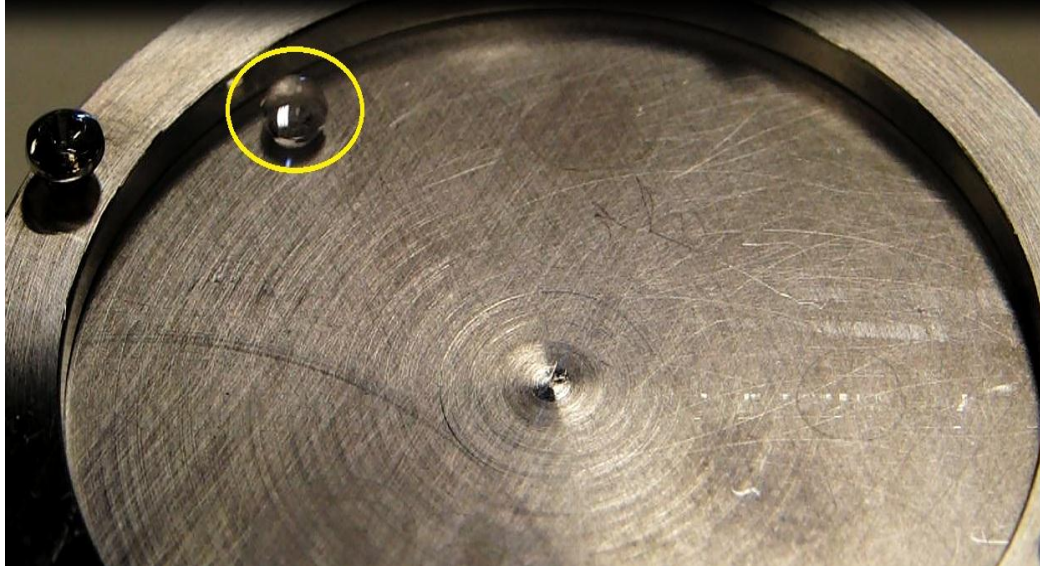


Figure 3.32: Film boiling regime

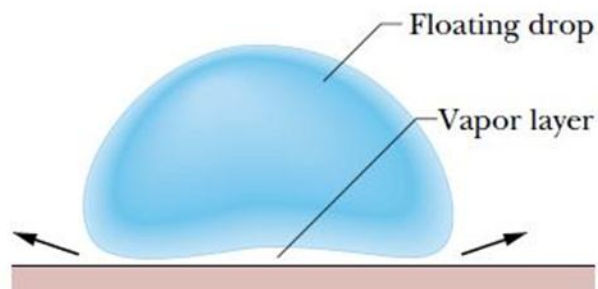


Figure 3.33: Leidenfrost drop in cross section [69]

3.3.1 Evaporation Time of Water Droplet

By depending on video recordings, the total evaporation time of a droplet of distilled water in the different pool boiling regimes was calculated and compared with the results of other researchers such as Abu-Mulaweh et.al [7]. By using the Escali L-600 digital scale, the mass of the single droplet was measured and found to be 35mg. However, for Abu-Mulaweh et.al.'s study, the value was 32mg. It should be stated that the calculations of the total evaporation time were conducted for three regimes only: the natural convection boiling regime, nucleate boiling regime, and film boiling regime. It was hard

to evaluate the evaporation time of the droplet in the transition boiling regime. The reason is the droplet during the transition boiling breaks into smaller balls, and some of these balls jump off the plate [7].

The total evaporation time is graphed against the excess temperature in Figure 3.34 and Figure 3.35. Figure 3.34 shows the evaporation time in the natural convection and nucleate boiling regimes. It can be obviously seen that when the excess temperature rises, the evaporation time drops. This reason is that in these two regimes increasing the wall temperature will increase the heat flux as it is shown in the general boiling curve (Figure 1.3). The experimental results of the evaporation time in natural convection regime show a little difference from the results reported by and Abu–Mulaweh et al. The evaporation time in the present work is shorter than that of Abu-Mulaweh et al. For example, at an excess temperature of 1 °C, the evaporation time was decreased by 31% compared with Abu–Mulaweh et al.’s findings. The droplet took 31s to evaporate in the present investigation, while, the evaporation time was 45s for Abu-Mulaweh et al.’s study. However, for the nucleate boiling regime, there is a good agreement [7].

The evaporation time in the film boiling regime is illustrated by Figure 3.35. Figure 3.35 obviously displays that when the excess temperature is raised, the droplet's lifetime starts to decrease. This reason is that increasing the wall temperature will increase the heat flux in film boiling because conduction and radiation between the drop and the plate are improved, shown in the boiling curve (Figure 1.3). The findings of the evaporation time in the film boiling regime agree well with the findings reported by Abu-Mulaweh et al. [7].

Comparing the evaporation time of the three regimes, it can be seen that the evaporation times in the natural convection and nucleate boiling regimes (Figure 3.34) are significantly shorter than those in film boiling regime (Figure 3.35) due to formation of a vapor layer between the plate and the droplet in film boiling regime. This layer turns to be as an insulator. As a result, the heat flux from the plate to the liquid ball is decreased [7].

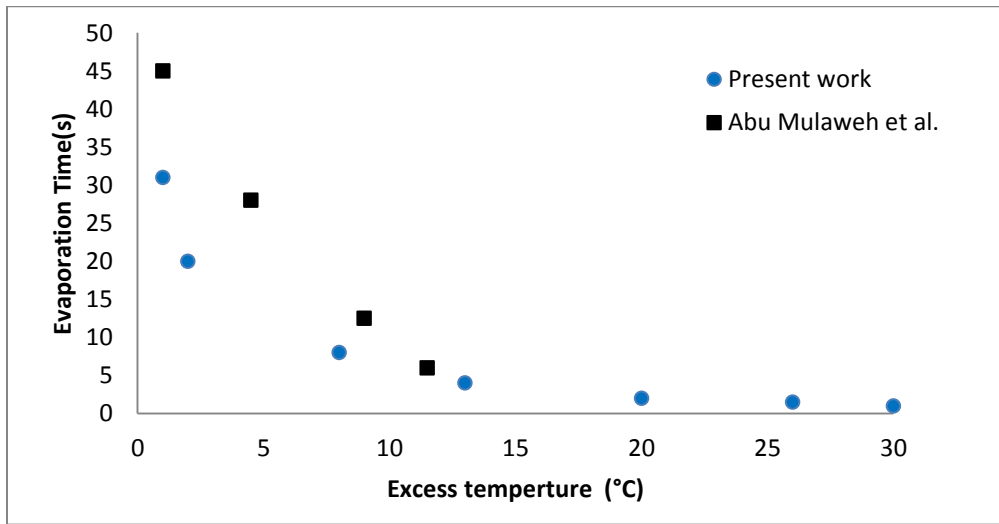


Figure 3.34: Evaporation time vs. excess temperature in the natural convection and nucleate boiling regimes

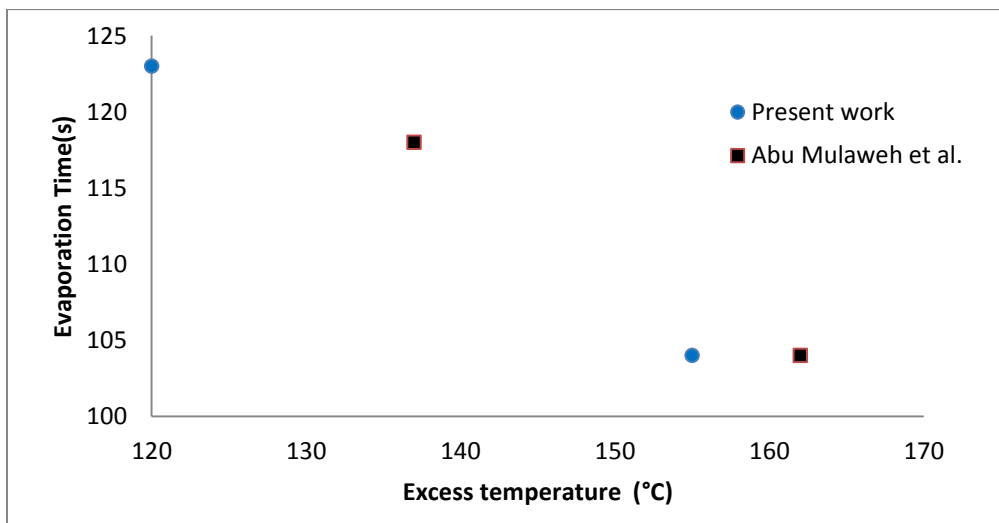


Figure 3.35: Evaporation time vs. excess temperature in the film boiling regime

4 Conclusions

In this chapter, the experimental results are summarized for three research studies. The following conclusions have been made from the study of surfactant, structured surfaces, and droplet boiling evaporation time observations.

4.1 Surfactants

The effect of surfactants on nucleate pool boiling heat transfer is investigated experimentally. It has been observed that adding a small amount of surfactant changes the water boiling phenomenon significantly. The salient conclusions are listed below:

- 1- The addition of small amounts of surfactant in water causes the nucleate boiling curve to shift to the left. The wall temperature drops greatly with an increase in the concentration of aqueous surfactant solutions. It is found that the maximum reduction in wall temperature for each surfactant was 5.76% for 300ppm SLS, 2.97% for 1600ppm EH-14, and 2.61% for 200ppm SA-9, compared with water.
- 2- The increase in concentration of the aqueous solution and heat flux lead to considerable enhancement in heat transfer coefficient. It is found that the optimum boiling heat transfer enhancement of SLS is higher than that of EH-14 and SA-9 compared to water. The maximum enhancement obtained is 66.27 % for 300ppm aqueous SLS solution. However, the maximum enhancement in heat transfer coefficient is 24.31% for 1600ppm EH-14, and 22.09% for 200ppm SA-9.
- 3- Compared to water, it is found that time required to reach boiling point for surfactant concentrations is reduced significantly. The maximum reduction for

each surfactant was 14.6% for 100ppm SLS, 9% for 800ppm EH-14, and 12.49% for 300ppm SA-9.

- 4- It is found that the heat flux, surfactant concentration, surface tension, and molecular weight are considered to be the main factors that lead to enhancement in nucleate pool boiling.
- 5- Boiling visualization shows that boiling with surfactant solutions compared with that in pure water is more vigorous. Bubbles are smaller in size, activate continuously, and collapse quickly. Also, the bubble departure frequency is higher than that of pure water.

4.2 Structured Surfaces

An experimental investigation has been made to study boiling performance of distilled water from plain and structured surfaces. Plain and seven structures have been machined of aluminum. One surface was with mushroomed fins; three surfaces were having rectangular channels, and the other three were with holes. The main conclusions are as follows:

- 1- Structured surfaces can enhance boiling heat transfer. The maximum enhancement was achieved by Holed 3 surface. The enhancement was 51.66% compared to plain surface.
- 2- As the spacing between channels or holes is decreased, the heat transfer coefficient is increased.
- 3- The bubbles with holed surfaces and mushroomed surface have almost spherical shape, while in plain and grooved surfaces they have an irregular shape.

4- Some enhanced surfaces show a big reduction in time to reach boiling point, while others show no reduction like Holed 3, Grooved 2, and Grooved 3 surfaces. For heat flux of 27.91 kW/m^2 , the maximum reduction achieved was 8.74% of Mushroomed surface and 8.19% for Holed 1 surface, while 8.58% enhancement in time to reach boiling point for Grooved 1 surface was attained at a heat flux of 35.08 kW/m^2 .

4.3 Droplet Boiling Evaporation Time Observations

The different regimes of pool boiling (natural convection boiling, nucleate boiling, transition boiling, and film boiling) were investigated with droplet dropping tests. The results showed that the boiling phenomenon of water droplet was completely different from one regime to another. Also, the total evaporation time of a droplet of sub-cooled water was measured and compared with results of Abu-Mulaweh et al.'s study. It was found that the evaporation times in the natural convection and nucleate boiling regimes are significantly shorter than those in film boiling regime. Compared to findings by Abu-Mulaweh et al., there is a fair agreement in evaporation times for nucleate and film boiling, but the evaporation times for natural convection boiling in the present study are shorter than those of Abu-Mulaweh et al.'s study. At an excess temperature of $1 \text{ }^\circ\text{C}$, the evaporation time was reduced by 31% compared with Abu-Mulaweh et al.'s findings.

4.4 Practical Engineering Drawbacks

The experimental data show that the structured surfaces and surfactants can enhance pool boiling heat transfer. However, further studies need to be carried out to investigate the practical engineering applications of these enhancement techniques. For example, these techniques can be applied in boilers of power plants, but many issues should be

taken in consideration. For example, the manufacturing cost of structured surfaces is one of these problems because these surfaces need to be fabricated with special features and dimensions. In addition, deposition is a big issue in boilers. This can lead to overheating and corrosion. Scale is the most well-known deposit, which is formed by salts that have partial solubility [72]. Therefore, treatment this issue with structured surfaces is not easy. From a design perspective, structured surfaces can have a stress concentration at sharp corners, which can lead to fatigue and corrosion cracking. Also, surfactant cost is another concern. It is important to evaluate the surfactant cost with the benefit of enhancing boiling heat transfer.

5 Future work

The following recommendations could be made for future work on three projects:

5.1 Surfactants

Further studies need to be carried out by measuring viscosity, surface tension, ionic nature, and contact angle of the surfactant solutions. Currently, undergraduate students (Remelisa Esteves and Nonso Onukwuba) study the viscosity of various surfactants and concentrations. Surface tensiometer device can be purchased for the lab.

Also, a new experimental setup is required to determine the effect of pressure on boiling heat transfer because the present investigation is done under atmospheric pressure condition to investigate the relationship between temperature changes with pressure. Finally, the effect of other surfactants can be investigated.

5.2 Structured Surfaces

The boiling heat transfer can be enhanced significantly by the grooved, holed, and mushroomed surfaces. Since the width of the channels, diameter of holes, and diameter of mushroomed fins for all the tested surfaces are the same, the next step would be to manufacture new surfaces with modifications in the width of the channels, the diameter of holes, and diameter of mushroomed fins, their depth, and the distance between the channels or holes and study their influence on pool boiling.

Also, the same enhanced surfaces implemented in this study could be used again to investigate other operating conditions like studying the effect of pressure, or using new fluids like refrigerants as working fluid. In addition, studying the effect of these surfaces

at high heat flux is necessary to investigate the CHF (critical heat flux) characteristics. So, new experimental setup may be required for that purpose.

5.3 Droplet Boiling Evaporation Time Observations

The results show that it is possible to study evaporation times of different regimes of boiling. In the future for comparing surfactant solution, evaporation times and boiling regimes can be investigated by using a droplet. Droplet evaporation comparison can be closely related to boiling phenomenon.

References

- [1] **Dikici, Birce**, Edidiong Eno, and **Marc Compere**. "Pool Boiling Enhancement with Environmentally Friendly Surfactant Additives." *Journal of Thermal Analysis and Calorimetry*, February 201, DOI 10.1007/s10973-013-3634-x.
- [2] **Dikici, Birce**, Edidiong Eno, and **Marc Compere**. "Nucleate Pool Boiling Enhancement Experiments for Heat Transfer Laboratory." ASME 2013 International Mechanical Engineering Congress and Exposition, Paper No. IMECE2013-63860, November 15–21, 2013: San Diego, California.
- [3] Disadvantages of Fossil Fuels. n.d. 26 May 2014 <http://www.conserve-energy-future.com/Disadvantages_FossilFuels.php>.
- [4] Park, Ki-Jung, Dongsoo Jung and Sang Eun Shim. "Nucleate boiling heat transfer in aqueous solutions with carbon nanotubes up to critical heat fluxes." *International Journal of Multiphase Flow* (2009): 525.
- [5] Witharana, Sanjeeva. BOILING OF REFRIGERANTS ON ENHANCED SURFACES AND BOILING OF NANOFUIDS. Licentiate Thesis. Stockholm, Sweden: The Royal Institute of Technology, 2003.
- [6] Incropera, Frank P., et al. Principles of Heat and Mass Transfer. New Jersey: John Wiley & Sons, Inc., 2003.
- [7] Abu-Mulaweh, Hosni I. and Josué Njock Libii. "Integration of boiling experiments in the undergraduate heat transfer laboratory." *International Journal of Mechanical Engineering Education* 31/3 (n.d.): 269-279.
- [8] Eduardo Cao: Heat Transfer in Process Engineering. BOILING, Chapter (McGraw-Hill Professional, 2010), AccessEngineering.
- [9] Cengel, Yunus A., and Afshin J. Ghajar. "Boiling and Condensation." *Heat and Mass Transfer: Fundamentals and Applications*. 4th ed. McGraw-Hill Higher Education, 2011. 515-560. Print.
- [10] Nukiyama S., 1934. Maximum and minimum values of heat transmitted from metal to boiling water under atmospheric pressure. *Journal of Society of Mechanical Engineers, Japan*, Vol. 37, pg.367.
- [11] Faghri, Amir, Yuwen Zhang and John R. Howell. "Advanced Heat and Mass Transfer." n.d. 1 June 2014 <<http://www.thermalfluidscentral.org/e-resources/download.php?id=1>>.

- [12] Zhang, Juntao. EXPERIMENTAL AND COMPUTATIONAL STUDY OF NUCLEATE POOL BOILING HEAT TRANSFER IN AQUEOUS SURFACTANT AND POLYMER SOLUTIONS. DOCTOR OF PHILOSOPHY (Ph.D.). Cincinnati: University of Cincinnati, 2004.
- [13] Yamagata, K., F. Kirano, K. Nishiwaka, and H. Matsuoka, *Mem. Fac. Eng. Kyushu*, 15, 98, 1955.
- [14] Rohsenow W.M., 1952. A method of correlating heat transfer data for surface boiling of liquids. *ASME Transactions*, Vol. 74, pp. 969-976.
- [15] Kutateladze, S. S., *Kotloturbostroenie*, 3, 10, 1948.
- [16] Zuber, N., *Trans. ASME*, 80, 711, 1958.
- [17] James G. Speight: *Chemical Process and Design Handbook. MANUFACTURE OF CHEMICALS*, Chapter (McGraw-Hill Professional, 2002), AccessEngineering.
- [18] IUPAC. *Compendium of Chemical Terminology*, 2nd ed. (the "Gold Book"). Compiled by A. D. McNaught and A. Wilkinson. Blackwell Scientific Publications, Oxford (1997). XML on-line corrected version: <http://goldbook.iupac.org> (2006-) created by M. Nic, J. Jirat, B. Kosata; updates compiled by A. Jenkins. ISBN 0-9678550-9-8. doi:10.1351/goldbook. Entry "critical micelle concentration, cmc".
- [19] Ana Domínguez, Aurora Fernández, Noemí González, Emilia Iglesias, and Luis Montenegro "Determination of Critical Micelle Concentration of Some Surfactants by Three Techniques", *Journal of Chemical Education*, Vol. 74 No. 10 October 1997, p. 1227-1231 (pdf)
- [20] Critical micelle concentration. 28 February 2013 . 10 June 2014
<http://en.wikipedia.org/wiki/Critical_micelle_concentration>.
- [21] Market Report: Global Surfactant Market. n.d. 14 Oct 2014
<<http://www.acmite.com/market-reports/chemicals/global-surfactant-market.html>>.
- [22] Yang, Y.M., Maa, J.R., 1983. Pool boiling of dilute surfactant solutions. *Journal of Heat Transfer* 105, 190–192.
- [23] Wasekar, V.M., and Manglik, R.M., 2002, "The Influence of Additive Molecular Weight and Ionic Nature on the Pool Boiling Performance of Aqueous Surfactant Solutions," *International Journal of Heat and Mass Transfer*, 45, pp. 483-493.

- [24] Wu, Wu-Tsann, Yu-Min Yang and Jer-Ru Maa. "Nucleate pool boiling enhancement by means of surfactant additives." *Experimental Thermal and Fluid Science* (1998): 195-209.
- [25] Hetsroni, G., et al. "Subcooled boiling of surfactant solutions." *International Journal of Multiphase Flow* (2002): 347–361.
- [26] Elghanam , R.I. , et al. "Experimental study of nucleate boiling heat transfer enhancement by using surfactant." *Ain Shams Engineering Journal* (2011): 195–209.
- [27] Nafey, A.S. , M.A. Mohamad and M.A. Sharafa. "Enhancement of solar water distillation process by surfactant additives." *Desalination* (2007): 514–523.
- [28] Hetsroni, G., Zakin, J.L., Lin, Z., Mosyak, A., Pancallo, E.A., and Rozenblit, R., 2001, "The Effect of Surfactants on Bubble Growth, Wall Thermal Patterns and Heat Transfer in Pool Boiling," *International Journal of Heat and Mass Transfer*, 44, pp. 485-497.
- [29] Zicheng, Hu , et al. "Pool Boiling Heat Transfer of Aqueous Surfactant Solutions." *Fourth International Conference on Intelligent Computation Technology and Automation*. Zhenjiang, Jiangsu, 212013, China: Jiangsu University, 2011. 841-844.
- [30] Levitskiy, S. P., Khusid, B. M., and Shul'man, Z. P., 1996, "Growth of Vapor Bubbles in Boiling Polymer Solutions-II. Nucleate Boiling Heat Transfer," *International Journal of Heat and Mass transfer*, 39(3), pp. 639-644.
- [31] P. Kotchaphakdee, M.C. Williams, Enhancement of nucleate pool boiling with polymer additives, *Int. J. Heat Mass Transfer* 13 (1970) 835–848.
- [32] P. Griffith, J.D. Wallis, The role of surface conditions in nucleate boiling, *Chem. Eng. Prog. Symp.* 56 (1960) 49–63.
- [33] J. Fujikaka, Heat Transfer Tube for Use in Boiling Type Heat Exchangers and Method of Producing the Same, US Patent 216, 1980, p. 826.
- [34] Das, A.K., P.K. Das and P. Saha. "Performance of different structured surfaces in nucleate pool boiling." *Applied Thermal Engineering* (2009): 3643–3653.
- [35] Cooke, Dwight and Satish G. Kandlikar. "Effect of open microchannel geometry on pool boiling enhancement." *International Journal of Heat and Mass Transfer* 55 (2012): 1004–1013.

- [36] Yu, Chih Kuang and Ding Chong Lu. "Pool boiling heat transfer on horizontal rectangular fin array in saturated FC-72." *International Journal of Heat and Mass Transfer* (2007): 3624–3637.
- [37] Hubner, Peter and Wolfgang Kunstler. "Pool boiling heat transfer at finned tubes: influence of surface roughness and shape of the fins." *ELSEVIER Science Ltd and IIR* (1997): 575-582.
- [38] Nimkar , Nitesh D., Sushil H. Bhavnani and Richard C. Jaeger. "Effect of nucleation site spacing on the pool boiling characteristics of a structured surface." *International Journal of Heat and Mass Transfer* 49 (2006): 2829–2839.
- [39] Ramaswamy, C., et al. "High-speed visualization of boiling from an enhanced structure." *International Journal of Heat and Mass Transfer* 45 (2002): 4761–4771.
- [40] Low Form Beakers. n.d. 21 Sept 2014 <<http://www.unitedsci.com/product-catalog/low-form-beakers>>.
- [41] Benchmark Hotplates, Stirrers and Hotplate Stirrers. Temperature Control Equipment. 28 May 2014 <http://www.benchmarkscientific.com/index_files/BenchmarkHotplatesStirrersandHotplateStirrers.htm>.
- [42] Self-Adhesive Thermocouples Molded Silicone Design. n.d. 5 May 2014 <<http://www.omega.com/pptst/SA2.html>>.
- [43] Portable Thermometer/Data Loggers with SD Card and Thermocouple Input. n.d. 29 May 2014 <http://www.omega.com/pptst/RDXL-SD_SERIES.html>.
- [44] FLIR Exx-Series." FLIR. Web. <<http://www.flir.com/cs/emea/en/view/?id=61457>>.
- [45] EX-FH20. n.d. 29 May 2014 <http://www.casio.com/products/archive/Digital_Cameras/High-Speed/EX-FH20/content/Special_Features/>.
- [46] ppm - parts per million. n.d. 15 Sept 2014 <http://www.engineeringtoolbox.com/ppm-d_1039.html>.
- [47] Richard, Cicely A. What Is the Difference Between Distilled Water & Tap Water? n.d. 15 Sept 2014 <http://www.ehow.com/about_5079200_difference-distilled-water-tap-water.html>.
- [48] Getan, Mahmoud Kamel. Heat Transfer in Pool Boiling with Surfactants. MS. thesis. Baghdad: University of Technology, 2009.

- [49] "Borosilicate Glass." Glass Properties. Cambridge Glassblowing Ltd
Camglassblowing.co.uk. Web. 5 Nov. 2014.
<<http://www.camglassblowing.co.uk/gproperties.htm>>.
- [50] SODIUM LAURYL SULFATE. n.d. 15 Sept 2014
<<http://chemicaland21.com/specialtychem/perchem/SODIUM%20LAURYL%20SULFATE.htm>>.
- [51] "ECOSURF(TM) EH-14 (90% Actives) Surfactant." Material Safety Data Sheet. 2013.
- [52] "ECOSURF™ SA-9 Surfactant." Material Safety Data Sheet. 2013.
- [53] "Borosilicate Glass." Skyline Components, LLC. Web. 5 Nov. 2014.
<<http://www.skylinecomponents.com/Borosilicate.html>>.
- [54] Toshiaki I, Yoshio T, Masanori M. "Enhancement of pool boiling heat transfer in water and ethanol/water mixtures with surface-active agent". International Journal of Heat and Mass Transfer. 2004, vol. 47, pp.5555-5563.
- [55] Hetsroni G, Mosyak A, Pogrebnyak E, Sher I, Segal Z. "Bubble growth in saturated pool boiling in water and surfactant solution". International Journal of Multiphase Flow, 2006, vol. 32, pp. 159-182.
- [56] Baloch, M.K., G. Hammed and A. Bano. "Effect of Electrolyte Concentration and Temperature on CMC of Surfactants." Jour.Chem. Soc.Pak (2002): 77-86.
- [57] Y.L. Tzanand, Y.M. Yang, Experimental study of surfactant effects on pool boiling heat transfer, Journal of Heat Transfer 112 (1990) 207±212.
- [58] Henneberg, M., Sanfeld, A., Bisch, P.M., 1980. Absorption–desorption barrier diffusional exchanges and surface instabilities of longitudinal waves for aperiodic regimes. J. Am. Inst. Chem. Eng. 27, 1002–1008.
- [59] Fritz W., 1935. Berechnung des maximal volume von dampfblasen. Phys. Z., 36, pg.379.
- [60] Wen D S, Wang B X. "Effects of surface wettability on nucleate pool boiling heat transfer for surfactant solutions". International Journal of Heat and Mass Transfer. 2002, vol. 45, pp. 1739-1747.
- [61] Hetsroni G, Mosyak A, Pogrebnyak E, Sher I, Segal Z. "Bubble growth in saturated pool boiling in water and surfactant solution". International Journal of Multiphase Flow, 2006, vol. 32, pp. 159-182.

- [62] B.H. Shah, R. Darby, The effect of surfactant on evaporative heat transfer in vertical film flow, *Int. J. Heat Mass Transfer* 16 (1973) 1889–1903.
- [63] Dong, Lining, Xiaojun Quan and Ping Cheng. "An experimental investigation of enhanced pool boiling heat transfer from surfaces with micro/nano-structures." *International Journal of Heat and Mass Transfer* (2014): 189–196.
- [64] S. Jun, S. Sinha-Ray, A.L. Yarin, Pool boiling on nano-textured surfaces, *Int. J. Heat Mass Transfer* 62 (2013) 99–111.
- [65] Das, A.K., P.K. Das and P. Saha. "Nucleate boiling of water from plain and structured surfaces." *Experimental Thermal and Fluid Science* 31 (2007): 967–977.
- [66] H.J. Ivey, Relationships between bubble frequency, departure diameter, and rise velocity in nucleate boiling, *Int. J. Heat Mass Transfer* 10 (1967) 1023–1040.
- [67] W. Nakayama, T. Daikoku, T. Nakajima, Effects of pore diameters and system pressure on saturated pool boiling heat transfer from porous surfaces, *J. Heat Transfer* 104 (1982) 286–291.
- [68] L.-H. Chien, R.L. Webb, Measurement of bubble dynamics on an enhanced boiling surface, *Exp. Thermal Fluid Sci.* 16 (3) (1998) 177–186.
- [69] Walker, J. (n.d.). Boiling and the Leidenfrost Effect. Cleveland State University.
- [70] http://darkwing.uoregon.edu/linke/papers/Walker_leidenfrost_essay.pdf, (2011).
- [71] A. Blanche, C. Clanet, and D. Quere, Leidenfrost drops, *Phys. Fluids* 15, 1632 (2003).
- [72] "Chapter 12- Boiler Deposits: Occurrence and Control." *Imagination at Work*. GE Power & Water, Water & Process Technologies. Web. 19 Nov. 2014. <http://www.gewater.com/handbook/boiler_water_systems/ch_12_boilerdeposits.jsp>.

Appendix A: Thermocouple Calibration

Type K thermocouple was calibrated in water bath in the range of ambient water temperature to the boiling point against another K type thermocouple. The sample of the calibration curve is shown in Figure A.

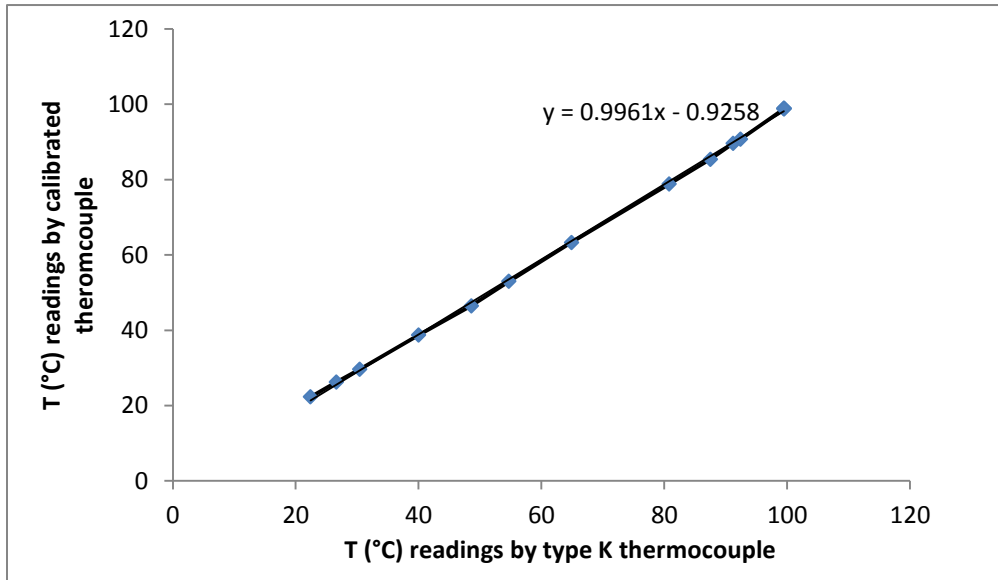


Figure A: Calibration of the thermocouple type k.

Table A: Data of calibration of the thermocouple type k.

Thermocouple type K	Calibrated thermocouple	ΔT (°C)
22.4	22.3	0.1
26.6	26.2	0.4
30.4	29.6	0.8
40	38.7	1.3
48.6	46.5	2.1
54.7	53	1.7
64.9	63.3	1.6
80.8	78.8	2
87.5	85.4	2.1
91.2	89.6	1.6
92.4	90.7	1.7
99.5	98.8	0.7
99.5	98.8	0.7
99.5	98.9	0.6
99.5	99	0.5

Appendix B: Experimental Data of Calculating Heat Flux for Boiling with Surfactants

The tables below show the experimental data of calculation heat flux by two different methods.

Table B.1: Surface temperature of heater at different settings vs. time.

Setting 1		Setting 2		Setting 3	
Time(s)	T_s (°C)	Time(s)	T_s (°C)	Time(s)	T_s (°C)
0	23.95	0	24.75	0	24.75
232	118	230	132	228	197.15
310	154.4	300	168.4	306	241.75
510	236.75	465	243.1	468	319.65
602	263.6	610	293.3	611	370.45
826	308.55	755	327.3	750	406.15
907	319.55	908	350.25	916	423.6
1010	333.95	1005	363.25	1008	420.4
1210	349.35	1215	375.75	1220	404.7
1340	355.95	1345	381.75	1344	398.6
1512	359.25	1521	387.4	1518	398.05
1648	362.1	1650	389	1655	398.7
1810	363.85	1815	389.8	1820	399.55

Table B.2: Heat flux values by Fourier's law

	Setting 1	Setting 2	Setting 3
T_s (°C)	360.28	386.98	398.72
T_w (°C)	110.84	116.91	119.3
ΔT (°C)	249.44	270.07	279.42
q'' ($\frac{W}{m^2}$)	94787.2	102626.6	106179.6
Power (W)	774.41	838.49	867.48

Table B.2: Calculation of heat flux by the second method.

Setting3			Setting 2			Setting 1			
t(minutes)	m (grams)	Δm	\dot{m}_b ($\frac{kg}{s}$)	m (grams)	Δm	\dot{m}_b ($\frac{kg}{s}$)	m (grams)	Δm	\dot{m}_b ($\frac{kg}{s}$)
0	712	1	1.66667E-06	712	1	1.66667E-06	712	1	1.66667E-06
10	711	21	0.000035	711	10	1.66667E-	711	8	1.33333E-

						05			05
20	690	65	0.0001083	701	41	6.83333E-05	703	32	5.33333E-05
30	625	67	0.00011166	660	53	8.83333E-05	671	34	5.66667E-05
40	558	65	0.00010833	607	56	9.33333E-05	637	37	6.16667E-05
50	493	64	0.00010666	551	55	9.16667E-05	600	36	0.00006
60	429	0	0	496	0	0	564	0	0
Average of \dot{m}_b ($\frac{kg}{s}$)			0.00011			0.000091			0.00006
Power (W)			248.27			205.387			135.42
Heat flux (W/m^2)			30383.23			25135.22			16572.67

Appendix C: Experimental Data of Nucleate Boiling of Water and Surfactants

The experimental data for water and surfactants, shown in the tables below, are obtained.

Table C.1: Heat flux vs. wall temperature (°C) for water

Heat flux (kW/m ²)	Run 1	Run 2	Run 3	Run 4	Run 5	T average
16.57	109.3	110.4	117.74	112.47	110.54	110.84
25.13	116.81	117.5	116.11	117.75	116.38	116.91
30.38	118.46	118.9	119.31	121	118.84	119.3

Table C.2: Heat flux vs. wall temperature (°C) for SLS surfactant

Heat flux (kW/m ²)	50ppm	100ppm	200ppm	300ppm	400ppm	500ppm
16.57	108.24	109.01	108.14	107.54	107.1	107.06
25.13	113.62	113.8	112.31	110.17	110.23	110.76
30.38	116.7	114.54	114.57	113.69	113.29	113.48

Table C.3: Heat flux vs. wall temperature (°C) for EH-14 surfactant

Heat flux (kW/m ²)	200ppm	400ppm	800ppm	1600ppm	2400ppm	3200ppm
16.57	110.07	110.28	109.22	108.72	110.15	109.86
25.13	116.49	116.04	115.14	115.58	113.89	115.66
30.38	118.08	117.73	116.31	115.75	116.63	118.1

Table C.4: Heat flux vs. wall temperature (°C) for SA-9 surfactant

Heat flux (kW/m ²)	200ppm	300ppm	400ppm	500ppm	600ppm
16.57	109.76	109.65	110.3	109.27	109.4
25.13	113.85	113.88	114.27	115	115.17
30.38	117.46	116.84	117	117.04	117.46

Table C.5: Heat flux vs. time to reach boiling point(s) for water

Heat flux (kW/m ²)	Run 1	Run 2	Run 3	Run 4	Mean
16.57	1202	1212	1292	1176	1220.5
25.13	998	986	988	994	991.5
30.38	810	802	817	820	812.25

Table C.6: Heat flux vs. time to reach boiling point(s) for SLS

Heat flux (kW/m ²)	50ppm	100ppm	200ppm	300ppm	400ppm	500ppm
16.57	1174	1042	1083	1130	1150	1104
25.13	1012	954	984	972	955	950
30.38	732	790	757	775	775	770

Table C.7: Heat flux vs. time to reach boiling point(s) for EH-14

Heat flux (kW/m ²)	200ppm	400ppm	800ppm	1600ppm	2400ppm	3200ppm
16.57	1140	1218	1170	1182	1158	1118
25.13	988	980	982	986	970	918
30.38	820	760	739	780	756	783

Table C.8: Heat flux vs. time to reach boiling point (s) for SA-9

Heat flux (kW/m ²)	200ppm	300ppm	400ppm	500ppm	600ppm
16.57	1126	1068	1084	1106	1076
25.13	996	988	924	964	970
30.38	750	764	757	747	755

Appendix D: Experimental Data of Water on Structured Surfaces

The experimental data of water from plain and structured surfaces are shown in tables below.

Table D.1: Experimental data of calculating heat flux

t (minutes)	Setting 1			Setting 2		
	m (grams)	Δm	$\dot{m}_b (\frac{kg}{s})$	m (grams)	Δm	$\dot{m}_b (\frac{kg}{s})$
0	1038	0	0	1038	0	0
20	1022	62	0.000103333	1010	77	0.000128333
30	960	60	0.0001	933	78	0.00013
40	900	65	0.000108333	855	80	0.000133333
50	835	0	0	775	0	0
Average of $\dot{m}_b (\frac{kg}{s})$			0.000103889			0.000130556
Power (w)			234.4772222			294.6638889
Heat flux (W/m ²)			27913.95503			35079.03439

Table D.2: Experimental data of pool boiling of water on plain and structured surfaces

Heat flux (kW/m ²)	Plain			Mushroomed					
	T _w (°C) R1	T _w (°C) R2	T _{ave} (°C)	T _w (°C) R1	T _w (°C) R2	T _{ave} (°C)			
27.91	105.74	104.94	105.34	104.28	104.78	104.53			
35.08	107.04	106.64	106.84	105.96	105.64	105.8			
Heat flux (kW/m ²)	Holed 1			Holed 2			Holed 3		
	T _w (°C) R1	T _w (°C) R2	T _{ave} (°C)	T _w (°C) R1	T _w (°C) R2	T _{ave} (°C)	T _w (°C) R1	T _w (°C) R2	T _{ave} (°C)
27.91	105.03	104.05	104.54	104.15	103.66	103.9	103.93	103.63	103.78
35.08	105.76	105.44	105.6	105.02	104.64	104.83	104.1	104.93	104.51
Heat flux (kW/m ²)	Grooved1			Grooved2			Grooved 3		
	T _w (°C) R1	T _w (°C) R2	T _{ave} (°C)	T _w (°C) R1	T _w (°C) R2	T _{ave} (°C)	T _w (°C) R1	T _w (°C) R2	T _{ave} (°C)
27.91	104.84	104.6	104.72	104.44	103.88	104.16	103.42	104.12	103.77
35.08	105.84	106.02	105.93	105.14	105.41	105.27	104.16	105.33	104.74

Table D.3: Experimental data of time to reach boiling point (s) for plain and structured surfaces.

Heat flux (kW/m ²)	Plain				Mushroomed			
	t(s) (Run 1)	t(s) (Run 2)	t _{ave} (s)		t(s) (Run 1)	t(s) (Run 2)	t _{ave} (s)	Reduction (%)
27.91	954	910	932		844	866	855	8.26
35.08	816	820	818		748	745	746.5	8.74
Heat flux (kW/m ²)	Grooved 1				Holed 1			
	t(s) (Run 1)	t(s) (Run 2)	t _{ave} (s)	Reduction (%)	t(s) (Run 1)	t(s) (Run 2)	t _{ave} (s)	Reduction (%)
27.91	868	836	852	8.58	878	907	892.5	4.23
35.08	755	768	761.5	6.9	734	768	751	8.19
Heat flux (kW/m ²)	Grooved 2				Holed 2			
	t(s) (Run 1)	t(s) (Run 2)	t _{ave} (s)	Reduction (%)	t(s) (Run 1)	t(s) (Run 2)	t _{ave} (s)	Reduction (%)
27.91	934	912	923	0.96	994	962	978	-4.93
35.08	818	815	816.5	0.18	831	853	842	-2.93
Heat flux (kW/m ²)	Grooved 3				Holed 3			
	t(s) (Run 1)	t(s) (Run 2)	t _{ave} (s)	Reduction (%)	t(s) (Run 1)	t(s) (Run 2)	t _{ave} (s)	Reduction (%)
27.91	1038	1028	1033	-10.83	952	946	949	-1.82
35.08	871	869	870	-6.35	856	860	858	-4.88

Appendix E: Experimental Data of Droplet Evaporation Time

The table below shows the experimental data of droplet evaporation time at different boiling regimes.

Natural and nucleate boiling regimes		
Surface temperature (°C)	Excess temperature (°C)	Time(s)
101	1	31
102	2	20
108	8	8
113	13	4
120	20	2
126	26	1.5
130	30	1
Film boiling regime		
220	120	123
255	155	104